William Robb Naylor

Model studies of the chiral and deconfinement transitions in QCD

Thesis for the degree of Philosophiae Doctor

Trondheim, September 2015

Norwegian University of Science and Technology
Faculty of Natural Sciences and Technology
Department of Physics

NTNU
Norwegian University of
Science and Technology

NTNU
Norwegian University of Science and Technology

Thesis for the degree of Philosophiae Doctor

Faculty of Natural Sciences and Technology
Department of Physics

© William Robb Naylor

978-82-326-1132-4 (print)
978-82-326-1133-1 (digital)
1503-8181

Doctoral theses at NTNU, 2015:238

Printed by NTNU Grafisk senter

Preface

This thesis is submitted to the Norwegian University of Science and Technology (NTNU) as partial fulfilment of the requirements for the degree of Philosophiae Doctor. It is the result of four years research at the Department of Physics at NTNU under the supervision of Professor Jens O. Andersen.

This thesis consists of two parts: In the second part we present the three papers that form the backbone of the thesis. In the first part, we provide a short introduction to the research field and motivate and elucidate the papers presented in the second part. It is hoped that this will make the papers presented accessible to someone new to the field or from a related field.

William Naylor

Trondheim, July 2015

To the non-physicist

The force that is responsible for holding the nucleus together and for creating protons and neutrons (via the binding of even smaller particles, called quarks) is the strong nuclear force. Of the four fundamental forces of nature, the strong force is (unsurprisingly) the strongest but also has extremely short range. Its short range arises from the fact that the force attracts to itself,[1] and thus produces very tangled configurations.

The theory of the strong nuclear force is Quantum ChromoDynamics (QCD). This theory accounts for the tangled nature of the force it describes. A result is that making calculations directly from the theory is almost impossible. Hence we follow the work of many others by instead using simplified models of QCD that approximate the theory for a certain range of temperatures and pressures. QCD is also studied experimentally via high energy collisions, such as the experiments ongoing at the Large Hadron Collider at CERN. A byproduct of these collisions is extremely intense magnetic fields. Currently there is disagreement between model calculations (which we do) and brute force calculations of QCD using supercomputers (lattice-QCD) as to what the effect of these large magnetic fields is on QCD.

In this thesis we give one of the most complete studies of a model of QCD including a magnetic field and explore some of the mathematical details that have arisen as people search for consensus between models and lattice-QCD. In addition, we investigate some of the subtleties that arise when comparisons are made between model studies and lattice-QCD and suggest ways in which these can be accounted for.

---

[1] What does it mean for a force to interact with itself? Well, imagining a long ranged force like electromagnetism we are prompted to think of field lines flowing from positive charges to negative charges. If this force was attracted to its self then instead of flowing evenly to the negative charge, the lines instead would all flow toward one another, and quickly become entangled.

Acknowledgements

This thesis simply would not be possible without the help of my supervisor Jens O. Andersen. I thank you for all the help with physics, getting me through the academic grind and for taking on someone with (essentially) a background in experimental quantum optics. My great thanks also goes to both Tomáš Brauner and Anders Tranberg for their help in the papers I co-authored with them. I don't think I ever learned more than in the weeks I spend hosted by the two of you.

Thinking now there is a horde of other names here at the department to whom this thesis owes some thanks. From the bones of the latex code seen here, stacks of questions about Mathematica and the irrelevant questions one asks to begin thinking about the answer in a new way, to help getting through teaching duties and what all those forms actually wanted me to write, there was a lot to be done that I didn't know how to do. Thanks to all that helped.

And thank you to friends and family for allowing me to keep on going.

List of Papers

Paper [1]
Jens O. Andersen, William R. Naylor and Anders Tranberg.
Chiral and deconfinement transitions in a magnetic background using the functional renormalization group with the Polyakov loop.
Journal of High Energy Physics, 1404:187, 2014.

Paper [2]
Jens O. Andersen, William R. Naylor and Anders Tranberg.
Inverse magnetic catalysis and regularization in the quark-meson model.
Journal of High Energy Physics, 1502:205, 2015.

Paper [3]
Jens O. Andersen, Tomáš Brauner and William R. Naylor.
Confronting effective models for deconfinement in dense quark matter with lattice data.
Submitted to Physical Review D, arXiv:1505.05925, 2015

Notation

Units

- Unless specifically stated we will work in natural units, where $\hbar = c = k_B = 1$.[2]

Vectors

- Three-vectors will be denoted by boldface and their components denoted by Latin indices, $\mathbf{p} = (p_1, p_2, p_3)$.
- Minkowskian four-vectors will be denoted by lower-case letters and their components denoted by Greek indices, $p = (p_0, \mathbf{p})$, and we use the signature $(+, -, -, -)$.
- We will use the Einstein summation convention, thus we have

$$\begin{aligned} p_i q_i &= p_1 q_1 + p_2 q_2 + p_3 q_3 \,, \\ p_\mu q_\mu &= p_0 q_0 - p_i q_i \,, \\ P_\mu Q_\mu &= P_0 Q_0 + p_i q_i \,. \end{aligned}$$

Definitions

- The Pauli matrices in flavour/isospin (we will almost exclusively work with two flavors) space will be denoted by τ_i otherwise by σ_i and, for reference, they are given by

---

[2] Using this elegant convention we have only a single unit, that of the electron-volt (eV). Thus, for example, dimensionally energies and masses are given in eV, distances by eV^{-1} and velocities are dimensionless.

$$\tau_1 = \begin{pmatrix} 0 & 1 \\ 1 & 0 \end{pmatrix} , \quad \tau_2 = \begin{pmatrix} 0 & -i \\ i & 0 \end{pmatrix} , \quad \tau_3 = \begin{pmatrix} 1 & 0 \\ 0 & -1 \end{pmatrix} .$$

We also use $\sigma^\mu \equiv (1, \sigma_i)$ and $\bar{\sigma}^\mu \equiv (1, -\sigma_i)$.

- The Gell-Mann matrices will be denoted by λ_i and, again for reference, we give them here

$$\lambda_1 = \begin{pmatrix} 0 & 1 & 0 \\ 1 & 0 & 0 \\ 0 & 0 & 0 \end{pmatrix} , \quad \lambda_2 = \begin{pmatrix} 0 & -i & 0 \\ i & 0 & 0 \\ 0 & 0 & 0 \end{pmatrix} , \quad \lambda_3 = \begin{pmatrix} 1 & 0 & 0 \\ 0 & -1 & 0 \\ 0 & 0 & 0 \end{pmatrix} ,$$

$$\lambda_4 = \begin{pmatrix} 0 & 0 & 1 \\ 0 & 0 & 0 \\ 1 & 0 & 0 \end{pmatrix} , \quad \lambda_5 = \begin{pmatrix} 0 & 0 & -i \\ 0 & 0 & 0 \\ i & 0 & 0 \end{pmatrix} ,$$

$$\lambda_6 = \begin{pmatrix} 0 & 0 & 0 \\ 0 & 0 & 1 \\ 0 & 1 & 0 \end{pmatrix} , \quad \lambda_7 = \begin{pmatrix} 0 & 0 & 0 \\ 0 & 0 & -i \\ 0 & i & 0 \end{pmatrix} , \quad \lambda_8 = \begin{pmatrix} 1 & 0 & 0 \\ 0 & 1 & 0 \\ 0 & 0 & -2 \end{pmatrix} .$$

Contents

Preface **i**

To the non-physicist **iii**

Acknowledgements **v**

List of papers **vii**

Notation **ix**

1 Introduction **1**
- 1.1 Papers and problems 2
- 1.2 Quantum chromodynamics 3
- 1.3 Phase diagram of QCD 7
- 1.4 Finite magnetic fields 8
- 1.5 Thesis outline 9

2 Model approach to QCD **13**
- 2.1 The quark meson model 13
- 2.2 The Nambu Jona-Lasinio model 15
- 2.3 Finite B 17
- 2.4 Polyakov loop 18

3 Theoretical Formalism **21**
- 3.1 Thermodynamic relations 21
- 3.2 Phase transitions 22
- 3.3 Thermal field theory 23
- 3.4 Functional renormalization group 27
- 3.5 Renormalization 29

4 Numerical methods **33**
4.1 Evaluation of $U_{k=0}(\rho, \Phi, \bar{\Phi})$ 34
4.2 Finding the critical temperatures 37

A Appendix **39**

1 Introduction

The work that comprises this thesis is mainly concerned with mapping out the location of the chiral and deconfinement phase transitions for strongly interacting matter. Confinement is perhaps the defining feature of quantum chromodynamics (QCD) and yet it remains poorly understood. This is mostly because of the difficulty in studying the non-perturbative regime of QCD. This thesis, and indeed the whole field of effective models for QCD, has arisen essentially as a response to this basic difficulty.

We use the two-flavor[1] quark meson (QM) and Nambu-Jona-Lasinio (NJL) models augmented by the Polyakov loop to study thermal equilibrium QCD for temperatures up to around 500 MeV. We primarily employ these models such that we can use standard calculational tools to make meaningful calculations for this region of the phase diagram of QCD. These models contain many of the same symmetries as QCD, in particular those relating to chiral symmetry. They do not, however contain any gluon degrees of freedom. The Polyakov loop is introduced to (a) add an approximate order parameter for deconfinement and (b) bring back into the model some of the effects of confinement (the suppression of quark degrees of freedom in the confined phase). In addition we include a constant classical background magnetic field, B, and investigate the effects this has on the phase diagram.

A complimentary approach to solving the non-perturbative regime of QCD is simply discretising space-time and solving QCD numerically, such an approach is called lattice QCD.[2] From our point of view this field has an important role to play, due to the difficulty in obtaining and interpreting experimental results and observations. Lattice QCD thus acts as an independent check of the results found in model studies. An important example is the behaviour of the chiral transition as a function of external magnetic field, which we will return to shortly. Lattice QCD is hindered by the sign problem (see for example Sec. 2 of [14]), which makes calculations at finite baryon chemical potential almost impossible. Thus models have an important role to play in the building of the phase diagram.

---

[1] We will only use the two lightest quark flavors, the up (u) and down (d) quarks. The charm, top and bottom quarks all have masses over a GeV and thus are beyond the energy scales we are exploring. The strange quark has a mass of 100 MeV, and thus a number of authors using effective models use three flavors, see for example [4, 5, 6, 7, 8, 9], however we are more interested in the behaviour of the transitions, than their exact values. Also, in paper [3] we will compare directly to lattice articles [10, 11] using two flavors.

1.1 Papers and problems

We present three papers in Part 2. The first paper is in essence a very simple paper. We follow up the work of Andersen and Tranberg [15] by extending the analysis of the QM model to include the Polyakov loop. Both works use a finite background magnetic field and chemical potential and go beyond mean field in using the functional renormalization group (RG), see Sec. 3.4. We concern ourselves in particular with the effect that the Polyakov loop has on the phase diagram, and with the various versions of the potential for the gauge sector.

During the time I have been undertaking my doctorate (2011-2015), there has been debate in the literature about the disagreement between lattice and model studies on the effect of a magnetic field on the chiral phase transition, and in particular the transition temperature T_c. Early lattice studies [16, 17] showed in agreement with model results that T_c increased with increasing B. However these results used heavy quark masses, later studies using light quarks, with physical values for the pion masses [13, 18, 19, 20, 21] showed the opposite behaviour (that T_c decreases with increasing B). This has led to a torrent of articles [22, 23, 24, 25, 26, 27, 28] investigating how models can be tweaked to reproduce these later lattice results. Motivated by the contrasting results of [22] and the RG extension of that work, we primarily investigate how various renormalization schemes effect the results of QM model calculations where the Yukawa coupling is allowed to vary with B.

In the third paper we look in greater depth at comparisons between lattice and model calculations. As we wish to investigate Polyakov loop coupled models, we must turn from physical three color QCD to QCD with two colors (2cQCD). The advantage of this is that lattice 2cQCD is free of the sign problem, and thus we are able to compare to lattice simulations at both zero and large chemical potential. In addition we use to the NJL model. Further discussion of the properties of 2cQCD is left to Sec. 2 of paper [3] and references therein.

---

[2] For a general review see [12], for results showing the behaviour of the chiral transition at physics quark masses see for example [13], and for the work we compare directly with in paper [3] see [10, 11].

1.2 Quantum chromodynamics

With the stage set, let us turn to the problem at hand: quantum chromodynamics. QCD is the correct theory of the strong interactions. The starting point for the theory is a Dirac Lagrangian for each of the six quark flavors. Interactions between the quarks are introduced by coupling them to a gauge field, exactly as in quantum electrodynamics (QED). The symmetry group of the gauge field is SU(3). This allows for colorless baryons, bound states of three quarks (such as the proton), and importantly this gauge group is non-abelian, which is central to the physics that this theory describes. The Lagrangian of QCD is, simply,

$$\mathcal{L}_{\text{QCD}} = \bar{\psi}(i\gamma^\mu D_\mu - m_0)\psi - \frac{1}{4} G^a_{\mu\nu} G^{\mu\nu}_a \,, \tag{1.1}$$

where D_μ is the covariant derivative coupling the fermions to the gauge bosons - the gluons - with $D_\mu = \partial_\mu - igA^a_\mu T^a$ and $G^a_{\mu\nu}$ is the non-abelian field strength. This compact form reflects the structure we have just described, but hides a lot of the mathematical detail. In more complete notation Eq. (1.1) is given by

$$\mathcal{L}_{\text{QCD}} = \bar{\psi}^\alpha_i (i\gamma^\mu \partial_\mu - m_i)\psi^\alpha_i + gA^a_\mu \, \bar{\psi}^\alpha_i \gamma^\mu t^a_{\alpha\beta} \psi^\beta_i - \frac{1}{4} G^a_{\mu\nu} G^{\mu\nu}_a \,, \tag{1.2}$$

with

$i = u, d, c, s, b, t$ is the quark flavor,

$\alpha = 1, 2, 3$ is the gauge/color index,

$a = 1, \ldots 8$ runs over the gluons,

$t^a_{\alpha\beta} = \frac{1}{2}\lambda^a_{\alpha\beta}$ with λ^a the Gell-Mann matrices,

$G^a_{\mu\nu} = \partial_\mu A^a_\nu - \partial_\nu A^a_\mu + gf^{abc} A^a_\mu A^b_\nu$ where f^{abc} are the structure constants of SU(3).

Given the definition of the structure constants as $[T^a, T^b] = if^{abc}T^c$ we see that the non-commutativity of the group immediately leads to an interaction term for the gluons.

The fact that the gauge bosons of QCD are self interacting leads to asymptotic freedom, and equally, color confinement.[3] Loosely, as a color-neutral hadron - either a quark-antiquark pair (a meson) or three quarks of color red, blue, green (a baryon) - is pulled apart the color field holding them together increases in strength. The further apart the components of the hadron are, the stronger the force between them, and thus the greater the energy in the field. At some point (on the order of fermi) the energy in the field is so great that it is energetically favourable to create a quark-antiquark pair to create (more) localised color neutral objects.

Mathematically these concepts are most simply expressed through the running of the QCD coupling constant $\alpha_s = g^2/(4\pi)$. g is the gauge coupling in Eq. (1.2) and is related to the beta function (which describes how the coupling within a theory changes with energy scale Q) via

$$\beta(g) = \frac{\partial g}{\partial \log(Q/\mu)}\,, \tag{1.3}$$

where μ is an arbitrary renormalization point. For an $SU(N_c)$ gauge theory with fermions in the fundamental representation the beta function is given by

$$\beta(g) = -\frac{g^3}{(4\pi)^2}\left(\frac{11}{3}N_c - \frac{2}{3}N_f\right) + \mathcal{O}(g^5)\,. \tag{1.4}$$

This result already tells us that QCD, which has $N_c = 3$ and $N_f = 6$ has a negative beta function and thus will be asymptotically free. Combining Eqs. (1.3) and (1.4) with the definition of α_s we arrive at

$$\alpha_s(Q) = \frac{\alpha_s(\mu)}{1 + (b_0\alpha_s(\mu)/2\pi)\log(Q/\mu)}\,, \tag{1.5}$$

where we have defined $b_0 \equiv (11N_c - 2N_f)/3$. This may be simplified by defining the energy scale

$$\Lambda_{\text{QCD}} \equiv \mu \exp\left\{\frac{-2\pi}{b_0\alpha_s(\mu)}\right\}\,, \tag{1.6}$$

---

[3] This part is mostly based on Secs. 16.6 and 7 and 17.2 of Peskin and Schroeder [29], see there for greater detail. We should note that asymptotic freedom also requires the negativity of the beta function, and thus we must also have a sufficiently low number of fermion flavors (see Eq. (1.4)).

which indicates the energy at which α_s becomes large. Eq. (1.5) is then given by

$$\alpha_s(Q) = \frac{2\pi}{b_0 \log(Q/\Lambda_{\mathrm{QCD}})}\,, \tag{1.7}$$

again encoding the coupling's dependence on the energy scale. It should be noted that this is only true for sufficiently low α_s. Experimentally this general picture is confirmed, as is shown in Fig. 1.1.

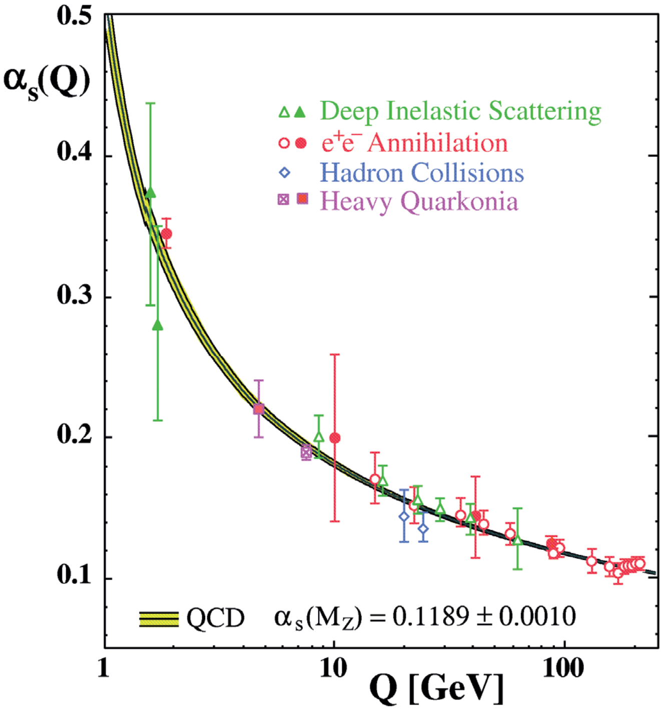

Figure 1.1: Summary of measurements of $\alpha_s(Q)$. The masses at which the charm and bottom quark freeze out is taken as 1.5 and 4.7 GeV respectively, at these points one can see small discontinuities in the theoretical prediction. Figure taken from Bethke, 2006 [30].

t

Despite this textbook knowledge of asymptotic freedom and the fine results shown in Fig. 1.1, an all encompassing definition of the deconfinement transition is still missing from QCD. It is clear that the transition is characterised by a change from hadronic degrees of freedom to quark degrees of freedom. We follow Fukushima [31] and others in coupling to the Polyakov loop (an order parameter for deconfinement in pure gauge theory [32, 33]) which is introduced in Sec. 2.4.

Due to the very construction of QCD the theory clearly exhibits exact *local* $SU(3)$ color symmetry. As a relativistic theory it is also invariant under the Poincaré group, that is both Lorentz transformations and translations in space and time. The Dirac spinor appears in combination with the Dirac adjoint, $\bar{\psi} = \psi^\dagger \gamma^0$, hence the Lagrangian is invariant under a $U(1)$ rotation of the quarks, resulting in the conservation of Baryon number. If we are lucky enough to have read Maggiore's fantastic introduction to quantum field theory (QFT) [34] we will also recall that we built our Dirac spinor out of a pair of left handed and right handed Weyl spinors such that it would be invariant under a parity transformation, $(t, \mathbf{x}) \to (t, -\mathbf{x})$, and of course this is carried over to the full theory, which is also time reversal and charge conjugation invariant. In the *chiral representation* the Dirac spinor and the gamma matrices are simply given as

$$\psi = \begin{pmatrix} \psi_L \\ \psi_R \end{pmatrix} , \qquad \gamma^\mu = \begin{pmatrix} 0 & \sigma^\mu \\ \bar{\sigma}^\mu & 0 \end{pmatrix} , \tag{1.8}$$

where $\psi_{L(R)}$ is a left (right) handed Weyl spinor (and ψ is a Dirac spinor). In this representation it is easy to see that if we neglect the mass term the quark sector is not only invariant under a total $U(1)$ rotation, but actually by two independent $U(1)$ rotations on the left and right handed parts:

$$\psi_L \to e^{i\theta_L} \psi_L \, , \qquad \psi_R \to e^{i\theta_R} \psi_R \, . \tag{1.9}$$

We may choose to instead encode these two rotations as

$$\psi \to e^{i\alpha} \psi \, , \qquad \psi \to e^{i\beta\gamma^5} \psi \, , \tag{1.10}$$

where we have defined $\alpha = (\theta_L + \theta_R)/2$ and $\beta = (\theta_R - \theta_L)/2$, the associated symmetries are then denoted $U(1)_V$ ('vector' - this corresponds to baryon number) and $U(1)_A$ ('axial') respectively. Using only the two lightest quark flavours we define

$$q = \begin{pmatrix} u \\ d \end{pmatrix} , \tag{1.11}$$

where u and d are Dirac spinors for the respective quarks. Again neglecting the mass term the fermionic sector of Eq. (1.1) can be broken into two equations for the left and right handed parts with a global $U(2)_L \times U(2)_R$ symmetry. It is customary to break this down into $SU(2)_L \times SU(2)_R \times U(1)_V \times U(1)_A$.[4] This extension of the chiral symmetry across two massless flavors will be centrally important to us when we go to build our Nambu-Jona-Lasinio (NJL) and Quark-Meson (QM) models. Note that although this is hidden in our notation q is also a three-vector in color space.

---

[4] The axial phase symmetry, $U(1)_A$, present in the classical theory is actually spontaneously broken in the QCD in a mechanism driven by instantons [35, 36]. For our purposes we ignore, for simplicity, this caveat, however it is noted that in both the NJL and QM models one can simply augment the Lagrangians given by a term violating this symmetry.

At low temperatures this chiral symmetry is broken by the condensation of q-$\bar{q}$ pairs into the *chiral condensate*, $\langle \bar{q}q \rangle$. The chiral condensate then serves as an order parameter for chiral symmetry. Thus, in the ground state the symmetry is reduced with $SU(2)_L \times SU(2)_R \rightarrow SU(2)_V$. At some sufficiently high temperature, T_c, the thermal energy will melt the chiral condensate and our chiral symmetry will be restored. This dynamic will be seen time and time again in the papers in Part 2 for various values of the chemical potential, the external magnetic field, the Yukawa coupling, the cutoff value, the parameter set for the gluonic sector and an external source term.

1.3 Phase diagram of QCD

The phase diagram of QCD is usually given in the temperature (T)-baryon chemical potential (μ_B) plane. Figure 1.2, taken from [37], gives a quantitative overview of this phase diagram. Figure 1.2 also denotes the regions of particular experimental significance. Firstly, we have the heavy ion collisions at the ALICE detector and the Super Proton Synchrotron (SPS) (both at CERN), the Relativistic Heavy Ion Collider (RHIC) in Brookhaven. We refer the reader to Ref. [38] for an introduction to heavy ion collisions. Beyond this, the region of very high temperature was created in the very early universe, and neutron stars have the correct properties such that they may be used for studying the low temperature high density region of the phase diagram. It is noted that observations of the quark-gluon plasma that presumably existed in the early universe are not directly observable, as it would have only existed long before cosmic microwave background was created and obscures our view of earlier times [37].

The phase diagram may be split into three main regions, firstly at low T and μ_B we have the hadronic phase, at sufficiently high temperatures the physics is dominated by a quark-gluon plasma and at high μ_B there exist several possible phases of quark matter. The hadronic phase is characterised by confinement of the quarks, and spontaneously broken chiral symmetry. The region is bounded by the ‘QCD transition’, where both chiral symmetry is restored and matter becomes deconfined. Above this transition temperature we have a region dominated by the quark-gluon plasma, which is believed

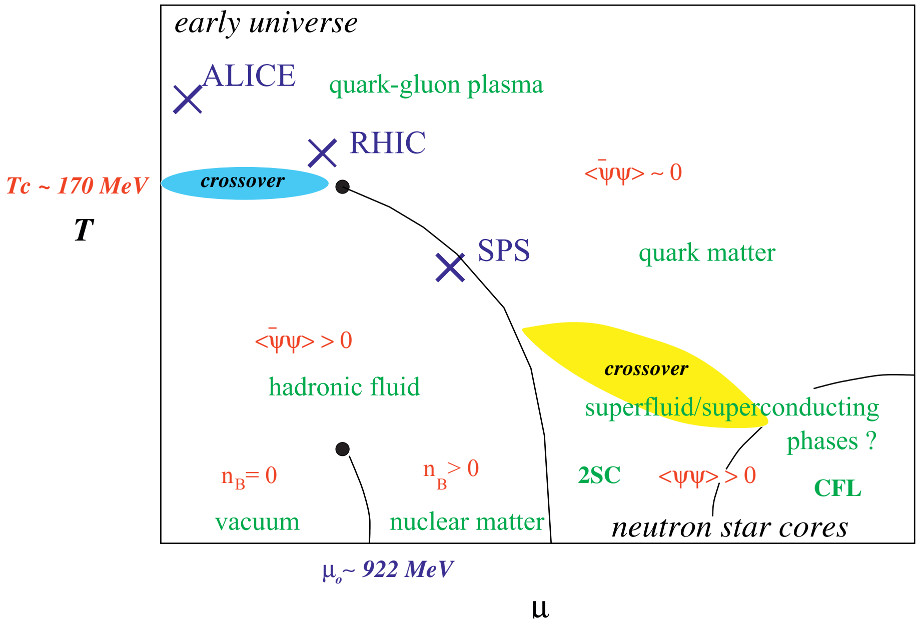
early universe
ALICE
quark-gluon plasma
RHIC
Tc ~ 170 MeV
crossover
T
$\langle\bar{\psi}\psi\rangle \sim 0$
SPS
quark matter
$\langle\bar{\psi}\psi\rangle > 0$
hadronic fluid
crossover
superfluid/superconducting
phases ?
$n_B = 0$
$n_B > 0$
2SC
$\langle\psi\psi\rangle > 0$
CFL
vacuum
nuclear matter
neutron star cores
$\mu_o \sim 922$ MeV
μ

Figure 1.2: A qualitative representation of the phase diagram of QCD in the T-μ_B plane. Figure taken from [37].

to be exactly what its name suggests. Indirect observation of this state was reported by CERN in 2000 and direct evidence from RHIC in 2005 [39, 40, 41, 42]. At high density there is believed to be found a color-flavor locked (CFL) phase, where quarks form Cooper pairs resulting in color-superconductivity. A number of other possible phases of quark matter have been proposed, see [43] for a review.

The extension of this phase diagram into the plane of magnetic fields was briefly discussed in Sec. 1.1 and we return to this in the next section. For further details see the recent review by Andersen et al. [44].

1.4 Finite magnetic fields

In papers [1] and [2] we focus on QCD in a strong magnetic background. The phase diagram of QCD is experimentally accessible in the high T ($\sim$250 MeV) and low baryon chemical potential through heavy ion collisions, and can be observed at high μ_B and low T through observations of heavy stars, in particular neutron stars and magnetars. However in both heavy ion collisions and magnetars, very strong magnetic fields can arise. Additionally the early universe was subjected to high magnetic fields and thus it's understanding is also aided by such studies.

In heavy ion collisions (which are exactly what their name suggests) if the two nuclei do not collide exactly head on, but rather with some finite impact parameter, b (see Fig. 1.3), then the geometry dictates that a magnetic field will be created. As the particles are ultrarelativistic (in the calculations presented below $\gamma \sim 100$) the ions are Lorentz contracted such that one should imagine two (slightly offset, and electromagnetically charged) crêpes travelling towards one another, as given by the large circles in Fig. 1.3. The motion of the charges is (to me) so like that of a curl operator ($\nabla\times$) it seems evident from Faradays law that we must have $\partial_t \mathbf{B} \neq 0$. The question for us is, is the magnitude of this induced (electromagnetic) magnetic field[5] strong enough to have an effect upon the states of our strongly (chromodynamically) interacting system.

In the appendix of [45] the magnetic field strength is estimated based on the charge density of the nuclei and is shown in Fig. 1.4(a). We see that the field's strength reaches a few m_π^2 ($\sim 10^{18}$ Gauss $\sim 10^{14}$ Tesla) with a centre of mass energy of 200 GeV per nucleon, which is approximately that used in RHIC. This result is in agreement with the calculations of [46] based on the ultrarelativistic quantum molecular dynamics (UrQMD) model (see [47]) shown in Fig. 1.4(b). Here the authors also show that $eB \sim 10^{-1} m_\pi^2$ at the SPS (CERN) collider and $eB \sim 15 m_\pi^2$ at the LHC. Clearly these fields are strong enough to impact the phase diagram of QCD.

The strength of magnetic field within magnetars is somewhat unclear. On the surface field strengths of $\sim 10^{14}$ Gauss are observed [48, 49] and its possible that fields of the same order as that seen in heavy ion collisions are present in the cores of these stars.

1.5 Thesis outline

In Chapter 2 we discuss the two models for QCD that we use, first the QM model and then, more briefly the NJL model. Here we will focus on how the models are constructed and which symmetries from QCD they contain.

---

[5] In this thesis we will simply use 'magnetic field' or similar, as we always refer to electromagnetic fields, and never chromomagnetic fields.

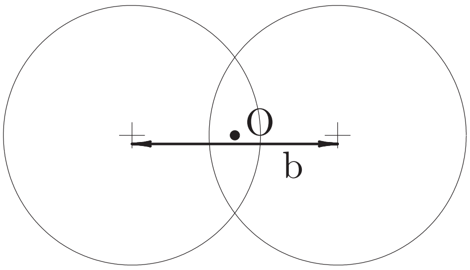

Figure 1.3: Basic geometry of heavy ion collisions. The circles represent the edges of the ions travelling into, and out of, the page. The impact parameter b is denoted along with the centre O of the collision, where magnetic field calculations are typically made.

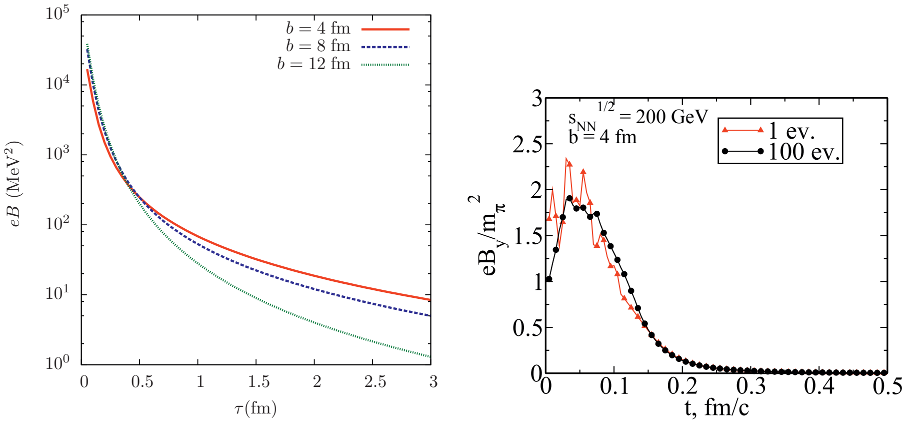

(a) Note that 10^4 MeV^2 corresponds to ∼0.5 m_π^2. Figure taken from Kharzeev et al. [45].

(b) 1 ev. is a single run of the UrQMD model, 100 ev. is the average of 100 runs. Figure taken from Skokov et al. [46].

Figure 1.4: Magnetic field strength at O for a gold-gold (Z=79) collision with a centre of mass energy of 200 GeV from [45] and [46]. The impact factor(s) are given in the plots.

We also introduce the coupling of these models to the external background gauge (from which the Polyakov loop is defined) and magnetic fields.

In Chapter 3 we give the the calculational methods used. Introducing first the basics of statistical thermal field theory, and defining the phase transitions we encouter time and time again in our papers. We introduce the functional renormalization group and give some calculational details. In this chapter we leave out a MF calculation of the QM model, as a very thorough explanation is given in [50].

Finally such that this thesis contributes more than simply fleshing out the theory around the papers presented in Part 2 we include a section on the numerical methods used in paper [1]. A great deal of time was spent during this thesis working through small numerical problems encountered in the calculations, and very little of this information is available in the literature. The hope of this section is that a prospective student can perform such calculations in the future with far greater ease and awareness of the possible potholes.

2 Model approach to QCD

There is a small section on page 340 of Zee's QFT in a nutshell [51] titled 'The Lagrangian as a mnemonic', which I have used a number of times to explain why it is effective theories are such a natural response to solving low temperature (non-perturbative) QCD. In the fifties many physicists felt that field theory was irrelevant for studying QCD and instead derived results general principles and in particular focusing on the symmetry structure of QCD. Then people realised they could take this approach further and encode those symmetries within an effective Lagrangian containing the symmetries they were studying. This comes with the obvious bonus that one can again use the well established machinery of QFT to analyse the Lagrangian.

Here we mostly aim to motivate and illustrate the construction of the Lagrangians of the QM and NJL models. The phase diagram predicted by the QM model is given in [1] and of course in the literature, notably (from our perspective) in [52, 53, 54, 50, 55, 15, 56, 57, 58, 59]. In the case of the (3-color) NJL model see for example [60, 4], and for the 2-color NJL model see [61, 62, 63, 64].

2.1 The quark meson model

To represent the chiral sector of low energy QCD an obvious starting point is a massless Dirac Lagrangian using the quark doublet $q = (u\, d)^T$ as given in Sec. 1.2. To add a mass term, $m\, \bar{q}q$, whilst maintaining our chiral $SU(2)_L \times SU(2)_R$ symmetry we couple all four of our bilinears[1] equally to an $SO(4)$ multiplet of mesonic fields (which in anticipation we will denote $(\sigma, \boldsymbol{\pi})$)

---

[1] The four bilinears are the left- and right-handed bilinears of both the u and d quarks, this is particularly evident in the chiral representation.

and use the fact that $SU(2)_L \times SU(2)_R$ is locally isomorphic to $SO(4)$ to maintain our chiral symmetry. The exact form of the coupling is $\bar{q}(\sigma + i\gamma^5 \boldsymbol{\tau} \cdot \boldsymbol{\pi})q$, which is called a Yukawa coupling. Our full Lagrangian will thus be

$$\mathcal{L}_{\mathrm{QM}} = \bar{q}\left(i\gamma^\mu \partial_\mu + g(\sigma + i\gamma^5 \boldsymbol{\tau} \cdot \boldsymbol{\pi})\right) q + \mathcal{L}(\sigma, \boldsymbol{\pi})\,, \tag{2.1}$$

where $\boldsymbol{\tau}$ are the Pauli matrices acting in isospin space and $\mathcal{L}(\sigma, \boldsymbol{\pi})$ must be $SO(4)$ symmetric. To give the quarks a spontaneously generated mass we simply employ the linear sigma model;

$$\mathcal{L}(\sigma, \boldsymbol{\pi}) = \frac{1}{2}\left((\partial\sigma)^2 + (\partial\boldsymbol{\pi})^2\right) + \frac{m^2}{2}(\sigma^2 + \boldsymbol{\pi}^2) - \frac{\lambda}{4}(\sigma^2 + \boldsymbol{\pi}^2)^2 - h\sigma\,, \tag{2.2}$$

which has built in spontaneous symmetry breaking (assuming m and λ are positive). Thus in the vacuum we may choose $\langle \boldsymbol{\pi} \rangle = 0$ and $\langle \sigma \rangle > 0$. We have added the term $-h\sigma$, which we ignore for now, but will return to later. Additionally we have introduced four couplings, g, m, h and λ, which we must fix to observables.[2]

If we look at the coupling introduced between the u and d quarks via mesonic fields (and as the nomenclature already suggests) the 4-vector of mesons represents the sigma meson[3] and the three pions. In the case of the pions the physically relevant degrees of freedom are $\pi^0 = \pi_3$ and $\pi^\pm = (\pi_1 \pm i\pi_2)/\sqrt{2}$.

We may now simply follow the textbook examples of [51] (Chap. VI.4) or [29] (Chap. 11.1) for spontaneous symmetry breaking. Using the SO(4) symmetry we expand out fields around a non-zero minimum, $v = \sqrt{m^2/\lambda}$, of the mesonic potential in the σ direction. We thus make our sigma field massive, and the pion fields become Goldstone bosons. Breaking this symmetry breaks the chiral symmetry of the model and thus our original $SU(2)_L \times SU(2)_R \times U(1)_V \times U(1)_A$ is broken down to $SU(2)_V \times U(1)_V \times U(1)_A$. Here the subscript V stands for vector, but it could also be interpreted as the symmetry group for isospin. Note that when we expand our fields around v we generate a quark mass term which is symmetric in the u and d flavors: $gv\,\bar{q}q$.

Currently our pions must be massless as they are Goldstone bosons, however in reality they have masses of approximate 140 MeV. Such that our model can reproduce these we have added the explicit chiral symmetry breaking term $-h\sigma$. In practice this gives us a parameter with we may tune the pion mass, however this must be treated with some care in the RG approach, as noted in Sec. 3.4.

---

[2] In addition we will later introduce a renormalization scale. The procedure of parameter fixing is well described in the literature and the papers in the second Part of this thesis. See [50] for an example in a mean field calculation and [1] using the functional renormalization group.

[3] The σ meson is a very broad resonance, with the particle data group giving its mass in the range 400-550 MeV [65]. In [66] the mass range is constricted to 400 ± 6 MeV.

In paper [1] we plot the phase diagram given by the QM model at finite B and μ_B and including the Polyakov loop using a numerical solution to the RG equations (see Sec. 3.4). In paper [2] we again explore the phase diagram of the QM model using mean field methods. In this paper we mainly focus on the effects of varying the Yukawa coupling parameter, g.

2.1.1 Chemical potential

For any conserved charge within a system we may add a chemical potential. In Papers [1] and [3] we add a baryon number potential, μ_B, corresponding to the conserved baryon number, although for simplicity we tend to use the quark chemical potential (which we refer to simply as the chemical potential, μ, with $3\mu = \mu_B$). The number density for quarks is $\bar{\psi}\gamma^0\psi$, thus in both the QM and the NJL models we simply supplement the Lagrangian (Eqs. (2.1) and (2.3) respectively) by the term $\mu\,\bar{q}\gamma^0 q$.

2.2 The Nambu Jona-Lasinio model

A standard textbook introduction to QCD (for example [51]) starts with a Dirac Lagrangian and promotes the global $U(1)$ symmetry to a *local* $U(1)$ gauge symmetry and in doing so couples to the gluons. In the NJL model we demote this global symmetry back to a local one, and integrate out the gauge fields.[4] When removing the gauge fields we replace single gluon exchange with a four fermion interaction term with a phenomenological (and dimensionful) coupling parameter, G, as indicated in Fig. 2.1. To maintain chiral symmetry this interaction will be introduced as above, coupling all four bilinears equally, and thus the simplest chirally symmetric Lagrangian for a two-flavour NJL model (although adding a quark mass term m_0, which breaks chiral symmetry) is

$$\mathcal{L}_{\text{NJL}} = \bar{q}\left(i\gamma^\mu\partial_\mu - m_0\right)q + G\left[(\bar{q}q)^2 + (\bar{q}i\gamma^5\boldsymbol{\tau}q)^2\right]. \tag{2.3}$$

---

[4] This is not how the model was initially created. It was first introduce by Yoichiro Nambu and Giovanni Jona-Lasinio in 1961 [67, 68] as a model for nucleons (not quarks). Hence the model includes chiral symmetry, but completely ignores confinement.

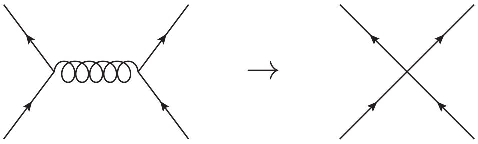

Figure 2.1: Integrating out the gluons from QCD the NJL model replaces single gluon exchange for a chirally symmetric four-fermion interaction.

Often the interaction term is expanded to include addition scalar and pseudoscalar interactions. In addition one may arrange these terms so as to explicitly break the $U(1)_A$ symmetry that is found in Eq. (2.3) (but not in the vacuum of QCD due to a quantum anomaly related to instantons [35, 69]). For an in depth article see [4], and see [44] for an overview at finite B. In the case of 2cQCD paper [3] gives an overview of the possible operators and a expands on the standard NJL formalism, particularly in breaking the chiral symmetry of the interaction term with

$$G\left[(\bar{q}q)^2 + (\bar{q}i\gamma^5\boldsymbol{\tau}q)^2\right] \to G(\bar{q}q)^2 + \lambda G(\bar{q}i\gamma^5\boldsymbol{\tau}q)^2\,, \tag{2.4}$$

where λ is a new (dimensionless) parameter. Results from the NJL model at finite B in 2cQCD are presented in [70].

2.2.1 Mean field approximation

In papers [2, 3] we employ the mean field approximation. By this we mean the one-loop effective potential where we treat the mesonic fields at tree level, or equally, work in the large N_c limit (but still use $N_c = 3$ or 2 as appropriate in our final expressions).

In the QM model the Lagrangian, Eq. (2.1), is already bilinear in the fermionic fields, so we may simply integrate over these. However the NJL model, as we have given it in Eq. (2.3), contains terms with higher powers of the fermionic fields. Thus, to examine the low energy degrees of freedom we first make a Hubbard-Stratonovich transformation from the quark degrees of freedom to collective (mesonic) degrees of freedom. This is done by introducing a set of auxiliary fields, in the case of the simple Lagrangian above, have have only σ- and π_i-type degrees of freedom and thus we introduce the fields $\sigma = -2G\,\bar{q}q$ and $\pi_i = -2G\,\bar{q}i\gamma^5\tau_i q$. One then adds to the Lagrangian a term of the form $\delta\mathcal{L} = -(\xi + 2Gf(\bar{q},q))^2/4G$, where ξ stands for the particular auxiliary field and $f(\bar{q},q)$ is chosen such that $\delta\mathcal{L} = 0$. In the example of σ we have $\delta\mathcal{L} = -(\sigma + 2G\bar{q}q)^2/4G$. After making this transform the Lagrangian then takes the form

$$\mathcal{L}_{\text{NJL}} = \bar{q}\left(i\gamma^\mu\partial_\mu - m_0 - \sigma - i\gamma^5\boldsymbol{\tau}\cdot\boldsymbol{\pi}\right)q - \frac{1}{4G}\left(\sigma^2 + \boldsymbol{\pi}^2\right) . \tag{2.5}$$

We are now able to exactly integrate out the (bilinear) fermionic fields and can deal simply with the mesonic fields (when working at mean field level).

2.3 Finite B

We raised two problems in the introduction that we wanted to address but are currently not included in our models, deconfinement and an external magnetic field. Here we introduce the basic mechanism for coupling to a magnetic field.

We examine the spectrum of a bosonic degree of freedom in a magnetic background. Considering only a classical constant background magnetic field with strength B aligned along the $\hat{z}$ direction. In Sec. 2 of [44] an equivalent derivation is given for fermions. The Lagrangian for our complex bosonic field is

$$\mathcal{L}_{\text{KG}} = \frac{1}{2}(D_\mu\phi)^* D^\mu\phi - \frac{1}{2}m^2\phi^*\phi\,, \tag{2.6}$$

where $D_\mu = \partial_\mu + ieA^{\text{EM}}_\mu$. We have some gauge freedom in our choice of A^{EM}_μ, and choose $A^{\text{EM}}_\mu = (0, 0, Bx_1, 0)$. The resulting equation of motion is

$$\begin{aligned} 0 &= \left(D_\mu D^\mu + m^2\right)\phi & (2.7)\\ &= \left(\partial_0^2 - \partial_1^2 - (\partial_2 - ieBx_1)^2 - \partial_3^2 + m^2\right)\phi\,, & (2.8)\end{aligned}$$

and we will have a similar equation for the field ϕ^*. Recalling the solution of the Klein Gordon equation, we suppose that ϕ takes the form $\phi = e^{i(p_0x_0 - p_2x_2 - p_3x_3)}f(x_1)$, which gives,

$$\left(-\partial_1^2 + (\partial_2 - eBx_1)^2\right)\phi = \left(E^2 - p_3^2 - m^2\right)\phi\,, \tag{2.9}$$

with $E = p_0$ and where we have been anticipating the physical meaning of the variables in our notation. Equation (2.9) is that of a harmonic oscillator, and the solutions are the Hermite polynomials, although we will not be primarily concerned with the exact space-time dependence of the wave function. Of greater import is that the energy spectrum is

$$E_n^2 = m^2 + p_3^2 + |eB|(2\ell + 1) \qquad \text{(bosons)}\,, \tag{2.10}$$

$$E_n^2 = m^2 + p_3^2 + |eB|(2\ell + 1 - s) \qquad \text{(fermions)}\,, \tag{2.11}$$

where we have given the result for fermions in addition, with s is the spin of the fermion and $\ell \in \mathbb{N}_0$ labels the energy of the associated Hermite polynomial. Note that we have gone (in spatial dimensions) from three continuous energy spectra, to a single one (along the x_3 axis) and a discrete variable, ℓ. ℓ labels the Landau levels of the system, which denotes the energy associated with the 'orbit' of the system.

The result of this is that we must make the substitutions

$$\mathbf{p} \to p_z + (2\ell + 1 - s)|eB|\,, \qquad \int \frac{\mathrm{d}^3 p}{(2\pi)^3} \to \frac{|eB|}{2\pi} \sum_{\ell=0}^{\infty} \int \frac{\mathrm{d}p_z}{2\pi}\,, \tag{2.12}$$

(but with $s = 0$ in the case of bosons) in our equations after transforming to momentum space. The RG implementation of this is given in [1], and a detailed version of the calculation is given in App. A of [15]. Note that in the case the momentum substitution is done both in the derivatives of the effective action and in the regulator. The mean field implementation is given in [2].

2.4 Polyakov loop

It is apparent that the models we are using do not contain gluons, and hence do not contain the mechanism for deconfinement as it stands in QCD. Additionally, at low temperatures the degrees of freedom in our two models include deconfined quarks, although we know that confinement means that the pions should dominate the physics. Thus following Fukushima [31] we add a constant temporal background gauge field, which as we will see suppresses the low temperature quarkyonic degrees of freedom. In addition the Polyakov loop, defined in terms of this background field, gives us an approximate order parameter for deconfinement.

The Polyakov loop, Φ, is a traced Wilson loop around the periodic Euclidean time direction [71, 72]. The thermal Wilson line, L, is

$$L(\mathbf{x}) = \mathcal{P}\exp\left[i \int_0^\beta d\tau A_4(\mathbf{x}, \tau) \right]\,, \tag{2.13}$$

where $\mathcal{P}$ is path ordering and $A_4 = it_a A_0^a$. Φ (and its conjugate, $\bar{\Phi}$ [5]) is given in terms of L as

$$\Phi = \frac{1}{N_c}\langle \mathrm{Tr}_c L(\mathbf{x})\rangle \,, \qquad \bar{\Phi} = \frac{1}{N_c}\langle \mathrm{Tr}_c L^\dagger(\mathbf{x})\rangle \,, \tag{2.14}$$

where the trace is in color space. The free energy of a static quark is related to the expectation value of the Polyakov loop via $\langle\Phi\rangle = e^{-\beta F}$ [73]. In QCD with static quarks adding a single test quark to the confined matter phase costs an infinite amount of energy, i.e. it is impossible and we have $\langle\Phi\rangle = 0$. Thus the Polyakov loop forms an order parameter for deconfinement. It should be noted though, that this order parameter behaves in the opposite manner to most other order parameters in that it is zero in the low temperature (confined) state, and becomes non-zero at high temperature. In true QCD this is only approximately true, as a (dynamical) quark can couple to a (dynamical) antiquark and hence the energy cost is not infinite, and as such the Polyakov loop only serves as an approximate order parameter for deconfinement.

As stated the Polyakov loop is introduced by coupling to a constant temporal background gauge field. Thus we replace the derivative operator acting on the quarks as $\partial_\mu \to \partial_\mu - i\delta_{\mu 0} t_a A_0^a$, where in the Polyakov gauge $t_a A_0^a$ can be written diagonally as $t_3 A_0^3 + t_8 A_0^8$. The Fermi-Dirac distribution function is generalised to (see Sec. VI of [44])

$$n_F^+(\Phi,\bar{\Phi};T,\mu) = \frac{1 + 2\bar{\Phi}e^{\beta(E-\mu)} + \Phi e^{2\beta(E-\mu)}}{1 + 3\bar{\Phi}e^{\beta(E-\mu)} + 3\Phi e^{2\beta(E-\mu)} + e^{3\beta(E-\mu)}}\,, \tag{2.15}$$

$$n_F^-(\Phi,\bar{\Phi};T,\mu) = n_F^+(\bar{\Phi},\Phi;T,-\mu)\,, \tag{2.16}$$

which in the confined and deconfined limits becomes

$$n_F^+(\Phi,\bar{\Phi};T,\mu) = \frac{1}{1+e^{3\beta(E-\mu)}} \qquad (\Phi \;\&\; \bar{\Phi} \to 0)\,, \tag{2.17}$$

$$n_F^+(\Phi,\bar{\Phi};T,\mu) = \frac{1}{1+e^{\beta(E-\mu)}} \qquad (\Phi \;\&\; \bar{\Phi} \to 1)\,. \tag{2.18}$$

showing, as mentioned in [1] the suppression of the quarkyonic degrees of freedom in the confined phase.

When adding the Polyakov loop one must also add a potential for the pure gauge sector, which we do in all papers presented in Part 2. In paper [1] we give three such options and present results with all three potentials, as well as varying the parameter $\hat{\gamma}$, which controls the μ_B dependence of the transition temperature of the gauge potential. In paper [2] we investigate the dependence of the chiral transition on the parameter T_0. See the papers for the specific form of them implementation.

---

[5] L is in general a complex operator, thus we have two independent operators for the Polyakov loop, however both in 2cQCD and with $\mu_B = 0$ $L \in \mathbb{R}$ and thus $\Phi = \bar{\Phi}$.

3 Theoretical Formalism

In the papers that are presented below much of the formalism behind the calculations is left out. This tower of theoretical knowledge is built up from the foundations of mechanics, both quantum and classical, through field theory and thermodynamics and finally with the formalism of equilibrium thermal field theory. In this section we present for reference the relevant results from thermodynamics and thermal field theory (and an interesting phase transition found in the work for paper [1]). We also present the ideas behind the functional renormalization group and some interesting points that arise in the calculation of the flow equation of the effective potential. Finally we outline the renormalization schemes used, which are of particular import to paper [2].

3.1 Thermodynamic relations

The expectation values of the chiral and deconfinement order parameters, σ and Φ, can be found by minimising the grand canonical potential,

$$\Phi_G = -T \log Z \,, \tag{3.1}$$

with respect to these variables. Φ_G is an extensive quantity (it doubles with a doubling of volume) and the action is calculating over an infinite volume in space, thus we work with the grand potential's density:

$$\Omega = \frac{\Phi_G}{V} = \frac{1}{\beta V} \log Z \tag{3.2}$$

In addition to allowing the determination of the chiral transition temperature and the deconfinement transition temperature we may also define the pressure, P, entropy, S, particle number densities, N_i, and the energy density $\mathcal{E}$ from Ω as

$$P = -\Omega\,, \qquad\qquad S = -\frac{\partial\Omega}{\partial T}\,, \tag{3.3}$$

$$N_i = -\frac{\partial\Omega}{\partial\mu_i}\,, \qquad\qquad \mathcal{E} = \Omega + TS + \mu_i N_i\,. \tag{3.4}$$

We have kept the particle number densities and chemical potentials general as we may have multiple chemical potentials. With two quark flavors with equal mass we may may include an isospin chemical potential, μ_I, as well as a baryon chemical potential, but we set $\mu_I = 0$ and only allow non-zero μ_B.

3.2 Phase transitions

Studying the pressure or number density of a specific state of matter will in many cases be beyond our aims, instead we mostly focus on finding the location of the phase transitions. Usually this means finding the temperature at which chiral symmetry is restored, T_c, or matter becomes deconfined, T_d, for any given quark chemical potential or external magnetic field. The textbook method (which works more or less in the case of chiral symmetry) goes as follows. One identifies an appropriate order parameter, O, which will be zero in the symmetric phase, and non-zero in the phase with broken symmetry. One can then classify the phase transition by the way in which the order parameter goes to zero.

A phase transition is *first order* where there is a discontinuous jump in O from a finite value to zero. A *second order* phase transition goes is an unbroken path from a finite value to zero but with a discontinuity in the first derivative of the order parameter. These 'exact' phase transitions (where the order parameter goes to zero) occur when an exact symmetry of the Lagrangian is broken/restored. For example in Sec. 5 of paper [3] we see the breaking of $U(1)_V = U(1)_B$ with increasing μ_B and the eventual formation of a finite diquark condensate. In Fig. 3.1 we gives examples of the behaviour of the order parameter for various transition types. Figs. 3.1(a) and 3.1(b) give 'exact' first and second order transitions respectively.

When the symmetry being restored is only approximate, as is the case of chiral symmetry in QCD (and our models) with non-zero quark masses, the phase transition also becomes approximate, with the order parameter transitioning to a low, but non-zero value. In these cases the critical temperature is often called the pseudo-critical temperature, although we will refrain from this excess. The definition of the critical temperature for an approximate first order phase transition is clear, it is the point at which we see a discontinuity in the order parameter, as is shown in Fig. 3.1(c). The definition of the critical temperature of a second order approximate phase transition is a little more ambiguous, as the the order parameter smoothly transitions from a high to low value. We will see in Sec. 4.2 that this was numerically a difficult point to deal with. The generally accepted standard definition of the critical temperature is the inflection point, where $\partial^2 O/\partial T^2 = 0$, however it is often more convenient or precise to define the phase transition where the order parameter is at a half of it's zero temperature value. This is shown in Fig 3.1(d).

Finally, as an interesting example originally observed in [74] (see specifically Figs. 1 and 2 of that paper), and also in our work towards [1], there develops a bifurcation in the chiral phase transition at very low T (below ~ 20 MeV). This occurs in the chirally symmetric quark meson model, evaluated with the functional renormalization group (see Sec. 3.4), where the first order phase transition bifurcates to an approximate first order transition at slightly lower chemical potential and a second order transition at slightly higher μ_B. The behaviour of the order parameter σ, the chiral order parameter, is shown in Fig. 3.2. The reason for this, and if it is of any physical significance is unclear, although presumably it is completely washed out in QCD, where the quarks have non-zero bare mass.

3.3 Thermal field theory

We see from Eq. (3.2) that the partition function is centrally important. Recalling our favourite book on thermal physics (for example [75]) we remember that the partition function is simply the sum over all Boltzmann factors, thus

$$Z = \sum_{\text{all states}} e^{-E(\text{state})/k_B T} = \mathrm{Tr}\, e^{-\beta H} = \int \mathrm{d}\phi \, \langle \phi | \, e^{-\beta H} \, | \phi \rangle \ , \tag{3.5}$$

where k_B is the Boltzmann constant, H is the Hamiltonian and ϕ is a component in a complete set of continuous states. Using the essential result of path

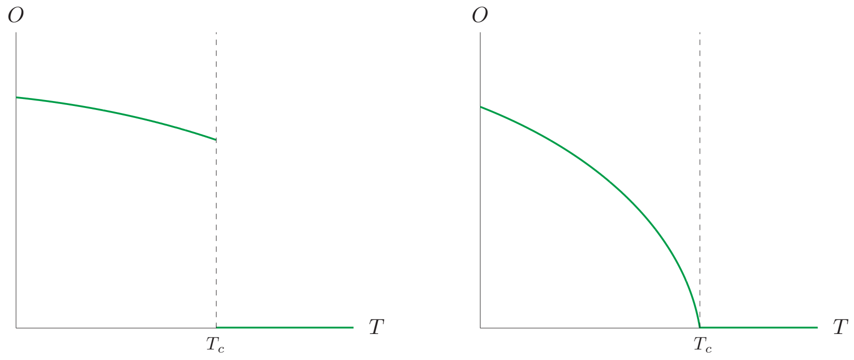

(a) Exact first order transition.

(b) Exact second order transition.

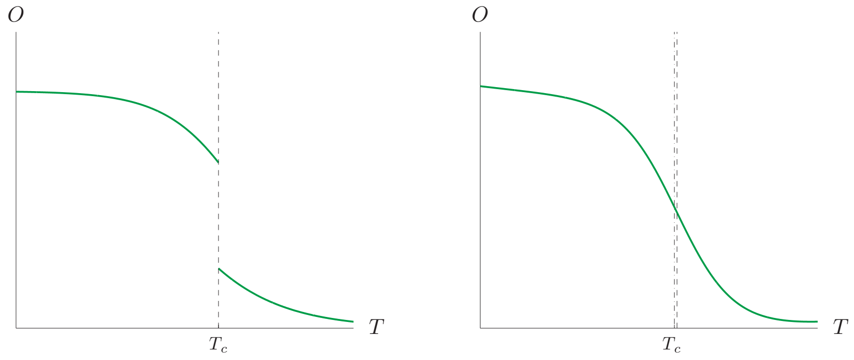

(c) First order transition restoring an approximate symmetry.

(d) Second order transition restoring an approximate symmetry.

Figure 3.1: Example curves for four different types of phase transitions. In (d) we show two transition temperatures, that at lower temperature (dashed-dotted) relates to the point at which $O(T) = O(0)/2$, while the higher temperature (dashed) line corresponds to the inflection point.

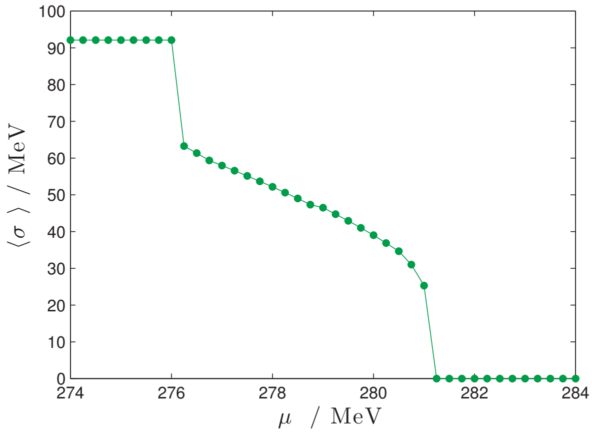

Figure 3.2: Chiral order parameter, $\langle\sigma\rangle$, at a function of μ at $T = 10$ MeV. We see an approximate first order transition at $\mu \approx 276$ MeV and a second order transition at $\mu \approx 281$ MeV.

integral formulation of quantum field theory (QFT) (see for example [51]),

$$\langle\phi_F|\, e^{-itH}\, |\phi_I\rangle = \int_{\phi_I,0}^{\phi_F,t} \mathcal{D}\phi\; e^{iS[\phi]} \,, \tag{3.6}$$

we see the partition function is a sum over closed ($x_I = x_F = x$) path integrals. In the formalism of thermal field theory this is made exact, and as a first step we rotate our time dimension to imaginary time, $t \to -i\tau$ and integrate from 0 to β. When all of the i's have been cancelled, and interpreting ϕ as a scalar field, we are left with

$$Z = \int_{\phi(\mathbf{x},0)=\phi(\mathbf{x},\beta)} \mathcal{D}\phi\; e^{-S_E[\phi]} \,, \tag{3.7}$$

where we integrate over all fields that satisfy $\phi(\mathbf{x},0) = \phi(\mathbf{x},\beta)$, that is all fields with period β/n (with $n \in \mathbb{N}_+$) in imaginary time. Due to the anticommutivity of fermionic fields (see Sec. 2.5 of [76]) the fermionic version of Eq. (3.7) is

$$Z = \int_{\psi(\mathbf{x},0)=-\psi(\mathbf{x},\beta)} \mathcal{D}\bar{\psi}\mathcal{D}\psi\; e^{-S_E[\bar{\psi},\psi]} \,, \tag{3.8}$$

with the sum now over anti-periodic fields. In both Eqs. (3.7) and (3.8)

$$S_E = \int_0^\beta \mathrm{d}\tau \int \mathrm{d}^3x\; \mathcal{L}_E \,, \tag{3.9}$$

with

$$\mathcal{L}_E = -\mathcal{L}(t \to -i\tau)\,. \tag{3.10}$$

In real space we see that we have an temporal integral over periodic boundary conditions. Once we have Fourier transformed to momentum space this will result in a sum over an infinite set of discretely spaced frequencies, the Matsubara frequencies, ω_n for bosons we have $\omega_n = 2n\pi T$ and for fermions $\omega_n = (2n+1)\pi T$.

We now turn to the evaluation of the grand potential for free fermions. This serves both as demonstrational for the most essential analytic tools we have at our disposal: Fourier transforms, Matsubara sums and Gaussian integration. This will also elucidate the basis of the mean field approximation calculations given in papers [2] and [3]. In these papers we end up with a Lagrangian bilinear in the fermionic fields and with a number of higher order terms for the mesonic/bosonic fields. As stated in Sec. 2.2.1, the mean field approximation the fluctuations of these bosonic fields are ignored and hence the results parallel the simplest case we present here.

We begin by Fourier transforming to momentum space using the relation

$$\psi(\tau, \mathbf{x}) = \frac{1}{\sqrt{\beta V}} \sum_n \int \frac{\mathrm{d}^3 p}{(2\pi)^3} \psi_n(\mathbf{p}) e^{i(\omega_n \tau + \mathbf{p}\cdot\mathbf{x})}\,, \tag{3.11}$$

thus the action is

$$S_E = \sum\!\!\!\!\!\!\int_{\mathbf{p}} \bar{\psi}_n(\mathbf{p})\; G^{-1}_{n,\mathbf{p}}\; \psi_n(\mathbf{p})\,. \tag{3.12}$$

where we have defined both

$$\sum\!\!\!\!\!\!\int_{\mathbf{p}} \equiv \sum_{n=\infty}^{\infty} \int \frac{\mathrm{d}^3 p}{(2\pi)^3}\,, \tag{3.13}$$

$$G^{-1}_{n,\mathbf{p}} \equiv i\gamma^0 \omega_n + \boldsymbol{\gamma}\cdot\mathbf{p} + m\,. \tag{3.14}$$

Substituting Eq. (3.12) into Eq. (3.8) we find for partition function,

$$Z = \int \mathcal{D}\bar{\psi}\mathcal{D}\psi\, \exp\left\{ -\sum\!\!\!\!\!\!\int_{\mathbf{p}} \bar{\psi}_n(\mathbf{p})\; G^{-1}_{n,\mathbf{p}}\; \psi_n(\mathbf{p}) \right\}\,. \tag{3.15}$$

This is simply a Gaussian integral and has solution $Z = \exp\{\mathrm{Tr}\,\ln G^{-1}_{n,\mathbf{p}}\}$.

Utilising relation 3.2 for Ω and that Tr ln $M =$ ln det M we have

$$\begin{aligned}
\Omega &= -T \sum\!\!\!\!\!\!\!\int_{\mathbf{p}} \ln \det G^{-1}_{n,\mathbf{p}} \\
&= -2T \sum\!\!\!\!\!\!\!\int_{\mathbf{p}} \ln \left[\omega_n^2 + \mathbf{p}^2 + m^2\right] \\
&= -4 \int \frac{\mathrm{d}^3 p}{(2\pi)^3} \left(\frac{1}{2} E_{\mathbf{p}} + T \ln\Big(1 + e^{-\beta E_{\mathbf{p}}}\Big) \right) \,, \qquad (3.16)
\end{aligned}$$

where in the first step we have simply evaluated the determinant in Dirac space and in the final line we have defined $E_{\mathbf{p}} \equiv \mathbf{p}^2 + m^2$ and explicitly evaluated the Matsubara sum as follows. We often obtain a sum of the form

$$X = \frac{1}{2} T \sum_{n=\infty}^{\infty} \ln(\omega_n^2 + a^2) \qquad (3.17)$$

which can be evaluated using complex contour integration, see Sec. 2.3.3 of [77], or [78], to give

$$\begin{aligned}
X &= \frac{1}{2} a + T \ln\big[1 - e^{-\beta a}\big] \qquad && (\text{bosons, } \omega_n = 2n\pi T) \,, \\
X &= \frac{1}{2} a + T \ln\big[1 + e^{-\beta a}\big] \qquad && (\text{fermions, } \omega_n = (2n+1)\pi T) \,.
\end{aligned}$$

3.4 Functional renormalization group

I find the ideas behind renormalization group flows particularly attractive. The Lagrangian details the physics present at the smallest length scale of the theory we are examining. The problem is reading off the physics over large length scales, where interactions may change the relevant degrees of freedom or symmetries and where the detailed properties of the system are not straightforwardly given.

We begin with the flow equation introduced by Wetterich [79] (for more general and pedagogical articles see [80, 81]) for the effective potential:

$$\partial_k \Gamma_k[\phi, \psi] = \frac{1}{2} \mathrm{Tr} \left[\frac{\partial_k R_{kB}}{\Gamma_k^{(2,0)} + R_{kB}} \right] - \mathrm{Tr} \left[\frac{\partial_k R_{kF}}{\Gamma_k^{(0.2)} + R_{kF}} \right] \,. \qquad (3.18)$$

$\Gamma_k^{(a,b)}[\phi, \psi]$ represents the ath functional derivative with respect to the mesonic fields and the bth with respect to the fermionic fields and k is the current energy scale in the RG flow. $R_{kB(F)}$ is the bosonic (fermionic) regulator function, which we will introduce shortly. The basic idea of the equation is as follows: At some suitably high energy scale, $k = \Lambda_{\mathrm{RG}}$, the physics is simply that given by the classical action, i.e. the tree level potential[1] (up to a factor $V\beta$). If we then imagine zooming out (lowering the energy scale) one 'step' and re-writing our action in terms of new effective masses and interactions. Then zooming out again, and repeating the process, and so on. Imagining now these steps as infinitesimal we have a 'flow' of the effective potential, with the high energy boundary condition being the tree level potential. When we reach $k = 0$ then the effective potential will be equal to the full quantum action. Equation (3.18) encodes (exactly) this flow from the classical to the quantum action.

The regulator functions, $R_{kB(F)}(p)$, control the flow equation. For the bosonic term in Eq. (3.18) we use the form[2]

$$R_{kB}(p) = (k^2 - \mathbf{p}^2)\,\theta(k^2 - \mathbf{p}^2)\,, \tag{3.20}$$

where $\theta(x)$ is the Heaviside step function. The cutoff ensures that modes far below the energy scale of the cutoff are heavy and decouple, whilst modes below but close to the cutoff are included in the flow. For modes above the cutoff ($\mathbf{p}^2 > k^2$), using this particular form of the regulator, the numerator of Eq. (3.18) ensures that those modes are not included.

In practice one cannot find an exact form of the flow equation for the QM model and approximations must be made. In paper [1] we use a truncated derivative expansion for the effective action in the local-potential approximation (where all of the terms in the expansion are left independent of the energy scale other than the effective potential for the mesonic fields and the Yukawa coupling). We then further approximate by ignoring the running of the Yukawa coupling. In addition we ignore any running of the Polyakov loop, and treat this as an independent classical background field as in the mean field case. We thus start with the following effective potential for the

---

[1] One has to be slightly careful in calculating absolute quantities, for example pressures, to include additive effects coming from the energies above Λ_{RG}. In Paper [1] we investigate the expectation values of the condensates, hence avoiding these problems.

[2] For fermions we use

$$R_{kF}(p) = \left(\sqrt{\frac{(p_0+i\mu)^2+k^2}{(p_0+i\mu)^2+\mathbf{p}^2}} - 1\right)(\gamma^\mu p_\mu + i\mu\gamma^0)\,\theta(k^2-\mathbf{p}^2)\,, \tag{3.19}$$

which incorporates the same properties as the bosonic regulator, whilst also simplifying the calculation of the flow equation.

$U(4)$ symmetric mesonic field $\rho = \phi^2/2 = (\sigma^2 + \boldsymbol{\pi}^2)/2$

$$\Gamma_k[\rho] = \int_0^\beta \mathrm{d}\tau \int \mathrm{d}^3x \left[\frac{1}{2}\left((\partial_\mu\sigma)^2 + (\partial_\mu\boldsymbol{\pi})^2\right) + U_k(\rho)\right. \tag{3.21}$$

$$\left. + \bar{q}\gamma_\mu D^\mu q + g\bar{q}(\sigma + i\gamma_5\boldsymbol{\tau}\cdot\boldsymbol{\pi})q\right], \tag{3.22}$$

where D^μ is the covariant derivative which couples to both the magnetic and gauge background fields as given in Secs. 2.3 and 2.4. As the effective potential we calculate is explicitly $U(4)$ symmetric the explicit symmetry breaking term ($h\sigma$) used to give the pions mass is dropped from the calculation initially (this amounts to not including it in the tree level potential), and instead adding it as a condition on the minimisation of effective potential when finding $\langle\sigma\rangle$ (see Chap. 4 for details). The derivation of the flow equation follows that of App. A of [15], other than the replacement of the Fermi-Dirac distribution function to their Polyakov loop extensions given in Eqs. (2.15) and (2.16).[3]

Finally we must add the gluonic potential, but as stated this not treated as scale dependent and thus may simply be added to the final result for $U_{k=0}(\rho)$ before calculation the expectation values of σ, Φ and $\bar{\Phi}$.

3.5 Renormalization

In paper [2] we compare the results of the QM model using dimensional regularization (commonly used in mean field model calculations) and a sharp cutoff (which we used in the RG calculations in paper [1]). Here we supplement the treatment in that paper of these two methods.

In Eq. (3.16) we have the divergent integral of the form $\int \mathrm{d}^3p\, \sqrt{\mathbf{p}^2 + m^2}$,[4] which remains in essence in the calculations in Part 2. A straightforward method for regulating the integral is to simply add a UV three-momentum cutoff, Λ_{UV}, integrating from zero momentum up to the energy scale Λ_{UV}

---

[3] Note also in the derivation in Eq. A.6 the second term is missing a factor -2, in Eq. A.9 the term '$+U_k''$' should read '$+2\rho U_k''$' and Eq. A.14 is missing a plus sign in the middle of the second line.

[4] Recall that we arrived at this form from a single free fermion with mass parameter m. We are also ignoring a factor coming from a sum over the spin states, and are in a medium with $T = B = 0$.

and ignoring anything above that. In this case the above integral,

$$\int \frac{\mathrm{d}^3 p}{(2\pi)^3} \sqrt{\mathbf{p}^2 + m^2} = \frac{1}{2\pi^2} \int_0^\infty \mathrm{d}p \, p^2 \sqrt{p^2 + m^2} \,, \tag{3.23}$$

becomes

$$\begin{aligned} \frac{1}{2\pi^2} \int_0^{\Lambda_{\text{UV}}} \mathrm{d}p \, p^2 \sqrt{p^2 + m^2} = \frac{1}{16\pi^2} \Bigg\{ & \Lambda_{\text{UV}} \sqrt{\Lambda_{\text{UV}}^2 + m^2} \, (2\Lambda_{\text{UV}}^2 + m^2) \\ & - m^4 \ln \left[\frac{\Lambda_{\text{UV}} + \sqrt{\Lambda_{\text{UV}}^2 + m^2}}{m} \right] \Bigg\} . \end{aligned} \tag{3.24}$$

This somewhat crude scheme is far more useful than it might seem, as if all of the relevant physics occurs below this scale this will approximately amount to subtracting a (infinite) constant from the potential. However we must be clear that in doing this we are quite explicitly redefining our theory with Λ_{UV} as a parameter in the new theory, which other quantities (masses, couplings) will depend upon, although hopefully only weakly.

In dimensional regularisation ([82, 83] or see [84] for a more pedagogical article) we instead allow dimension of integration to vary, and then use this to find the form of the renormalization terms required to render the integral finite. We use the modified minimal subtraction scheme ($\overline{\text{MS}}$) where,

$$\int \frac{\mathrm{d}^3 p}{(2\pi)^3} \to \left(\frac{e^{\gamma_E} \Lambda_{\text{DR}}^2}{4\pi} \right)^\epsilon \int \frac{\mathrm{d}^d p}{(2\pi)^d} \,, \tag{3.25}$$

with $d = 3 - 2\epsilon$ and $e^{\gamma_E}/4\pi$ is added to simplify later calculations. Λ_{DR} is the renormalization scale associated with the scheme, which is added to keep the integral dimensionally consistent while d is varied. Switching to polar coordinate and then integrating and expanding in powers of ϵ up to zeroth order we obtain (see [50] or pages 249-251 of [51])

$$\begin{aligned} & \left(\frac{e^{\gamma_E} \Lambda_{\text{DR}}^2}{4\pi} \right)^\epsilon \int \frac{\mathrm{d}^d p}{(2\pi)^d} \sqrt{p^2 + m^2} \\ & \qquad = \left(\frac{e^{\gamma_E} \Lambda_{\text{DR}}^2}{4\pi} \right)^\epsilon \frac{2\pi^{d/2}}{\Gamma(d/2)} \frac{1}{(2\pi)^d} \int_0^\infty \mathrm{d}p \, p^{d-1} \sqrt{p^2 + m^2} \\ & \qquad = - \frac{m^4}{32\pi^2} \left(\frac{\Lambda_{\text{DR}}^2}{m^2} \right)^\epsilon \left(\frac{1}{\epsilon} + \frac{3}{2} \right) . \end{aligned} \tag{3.26}$$

Taking the limit as $\epsilon \to 0$ we are left with a divergent term, $-m^4/32\pi^2\epsilon$ which may be removed by renormalizing the mass term. The final result is $-m^4/32\pi^2[\log(\Lambda_{\mathrm{DR}}^2/m^2) + (3/2)]$.

Here we have only considered a fermion in the vacuum. Although the finite temperature terms are inherently finite, the inclusion of a magnetic field leads to some additional divergencies. A divergent term explicitly dependent upon the magnetic field can be removed by renormalization of the magnetic field. In addition the sums over Landau levels are divergent and are regulated using the Hurwitz zeta function,

$$\zeta(s, a) \equiv \sum_{k=0}^{\infty} \frac{1}{(k+a)^s} \,. \tag{3.27}$$

The sums are simply expressed in terms of ζ and then the result is from the analytic continuation of ζ to negative s is inherently finite. For full details of the calculation see [50].

Although both schemes are equally applicable to the QM model, authors almost exclusively use dimensional regularization (in mean field treatments), presumably due to the weaker renormalization scale dependence of dimensional regularization and that the method preserves gauge invariance.

4 Numerical methods

There is scant information in the literature on the numerical methods behind the calculation of the flow equation presented in [1], something we are also guilty of. The task at hand is to evaluate the following equation:

$$
\begin{aligned}
\partial_k U_k(\rho,\Phi,\bar{\Phi};T,\mu,B) = {} & \frac{k^4}{12\pi^2}\left\{\frac{1}{\omega_{1,k}}\left[1+2n_B(\omega_{1,k})\right]+\frac{1}{\omega_{k,2}}\left[1+2n_B(\omega_{2,k})\right]\right\} \\
& + k\frac{|qB|}{2\pi^2}\sum_{\ell=0}^{\infty}\frac{1}{\omega_{1,k}}\sqrt{k^2-p_\perp^2(q,\ell,0)}\,\theta\left(k^2-p_\perp^2(q,\ell,0)\right)\left[1+2n_B(\omega_{1,k})\right] \\
& - \frac{N_c}{2\pi^2}k\sum_{s,f,\ell=0}^{\infty}\frac{|q_fB|}{\omega_{q,k}}\sqrt{k^2-p_\perp^2(q_f,\ell,s)}\,\theta\left(k^2-p_\perp^2(q_f,\ell,s)\right) \\
& \times\left[1-n_F^+(\omega_{q,k},\Phi,\bar{\Phi})-n_F^-(\omega_{q,k},\Phi,\bar{\Phi})\right]\ , \qquad (4.1)
\end{aligned}
$$

where $\omega_{1,k} = \sqrt{k^2+U_k'}$, with $U_k' = \partial U_k/\partial\rho$, $\omega_{2,k} = \sqrt{k^2+U_k'+2U_k''\rho}$, $\omega_{q,k} = \sqrt{k^2+2g^2\rho}$, $p_\perp^2(q,m,s) = (2\ell+1-s)|qB|$, $n_B(x) = 1/(e^{\beta x}-1)$ and $n_F^\pm(\omega_{q,k},\Phi,\bar{\Phi})$ are the generalised Fermi-Dirac distribution functions defined in Eqs. (2.15) and (2.16) with $E=\omega_{q,k}$. As noted in [15] there are two main methods used to solve this equation. One possibility is to use a polynomial expansion around the k-dependent minimum. The expansion is truncated and the coupled equations for the coefficients of the terms in the series are solved, see [59] for a calculation using this method. Here instead we discretise all of the variables $(\rho,\Phi,\bar{\Phi},T,\mu,B)$, and solve the equation using standard numerical methods (described below). This is done in C++, although we calculate the gluonic potential and find the transition temperatures T_c and T_d using MatLab.

To find the expectation value of our three order paramters, σ, Φ and $\bar{\Phi}$ we evaluate U_k on a grid in $(\rho,\Phi,\bar{\Phi})$-space, ultimately giving us $U_{k=0}(\rho,\Phi,\bar{\Phi})$.

We then add to this result the gauge potential, $U_{\text{glue}}(\Phi, \bar{\Phi})$ (which can be straightforwardly calculated given its simple analytic form). Finally in the minimisation procedure we must re-introduce the explicit symmetry breaking parameter described in Sec. 3.4. Thus finding $\langle\sigma\rangle$, $\langle\Phi\rangle$ and $\langle\bar{\Phi}\rangle$ we find the value of $\phi = \sqrt{2\rho}$, Φ and $\bar{\Phi}$ that minimise $U_{k=0} + U_{\text{glue}} + h\phi$. This procedure can be then repeated for different values of T, B and μ to build up the phase diagram.

4.1 Evaluation of $U_{k=0}(\rho, \Phi, \bar{\Phi})$

The major difficulty in the above (other than the sheer size of the phase space we examine) is the evaluation of $U_{k=0}(\rho, \Phi, \bar{\Phi})$. We use a grid in ρ from 0 to 8000 MeV^2 in 200 (evenly spaced) steps, corresponding roughly to the region 0 to 126 MeV in σ. Note that this implies that the spacing of the steps in σ is not even, with greater step density at higher σ.

We then step through the differential equation using a fourth order Runga-Kutta method. Each step requires the evaluation of first and second order derivative of U_k, along with a number of different sums over Landau levels for the various charged particles.[1] We define a dimensionless RG time, $t = \log(k/\Lambda_{\text{RG}})$, with $\Lambda_{\text{RG}} = 500$ MeV, and use this as the controlling parameter for the RG flow. We run from $t = 0$ to $t = -6$, corresponding to $\Lambda_{\text{RG}} = 500$ MeV to $\Lambda_{\text{RG}} \approx 1$ MeV. At this point the position of the minimum of the potential is stable in RG time. It was shown in [74] that by running to $t = -\infty$ ($k = 0$ MeV) the potential actually becomes convex, and the minimum is thus no longer uniquely defined.

4.1.1 Complex nature of the potential

Due to the derivative term in the bosonic frequencies (for example $\omega_{1,k} = \sqrt{k^2 + U_k'}$) U_k becomes complex (although the boundary condition is real). This has two major implications, first we must decide what to do with the complex part of $U_{k=0}$. $U_{k=0}$ is a potential energy and thus $\text{Re}[U_{k=0}]$ is simply the energy of that particular state, the imaginary part is then interpreted as the decay rate of the state, see [85]. As such we ignore the imaginary part in the minimisation procedure above, although we include it completely when calculating $U_{k=0}$. In addition we encountered numerical problems with the continuity of the phase of the complex number, and had to explicitly control this at each step of the integration.

---

[1] The sums over Landau levels are done by brute force. Although note that each sum is truncated by a term of the form $\theta(k^2 - (2\ell + 1)|qB|)$, thus this is only numerically intensive for small ($\lesssim 0.5\ m_\pi$) magnetic field strengths.

4.1.2 Adaptive Runga-Kutta, noise and numerical differentiation

The keen reader will notice that the derivative terms in Eq. (4.1) not only give complex bosonic frequencies, but at some points we obtain $\omega_{k,1/2} = 0$ resulting in undefined (infinite) points in $\partial_k U_k$. Due to the numerical integration, this ultimately leads to 'noise' in the final result for $U_{k=0}$, although this noise is approximately constrained to the part of the potential that lies to the left of the minimum (as in this region $U_k' < 0$). Although these points (where $\omega_{k,1/2} = 0$) are only created to the left of the minimum, in taking the derivative of the potential, we use the sixth order finite difference method to calculate U_k' and U_k'', which necessarily links the values of $U_k(\rho_i)$ to those between ρ_{i-3} and ρ_{i+3}. In later steps of the integration these errors are further linked to surrounding points. In this way these errors can have some effect upon the minimum of the potential. Figure 4.1 gives $U_{k=0}$ for a point in the centre of the phase diagram ($T = 40$ MeV, $\mu = 100$ MeV, $B = 0$, $\Phi = \bar{\Phi} = 1$) below the chiral transition temperature and at the

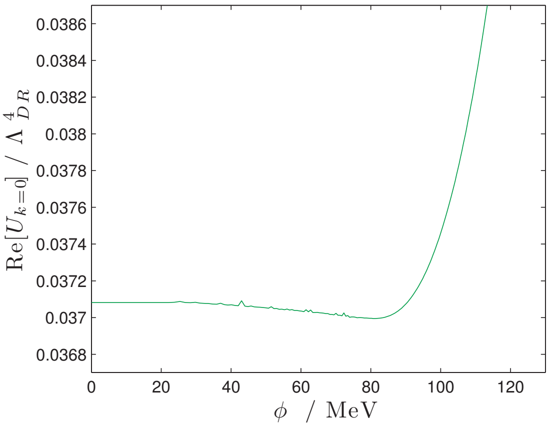

Figure 4.1: $U_{k=0}$ for $T = 40$ MeV, $\mu = 100$ MeV, $B = 0$, $\Phi = \bar{\Phi} = 1$ and at the physical point. We see visible noise for $\phi \lesssim 85$ MeV originating from points in the flow where $\omega_{k,1}$ or $\omega_{k,2}$ are zero.

physical point (i.e. using physical masses for the pions), it thus represents a fairly typical curve for the potential (where chiral symmetry is broken). There exist, however, some parts of the phase diagram (for example in the chiral limit and with $\mu = 0$), where noise is reduced to the point of being completely unnoticeable on a plot such as Fig. 4.1. Varying the input values of the Polyakov loop or the magnetic field seems not to have any great effect upon the relative strength of this noise.

Due to this noise it becomes both time consuming and inaccurate to use an adaptive Runga-Kutta method for solving the differential equation. The step size can decrease drastically even with fairly large error tolerances when encountering these points, however the quality (judged by the relative levels of noise) of the output $U_{k=0}$ is usually much worse. Instead we use a pre-set step size that increases as we step through the integration. The results are checked by comparison to existing calculations [74, 15] for a limited range of the phase space, to calculating using significantly smaller step size, and to an independent program written to solve the equation for a slightly expanded initial Lagrangian.

We are essentially concerned with the expectation value of our order parameters, and thus only in the minimum of $U_{k=0} + U_{\text{glue}} + h\phi$. The combined effect of $U_{\text{glue}} + h\phi$ is to push the minimum to slightly higher ϕ values, thus moving the point of interest further away from the region where the noise would affect our results. In the plots given in paper [1] the effects of this noise are insignificant as compared to the errors resulting from the procedure we use to find the transition temperatures (see Sec. 4.2).

We must take into account the numerical derivative when we choose the step spacing $\Delta\rho = \rho_{i+1} - \rho_i$. If this is chosen too small, then in the finite difference derivative we end up taking the difference of numbers that are very similar, and dividing by (in our case the seventh power of) a small number. We use 200 points ($\Delta\rho = 40$ MeV), as we see diminishing returns in terms of accuracy as we increase above this number.

4.1.3 Polyakov loop order parameters

As noted in [1] the surface $U_{k=0}(\Phi, \bar{\Phi})$ is extremely smooth, and as such we construct this via interpolation from an 8×8 grid in $\Phi \times \bar{\Phi}$-space, with $\Phi,\ \bar{\Phi} \in [0, 1]$. We checked this interpolation against additional data at various points in the phase diagram and found negligible errors (on the order 0.1%).

4.2 Finding the critical temperatures

Working in the chiral limit ($h = m_\pi = 0$) the chiral phase transition is a first order transition at low T and high μ and second order elsewhere (see Fig. 1 of [74]). Thus finding the critical temperature T_c amounts to finding the lowest temperature for which $\langle\sigma\rangle = 0$. This can be done numerically very easily, furthermore, we can use previously known points in the phase diagram to inform later ones to quickly build up the entire phase diagram.

At the physical point the chiral phase transition is a cross-over transition, like that of Fig. 3.1(d). In this case we would ideally use the inflection point of the curve as the definition of the critical temperature, but doing this directly from the data would require a step size in ρ that is unpractical using our numerical method. Thus we must fit the function first, and then find the inflection point the fitted function. As a fitting function we use

$$a + b\left(\frac{\pi}{2} - \mathrm{arcTan}[c(T-d)]\right) , \tag{4.2}$$

where a, b, c and d are fit parameters. In [15] a different fitting function was used, however we found this less effective at high μ.

For the deconfinement transition coupled to the matter sector we always have a cross-over transition. However due to a change in the shape of both $\Phi(T)$ and $\bar{\Phi}(T)$ we are not able to find a single function that can suitably fit the transition for all values of μ. As such, we interpolate Φ and $\bar{\Phi}$ in T and find the point at which these interpolations are equal to 1/2.

A Appendix

A.1 Useful sources and references

For the interested student, and in gratitude to those that have provided great material from which I can work let me elaborate on some possible further reading.

First, most of this thesis was written with the theses of the former members of Jens' group, Lars K. [86], Lars L. [87] and Rashid K. [88] along with Peskin and Schroeder [29], Zee [51] and Maggiore's modern introduction [34] at hand. I highly recommend the chapters 2 and 3 of [34] as a strong theoretical/group theoretical basis for the study of QFT. In addition Lars K.'s master's thesis [77] is accurately written and the Preliminaries section provides a useful reference and the section on the NJL model is far beyond what is presented here.

For paper [1] the RG calculations of Schaefer et al. [74, 55, 58] seem like foundational material. In addition Skokov's [57] and Andersen and Traberg's [15] works are clear precursors to our paper. The work of Kamikado and Kanazawa [59] is also well worth reading for a treatment beyond the LPA.

For paper [2] I recommend only Fraga's paper [22] although [50] may prove helpful as a reference.

For paper [3] the lattice papers of Boz, Cotter and co-authors are essential reading [10, 11]. Additionally the following 2cQCD papers were of great help to me [63, 64, 89].

Bibliography

[1] J. O. Andersen, W. R. Naylor, and A. Tranberg. Chiral and deconfinement transitions in a magnetic background using the functional renormalization group with the Polyakov loop. *JHEP*, 1404:187, 2014.

[2] J. O. Andersen, W. R. Naylor, and A. Tranberg. Inverse magnetic catalysis and regularization in the quark-meson model. *JHEP*, 1502:042, 2015.

[3] J. O. Andersen, T. Brauner, and W. R. Naylor. Confronting effective models for deconfinement in dense quark matter with lattice data. *Submitted to Phy. Rev. D*, 2015.

[4] M. Buballa. Njl-model analysis of dense quark matter. *Phys. Rept.*, 407:205, 2005.

[5] M. Ciminale, R. Gatto, N.D. Ippolito, G. Nardulli, and M. Ruggieri. Three flavor Nambu-Jona Lasinio model with Polyakov loop and competition with nuclear matter. *Phys.Rev.*, D77:054023, 2008.

[6] W. Fu, Z. Zhang, and Y. Liu. 2+1 flavor Polyakov-Nambu-Jona-Lasinio model at finite temperature and nonzero chemical potential. *Phys.Rev.*, D77:014006, 2008.

[7] K. Fukushima. Phase diagrams in the three-flavor Nambu-Jona-Lasinio model with the Polyakov loop. *Phys.Rev.*, D77:114028, 2008.

[8] B.-J. Schaefer, M. Wagner, and J. Wambach. Thermodynamics of (2+1)-flavor QCD: Confronting Models with Lattice Studies. *Phys.Rev.*, D81:074013, 2010.

[9] H. Mao, J. Jin, and M. Huang. Phase diagram and thermodynamics of the Polyakov linear sigma model with three quark flavors. *J.Phys.*, G37:035001, 2010.

[10] S. Cotter, P. Giudice, S. Hands, and J.-I. Skullerud. Towards the phase diagram of dense two-color matter. *Phys.Rev.*, D87(3):034507, 2013.

[11] T. Boz, S. Cotter, L. Fister, D. Mehta, and J.-I. Skullerud. Phase transitions and gluodynamics in 2-colour matter at high density. *Eur.Phys.J.*, A49:87, 2013.

[12] P. Petreczky. Lattice QCD at non-zero temperature. *J.Phys.*, G39:093002, 2012.

[13] G. Endrodi, Z. Fodor, S.D. Katz, and K.K. Szabo. The QCD phase diagram at nonzero quark density. *JHEP*, 1104:001, 2011.

[14] P. de Forcrand. Simulating QCD at finite density. *PoS*, LAT2009:010, 2009.

[15] J. O. Andersen and A. Tranberg. The chiral transition in a magnetic background: finite density effects and the functional renormalization group. *Journal of High Energy Physics*, 08:002, 2012.

[16] M. D'Elia, S. Mukherjee, and F. Sanfilippo. QCD Phase Transition in a Strong Magnetic Background. *Phys.Rev.*, D82:051501, 2010.

[17] M. D'Elia and F. Negro. Chiral Properties of Strong Interactions in a Magnetic Background. *Phys.Rev.*, D83:114028, 2011.

[18] G.S. Bali, F. Bruckmann, G. Endrodi, Z. Fodor, S.D. Katz, et al. QCD quark condensate in external magnetic fields. *Phys.Rev.*, D86:071502, 2012.

[19] G.S. Bali, F. Bruckmann, G. Endrodi, Z. Fodor, S.D. Katz, et al. The QCD phase diagram for external magnetic fields. *JHEP*, 1202:044, 2012.

[20] F. Bruckmann, G. Endrodi, and T. G. Kovacs. Inverse magnetic catalysis and the Polyakov loop. *JHEP*, 1304:112, 2013.

[21] G.S. Bali, F. Bruckmann, G. Endrodi, F. Gruber, and A. Schaefer. Magnetic field-induced gluonic (inverse) catalysis and pressure (an)isotropy in QCD. *JHEP*, 1304:130, 2013.

[22] E.S. Fraga, B.W. Mintz, and J. Schaffner-Bielich. A search for inverse magnetic catalysis in thermal quark-meson models. *Phys.Lett.*, B731:154–158, 2014.

[23] M. Ferreira, P. Costa, D. P. Menezes, C. Providência, and N. Scoccola. Deconfinement and chiral restoration within the SU(3) Polyakov–

Nambu–Jona-Lasinio and entangled Polyakov–Nambu–Jona-Lasinio models in an external magnetic field. *Phys.Rev.*, D89(1):016002, 2014.

[24] R.L.S. Farias, K.P. Gomes, G.I. Krein, and M.B. Pinto. Importance of asymptotic freedom for the pseudocritical temperature in magnetized quark matter. *Phys.Rev.*, C90(2):025203, 2014.

[25] M. Ferreira, P. Costa, O. Lourenço, T. Frederico, and C. Providência. Inverse magnetic catalysis in the (2+1)-flavor Nambu-Jona-Lasinio and Polyakov-Nambu-Jona-Lasinio models. *Phys.Rev.*, D89(11):116011, 2014.

[26] E.J. Ferrer, V. de la Incera, and X.J. Wen. Quark Antiscreening at Strong Magnetic Field and Inverse Magnetic Catalysis. *Phys.Rev.*, D91(5):054006, 2015.

[27] A. Ayala, M. Loewe, and R. Zamora. Inverse magnetic catalysis in the linear sigma model with quarks. *Phys.Rev.*, D91(1):016002, 2015.

[28] N. Mueller and J. M. Pawlowski. Magnetic catalysis and inverse magnetic catalysis in QCD. *arXiv:1502.08011 [hep-ph]*, 2015.

[29] M. E. Peskin and D. V. Schroeder. *An introduction to quantum field theory*. Westview Press Reading (Mass.), Boulder (Colo.), 1995. Autre tirage : 1997.

[30] S. Bethke. Experimental tests of asymptotic freedom. *arXiv:0606035 [hep-ex]*, 2006.

[31] K. Fukushima. Chiral effective model with the Polyakov loop. *Phys.Lett.*, B591:277–284, 2004.

[32] B. Svetitsky and L. G. Yaffe. Critical Behavior at Finite Temperature Confinement Transitions. *Nucl.Phys.*, B210:423, 1982.

[33] L. G. Yaffe and B. Svetitsky. First-order phase transition in the su(3) gauge theory at finite temperature. *Phys. Rev. D*, 26:963–965, Aug 1982.

[34] Michele Maggiore. *An modern introduction to quantum field theory*. Oxford University Press, Oxford, 2005.

[35] G. 't Hooft. Computation of the quantum effects due to a four-dimensional pseudoparticle. *Phys. Rev. D*, 14:3432–3450, Dec 1976.

[36] G. 't Hooft. Symmetry breaking through bell-jackiw anomalies. *Phys. Rev. Lett.*, 37:8–11, Jul 1976.

[37] S. Hands. The Phase diagram of QCD. *Contemp.Phys.*, 42:209–225, 2001.

[38] C.-Y. Wong. *Introduction fo High-Energy Heavy-Ion Collisoins.* World Scientific, Singapore, 1994.

[39] BRAHMS Collaboration. Quark gluon plasma and color glass condensate at RHIC? The Perspective from the BRAHMS experiment. *Nucl.Phys.*, A757:1–27, 2005.

[40] PHENIX Collaboration. Formation of dense partonic matter in relativistic nucleus-nucleus collisions at RHIC: Experimental evaluation by the PHENIX collaboration. *Nucl.Phys.*, A757:184–283, 2005.

[41] B.B. Back, M.D. Baker, M. Ballintijn, D.S. Barton, B. Becker, et al. The PHOBOS perspective on discoveries at RHIC. *Nucl.Phys.*, A757:28–101, 2005.

[42] STAR Collaboration. Experimental and theoretical challenges in the search for the quark gluon plasma: The STAR Collaboration's critical assessment of the evidence from RHIC collisions. *Nucl.Phys.*, A757:102–183, 2005.

[43] M. G. Alford, A. Schmitt, K. Rajagopal, and T. Sch afer. Color superconductivity in dense quark matter. *Rev.Mod.Phys.*, 80:1455–1515, 2008.

[44] J. O. Andersen, W. R. Naylor, and A. Tranberg. Phase diagram of QCD in a magnetic field: A review. *arXiv:1411.7176 [hep-ph]*, 2014.

[45] D. E. Kharzeev, L. D. McLerran, and H. J. Warringa. The effects of topological charge change in heavy ion collisions: "event by event p and cp violation". *Nucl. Phys. A*, 803:227, 2008.

[46] V. Skokov, A. Y. Illarionov, and V. Toneev. Estimate of the magnetic field strength in heavy-ion collisions. *Int. J. Mod.Phys. A*, 24:5925, 2009.

[47] M. et al. Bleicher. Relativistic hadron-hadron collisions in the ultra-relativistic quantum molecular dynamics model (urqmd). *arXiv:9909407 [hep-ph]*, 1999.

[48] R. C. Duncan and C. Thompson. Formation of very strongly magnetized neutron stars - implications for gamma-ray bursts. *Astrophys. J.*, 392:L9, 1992.

[49] C. Kouveliotou. Magnetars. *Proc. Natl. Acad. Sci. USA*, 96:5351, 1999.

[50] J. O. Andersen and R. Khan. Chiral transition in a magnetic field and at finite baryon density. *Phys. Rev. D*, 85:065026, 2012.

[51] A. Zee. *Quantum field theory in a nutshell.* Princeton University Press, Princeton, 2010.

[52] B.-J. Schaefer, J. M. Pawlowski, and J. Wambach. Phase structure of the polyakov-quark-meson model. *Phys. Rev. D*, 76:074023, Oct 2007.

[53] V. Skokov, B. Stokic, B. Friman, and K. Redlich. Meson fluctuations and thermodynamics of the polyakov-loop-extended quark-meson model. *Phys. Rev. C*, 82:015206, Jul 2010.

[54] B. Stokic, B. Friman, and K. Redlich. The Functional Renormalization Group and O(4) scaling. *Eur.Phys.J.*, C67:425–438, 2010.

[55] T. K. Herbst, J. M. Pawlowski, and B.-J. Schaefer. The phase structure of the Polyakov–quark-meson model beyond mean field. *Phys.Lett.*, B696:58–67, 2011.

[56] K. Kamikado, N. Strodthoff, L. von Smekal, and J. Wambach. Fluctuations in the quark-meson model for QCD with isospin chemical potential. *Phys.Lett.*, B718:1044–1053, 2013.

[57] V. Skokov. Phase diagram in an external magnetic field beyond a mean-field approximation. *Phys. Rev. D*, 85:034026, Feb 2012.

[58] T. K. Herbst, J. M. Pawlowski, and B.-J. Schaefer. Phase structure and thermodynamics of QCD. *Phys.Rev.*, D88(1):014007, 2013.

[59] K. Kamikado and T. Kanazawa. Chiral dynamics in a magnetic field from the functional renormalization group. *JHEP*, 1403:009, 2014.

[60] S.P. Klevansky and Richard H. Lemmer. Chiral symmetry restoration in the Nambu-Jona-Lasinio model with a constant electromagnetic field. *Phys.Rev.*, D39:3478–3489, 1989.

[61] J.B. Kogut, Misha A. Stephanov, and D. Toublan. On two color QCD with baryon chemical potential. *Phys.Lett.*, B464:183–191, 1999.

[62] T. Brauner, K. Fukushima, and Y. Hidaka. Two-color quark matter: $\mathrm{U(1)_a}$ restoration, superfluidity, and quarkyonic phase. *Phys. Rev. D*, 80:074035, Oct 2009.

[63] J. O. Andersen and T. Brauner. Phase diagram of two-color quark matter at nonzero baryon and isospin density. *Phys.Rev.*, D81:096004, 2010.

[64] A. Amador and J. O. Andersen. Two-color qcd in a strong magnetic field: The role of the polyakov loop. *Phys. Rev. D*, 88:025016, Jul 2013.

[65] K.A. Olive and Particle Data Group. Review of particle physics. *Chinese Physics C*, 38(9):090001, 2014.

[66] I. Caprini, G. Colangelo, and H. Leutwyler. Mass and width of the lowest resonance in qcd. *Phys. Rev. Lett.*, 96:132001, Apr 2006.

[67] Y. Nambu and G. Jona-Lasinio. Dynamical model of elementary particles based on an analogy with superconductivity. i. *Phys. Rev.*, 122:345–358, Apr 1961.

[68] Y. Nambu and G. Jona-Lasinio. Dynamical model of elementary particles based on an analogy with superconductivity. ii. *Phys. Rev.*, 124:246–254, Oct 1961.

[69] G. 't Hooft. How Instantons Solve the U(1) Problem. *Phys.Rept.*, 142:357–387, 1986.

[70] A. A. Cruz and J. O. Andersen. Two-color qcd in a strong magnetic field: The role of the polyakov loop. *Phys. Rev. D*, 88:025016, 2013.

[71] A.M. Polyakov. Thermal properties of gauge fields and quark liberation. *Physics Letters B*, 72(4):477 – 480, 1978.

[72] L. Susskind. Lattice models of quark confinement at high temperature. *Phys. Rev. D*, 20:2610–2618, Nov 1979.

[73] K. Holland and U.-J. Wiese. The Center symmetry and its spontaneous breakdown at high temperatures. *arXiv:0011193 [hep-ph]*, 2000.

[74] B.-J. Schaefer and J. Wambach. The phase diagram of the quark-meson model. *Nuclear Physics A*, 757:479 – 492, 2005.

[75] D.V. Schroeder. *An introduction to thermal physics*. Addison Wesley Longman, United States, 2000.

[76] J. I. Kapusta. *Finite temperature field theory*. Cambridge University Press, Cambridge, 2005.

[77] L. T. Kyllingstad. Pion condensation in effective theories. Master's thesis, Norwegian University of Science and Technology, 2007.

[78] M. le Ballac. *Thermal field theory.* Cambridge University Press, Cambridge, 1996.

[79] C. Wetterich. Exact evolution equation for the effective potential. *Phys. Lett. B*, 301:90, 1993.

[80] O. J. Rosten. Fundamentls of the exact renormalization group. *Physics Reports*, 511:177–272, 2012.

[81] J. Berges, N. Tetradis, and C. Wetterich. Nonperturbative renormalization flow in quantum field theory and statistical physics. *Phys.Rept.*, 363:223–386, 2002.

[82] G. 't Hooft. Dimensional regularization and the renormalization group. *Nuclear Physics B*, 61(0):455 – 468, 1973.

[83] S. Weinberg. New approach to the renormalization group. *Phys. Rev. D*, 8:3497–3509, Nov 1973.

[84] G. P. Lepage. What is renormalization? *arXiv:0506330 [hep-ph]*, 1989.

[85] E. J. Weinberg and A. Wu. Understanding complex perturbative effective potentials. *Phys. Rev. D*, 36:2474–2480, Oct 1987.

[86] L. T. Kyllingstad. *Aspects of QCD thermodynamics through scalar field theory and NJL models.* PhD thesis, Norwegian University of Science and Technology, 2011.

[87] L. E. Leganger. *Matter in extreme conditions.* PhD thesis, Norwegian University of Science and Technology, 2011.

[88] R. Khan. *Thermal resummation in scalar theories.* PhD thesis, Norwegian University of Science and Technology, 2012.

[89] N. Strodthoff and L. von Smekal. Polyakov-Quark-Meson-Diquark Model for two-color QCD. *Phys.Lett.*, B731:350–357, 2014.

[90] W. Broniowski, F. Giacosa, and V. Begun. Why the sigma meson should not be included in thermal models. *arXiv:1506.01260 [nucl-th]*, 2015.

Paper I

Chiral and deconfinement transitions in a magnetic background using the
functional renormalization group with the Polyakov loop.
JHEP, 1404:187, 2014.

Published for SISSA by Springer

Received: *November 22, 2013*
Revised: *January 22, 2014*
Accepted: *March 24, 2014*
Published: *April 30, 2014*

Chiral and deconfinement transitions in a magnetic background using the functional renormalization group with the Polyakov loop

Jens O. Andersen,[a] William R. Naylor[a] and Anders Tranberg[b]

[a] *Department of Physics, Norwegian University of Science and Technology,*
Høgskoleringen 5, N-7491 Trondheim, Norway
[b] *Faculty of Science and Technology, University of Stavanger,*
N-4036 Stavanger, Norway
E-mail: `andersen@tf.phys.ntnu.no`, `william.naylor@ntnu.no`,
`anders.tranberg@uis.no`

Abstract: We use the Polyakov loop coupled quark-meson model to approximate low energy QCD and present results for the chiral and deconfinement transitions in the presence of a constant magnetic background B at finite temperature T and baryon chemical potential μ_B. We investigate effects of various gluonic potentials on the deconfinement transition with and without a fermionic backreaction at finite B. Additionally we investigate the effect of the Polyakov loop on the chiral phase transition, finding that magnetic catalysis at low μ_B is present, but weakened by the Polyakov loop.

Keywords: Thermal Field Theory, Renormalization Group, Phase Diagram of QCD

ArXiv ePrint: 1311.2093

Open Access, © The Authors.
Article funded by SCOAP^3.

doi:10.1007/JHEP04(2014)187

Contents

1 Introduction 1

2 Quark-meson model and the functional renormalization group 2

3 Adding the Polyakov loop 4

4 Numerical implementation and the glue potential 7

5 Results at finite magnetic field 10

6 Summary and outlook 14

1 Introduction

Knowledge of the equation of state and the phase diagram of QCD is essential in understanding the properties of the deconfined matter created in heavy-ion collisions as well as the properties of compact stars and their quark cores. In non-central heavy-ion collisions, large time-dependent magnetic fields are generated during the experiment [1–3]. The maximum strength of these magnetic fields is on the order of 10^{19} Gauss ($qB \sim 6m_\pi^2$). Likewise, very strong magnetic fields exist inside magnetars [4]. These may be several orders of magnitude larger than the magnetic fields in ordinary neutron stars. On the surface, the magnetic field may be as strong as 10^{14}–10^{15} Gauss and it could be as strong as 10^{16}–10^{19} Gauss in the interior of the star. This has spurred the interest in strongly interacting matter at finite temperature, density and magnetic field, see for example ref. [5] for a recent review.

The phase boundary in (T, μ_B, B) space is therefore of great interest; however due to the infamous sign problem, one cannot use the standard techniques of lattice calculations at finite μ_B. At zero μ_B and finite B, there is no sign problem and so one can calculate the phase diagram in the T, B plane using Monte-Carlo methods. Recent lattice calculations [6, 7] suggest that for physical quark masses, the transition temperature for the chiral transition is a decreasing function of the magnetic field B, while for larger values of the quark masses corresponding to $m_\pi \simeq 400\,\text{MeV}$, the temperature is an increasing function of B [8, 9]. The qualitative behavior of the transition temperature for physical quark masses is in disagreement with model calculations using either the (Polyakov-loop extended) Nambu-Jona-Lasinio ((P)NJL) model or the (Polyakov-loop extended) quark-meson model ((P)QM); in these models, the critical temperature is an increasing function of the magnetic field, see e.g. [10–20]. Possible resolutions to the disagreement have been suggested [21–28] and we will discuss these at the end of the paper.

In a previous paper [17], two of us used the two-flavor three-color quark-meson model and the functional renormalization group [29] to map out the phase diagram in the $\mu_B - T$ plane for different values of the magnetic field (see also refs. [30, 31]). In the present paper, we add the Polyakov loop to the model to include certain aspects of confinement [32, 33]. In particular, we investigate a set of possible implementations of the Polyakov loop and how they effect both the chiral and deconfinement transitions. In the context of the functional renormalization group, this was studied in ref. [16] at zero baryon chemical potential.

The paper is organized as follows: in section 2 we briefly discuss the functional renormalization group implementation of the quark-meson model in a constant magnetic background. In section 3 we add the Polyakov loop variable to the model and review the three gluonic potentials we have used in this work. Section 4 explains the numerical implementation and the effects of the various gluonic potentials. In section 5 we discuss our results for the deconfinement and chiral transitions. Finally, in section 6, we summarise the main results and comment on the disagreement between lattice and model calculations at finite B and $\mu_B = 0$.

JHEP04(2014)187

2 Quark-meson model and the functional renormalization group

The quark meson model is the linear sigma model coupled to two massless quark flavors via a Yukawa coupling. The $O(4)$-invariant Euclidean Lagrangian for the model is

$$\begin{aligned}\mathcal{L} = \bar{\psi}\big[\gamma_\mu D_\mu - \mu\gamma_4 + g(\sigma - i\gamma_5\boldsymbol{\tau}\cdot\boldsymbol{\pi})\big]\psi + \frac{1}{2}\big[(\partial_\mu\sigma)^2 + (\partial_\mu\boldsymbol{\pi})^2\big] \\ +\frac{1}{2}m^2\big[\sigma^2 + \boldsymbol{\pi}^2\big] + \frac{\lambda}{4}\big[\sigma^2 + \boldsymbol{\pi}^2\big]^2 - h\sigma\,,\end{aligned} \tag{2.1}$$

where σ is the sigma field, $\boldsymbol{\pi}$ denotes the pions, $(\pi_1, \pi_2, \pi_3 \equiv \pi_0)$ and $\boldsymbol{\tau}$ are the Pauli matrices, $\mu = \mathrm{diag}(\mu_u, \mu_d)$ is the quark chemical potential, where μ_u and μ_d are the chemical potential for the u and d quarks, respectively. We set $\mu_u = \mu_d$ so that we are working at zero isospin chemical potential, $\mu_I = \frac{1}{2}(\mu_u - \mu_d) = 0$. The baryon chemical potential is given by $\mu_B = 3\mu$. When we couple the quark-meson model to an Abelian gauge field, we replace the partial derivatives by the covariant ones for the charged quarks as well as for the charged pions. The covariant derivative D_μ couples to the charged fields, $D_\mu = \partial_\mu - iqA_\mu^{\mathrm{EM}}$, where q is the charge of the field, $2/3e$, $-1/3e$ and $\pm e$ for the up quark, down quark, and the charged pions respectively. With the addition of the Polyakov loop, given in section 3, a coupling between the quarks and a constant background gauge field is added to the covariant derivative. The Euclidean γ matrices are given by $\gamma_j = i\gamma_M^j$, $\gamma_4 = \gamma_M^0$, and $\gamma_5 = -\gamma_M^5$, where the index M denotes Minkowski space. The fermion field is an isospin doublet,

$$\psi = \begin{pmatrix} u \\ d \end{pmatrix}. \tag{2.2}$$

The coupling to the Maxwell field reduces the $O(4)$ symmetry, or equally, $\mathrm{SU}(2)_V \times \mathrm{SU}(2)_A$ to $\mathrm{U}(1) \times \mathrm{U}(1)_A$ simply because the electric charges of the u and d quarks are different. The first term is a symmetry that corresponds to a rotation of the u and d fields with opposite phase, $u \to ue^{i\delta}$ and $d \to de^{-i\delta}$. The complex field $\Delta \equiv \frac{1}{\sqrt{2}}(\pi_1 + i\pi_2) \equiv \pi^+$ is simultaneoeusly rotated $\Delta \to \Delta e^{2i\delta}$. The second is a chiral rotation of the u and d fields with opposite phase, $u \to e^{i\gamma_5\delta}u$ and $d \to e^{-i\gamma_5\delta}d$. The complex field $\upsilon \equiv \frac{1}{\sqrt{2}}(\sigma + i\gamma_5\pi_0)$ is simultaneously rotated $\upsilon \to e^{2i\gamma_5\delta}\upsilon$. The $O(4)$ invariant $\sigma^2 + \pi_0^2 + \pi_1^2 + \pi_2^2$ now splits into the two $O(2)$ invariants $\upsilon^\dagger\upsilon$ and $\pi^+\pi^-$, where $\pi^- = \Delta^\dagger/\sqrt{2}$. In this case, we have in principle two Yukawa couplings, two mass terms and three different coupling constants.

If $h \neq 0$, the $\mathrm{U}(1)_A$ symmetry is explicitly broken, otherwise it is spontaneously broken in the vacuum. Either way, the symmetry is reduced. If the symmetry is broken spontaneously, the π_0 is a Goldstone boson, while if the symmetry is broken explicitly it is a pseudo-Goldstone boson. The charged bosons are no longer (pseudo)Goldstone bosons. The $\mathrm{U}(1)_A$ symmetry is broken in the vacuum by a nonzero expectation value ϕ for the sigma field and we make the replacement

$$\sigma \to \phi + \tilde{\sigma}\,, \tag{2.3}$$

where $\tilde{\sigma}$ is a quantum fluctuating field. The tree-level potential then becomes

$$U_\Lambda = \frac{1}{2}m_\Lambda^2\phi^2 + \frac{\lambda_\Lambda}{4}\phi^4 - h\phi\,. \tag{2.4}$$

Note that we have introduced a subscript Λ on U, m^2, and λ, where Λ is the ultraviolet cutoff of the theory. This is a reminder that these are unrenormalized quantities.[1]

We will follow Wetterich's implementation of the renormalization group ideas based on the effective average action $\Gamma_k[\varphi]$ [29]. This action is a functional of a set of background fields that are denoted by φ. $\Gamma_k[\varphi]$ satisfies an integro-differential flow equation in the variable k, to be specified below. The subscript k indicates that all the modes p between the ultraviolet cutoff Λ of the theory and k have been integrated out. When $k = \Lambda$ no modes have been integrated out and Γ_Λ equals the classical action S. On the other hand, when $k = 0$, all the momentum modes have been integrated out and Γ_0 equals the full quantum effective action. The flow equation then describes the flow in the space of effective actions as a function of k.

In order to implement the renormalization group ideas, one introduces a regulator function $R_k(p)$. The function $R_k(p)$ is large for $p < k$ and small for $p > k$ whenever $0 < k < \Lambda$, and $R_\Lambda(p) = \infty$. These properties ensure that the modes below k are heavy and decouple, and only the modes between k and the UV cutoff Λ are light and integrated out. The choice of regulator function has been discussed in detail in the literature and some choices are better than others due both to their analytical and stability properties, see for example [34].

The flow equation for the effective action cannot be solved exactly so one must make tractable and yet physically sound approximations. The first approximation in a derivative expansion is the local-potential approximation (LPA) where the flow equation for Γ_k reduces to a flow equation for an effective potential $U_k(\phi)$. In this case one sets the wave-function renormalization factors equal to one.[2] Going beyond the local-potential approximation, one would have to solve a set of coupled equations for the wave-function renormalization factors as done in the recent paper by Kamikado and Kanazawa [19].[3] Moreover, since the $\mathrm{SU}(2)_A$ symmetry is broken by the magnetic field, as explained above, the effective potential is therefore a function of these two invariants. This is similar to the case of two-color QCD with a baryon chemical potential [35] or three-color QCD with an isospin chemical potential [36]. In the LPA, the effective action then takes the form

---

[1] The symmetry breaking term is equivalent to an external field that does not flow and therefore $h = h_\Lambda$.

[2] Higher-order derivative operators that are consistent with the symmetries are also neglected in the LPA.

$$\Gamma_k\big[|\upsilon|,|\Delta|\big] = \int_0^\beta d\tau \int d^3x \bigg\{ \frac{1}{2}\big[(\partial_0\sigma)^2 + (\partial_0\boldsymbol{\pi}^2)\big] + \frac{1}{2}\big[(\nabla\sigma)^2 + (\nabla\boldsymbol{\pi}^2)\big] + U_k(|\upsilon|,|\Delta|) \bigg\} . \tag{2.5}$$

However, since we do not have a charged pion condensate, the effective potential can be evaluated at $\pi^+\pi^- \equiv 0$, but the flow equation still depends on both partial derivatives, $\frac{\partial U_k}{\partial|\upsilon|}$ and $\frac{\partial U_k}{\partial|\Delta|}$, of the potential U_k in field space. At the mean-field level these derivatives are identical, beyond they are not. In order to make the problem numerically tractable, we make the approximation that they are equal. With these approximations and defining $\rho = |\upsilon|$, the flow equation for the potential $U_k[\rho, 0]$ then reads [16, 17]

$$\begin{aligned}
\partial_k U_k[\rho,0] = {} & \frac{k^4}{12\pi^2}\bigg\{ \frac{1}{\omega_{1,k}}[1+2n_B(\omega_{1,k})] + \frac{1}{\omega_{k,2}}[1+2n_B(\omega_{2,k})] \bigg\} \\
& + k\frac{|qB|}{2\pi^2}\sum_{m=0}^{\infty}\frac{1}{\omega_{1,k}}\sqrt{k^2 - p_\perp^2(q,m,0)}\,\theta\big(k^2 - p_\perp^2(q,m,0)\big)[1+2n_B(\omega_{1,k})] \\
& - \frac{N_c}{2\pi^2}k\sum_{s,f,m=0}^{\infty}\frac{|q_fB|}{\omega_{q,k}}\sqrt{k^2 - p_\perp^2(q_f,m,s)}\,\theta\big(k^2 - p_\perp^2(q_f,m,s)\big)\big[1 - n_F^+(\omega_{q,k}) - n_F^-(\omega_{q,k})\big] ,
\end{aligned} \tag{2.6}$$

where we have defined $\omega_{1,k} = \sqrt{k^2 + U_k'}$, $\omega_{2,k} = \sqrt{k^2 + U' + 2U_k''\rho}$, $\omega_{q,k} = \sqrt{k^2 + 2g^2\rho}$, $p_\perp^2(q,m,s) = (2m+1-s)|qB|$, $n_B(x) = 1/(e^{\beta x} - 1)$, $\rho = \frac{1}{2}\phi^2$ and $n_F^\pm(x) = 1/(e^{\beta(x\pm\mu)} + 1)$, however the fermionic distribution functions will be transformed to eqs. (3.3) and (3.4) when we add the Polyakov loop.

At zero temperature, the Bose distribution function vanishes and the Fermi distribution function becomes a step function. Furthermore, if we set $\mu = 0$, this step function vanishes and we obtain the flow equation in the vacuum.

3 Adding the Polyakov loop

The Polyakov loop Φ is given by the thermal expectation value of the trace of the Wilson line, i.e.

$$\Phi = \frac{1}{N_c}\langle \mathrm{Tr}_c\, L\rangle , \tag{3.1}$$

where the trace is in color space and

$$L = \mathcal{P}\exp\left[i\int_0^\beta d\tau\, A_4 \right] , \tag{3.2}$$

---

[3] In this work, since a magnetic field breaks rotational symmetry, one must use two different wave-function renormalization factors $Z_k^\parallel$ and $Z_k^\perp$, where $\parallel$ and $\perp$ are the parallel and perpendicular directions relative to the magnetic field.

where $A_4 = iA_0$ and $A_0 = \delta_{\mu 0}\mathcal{A}_a^\mu t^a$. Here $\mathcal{A}_a^\mu$ are the $\mathrm{SU}(3)_c$ gauge fields and the generators are $t^a = \frac{1}{2}\lambda^a$, where λ^a are the Gell-Mann matricies. The Wilson line is a complex variable and so Φ is not equal to $\bar{\Phi} = \frac{1}{N_c}\langle \mathrm{Tr}_c\, L^\dagger \rangle$ in general. It is known that $\Phi = \bar{\Phi}$ at mean field level, but in the present work this is only true at zero baryon chemical potential. The Polyakov loop is an order parameter for deconfinement in pure-glue QCD. Under the center symmetry Z_N, it transforms as $\Phi \to e^{2\pi i n/N_c}$, where $n = 0, 1, 2 \ldots, N_c - 1$. At low temperatures, i.e. in the confined phase, we have $\Phi \approx 0$, while in the deconfined phase we have $\Phi \approx 1$.

Coupling the Polyakov loop to the QM model gives a more physically accurate model of the quark sector and allows us to explore both the chiral and deconfinement transitions of low energy QCD. This is done by introducing a constant background temporal gauge field $\delta_{\mu 0}\mathcal{A}_a^\mu$ via the covariant derivative for the quarks $D_\mu \to D_\mu - i\delta_{\mu 0}\mathcal{A}_a^\mu t^a$ (however the covariant derivative acting on the pions remains unchanged) and adding a phenomenological potential for the gluonic sector (discussed below). The Polyakov gauge is particularly convenient for calculations as the Wilson line is then a diagonal matrix, $L = e^{i(\lambda^3 A_3 + \lambda^8 A_8)/2T}$. Utilizing this and the mean field solution for the effective potential the quark distribution functions are found to be transformed from the standard Fermi-Dirac distribution functions to

$$n_F^+(\Phi, \bar{\Phi}; T, \mu) = \frac{1 + 2\bar{\Phi}e^{\beta(E_q-\mu)} + \Phi e^{2\beta(E_q-\mu)}}{1 + 3\bar{\Phi}e^{\beta(E_q-\mu)} + 3\Phi e^{2\beta(E_q-\mu)} + e^{3\beta(E_q-\mu)}}\,, \tag{3.3}$$

$$n_F^-(\Phi, \bar{\Phi}; T, \mu) = n_F^+(\bar{\Phi}, \Phi; T, -\mu)\,. \tag{3.4}$$

These are then substituted back into the renormalization group flow equation (2.6). This form is a particularly promising result, as in the confining limit (Φ and $\bar{\Phi} \to 0$) we obtain a Fermi-Dirac-like distribution function for states of three quarks, however as Φ and $\bar{\Phi} \to 1$ the functions $n_F^\pm$ are equal to the standard Fermi-Dirac distribution functions, as they should be.

A number of forms for the gluonic potentials have been proposed and investigated at mean field level for the PNJL model [37] and the PQM model with $\mu = 0$ [38]. In this work we will investigate three different gluon potentials. Since the Polyakov loop variable is the order parameter for the $Z(3)$ center symmetry of pure-glue QCD, a Ginzburg-Landau type potential should incorporate this. A polynomial expansion then leads to [39]

$$\frac{U_{\mathrm{poly}}}{T^4} = -\frac{b_2(T)}{2}\Phi\bar{\Phi} - \frac{b_3}{6}(\Phi^3 + \bar{\Phi}^3) + \frac{b_4}{4}(\Phi\bar{\Phi})^2\,, \tag{3.5}$$

where the coefficients are

$$b_2(T) = 6.75 - 1.95\left(\frac{T_0}{T}\right) + 2.624\left(\frac{T_0}{T}\right)^2 - 7.44\left(\frac{T_0}{T}\right)^3, \tag{3.6}$$

$$b_3 = 0.75\,, \tag{3.7}$$

$$b_4 = 7.5\,. \tag{3.8}$$

The coefficients $b_2(T)$, b_3, and b_4 are chosen such that the Polyakov loop potential reproduces the equation of state and temperature dependence of Φ around the transition

JHEP04(2014)187

at $\mu = 0$. The parameter T_0 is the transition temperature for pure-glue QCD lattice calculations [40].

In refs. [41, 42], another form for the Polyakov loop potential based on the SU(3) Haar measure was proposed:

$$\frac{U_{\text{log}}}{T^4} = -\frac{a(T)}{2}\Phi\bar{\Phi} + b(T)\ln\left[1 - 6\,\bar{\Phi}\Phi + 4(\Phi^3 + \bar{\Phi}^3) - 3(\bar{\Phi}\Phi)^2\right], \tag{3.9}$$

where the coefficients are

$$a(T) = 3.51 - 2.47\left(\frac{T_0}{T}\right) + 15.2\left(\frac{T_0}{T}\right)^2, \tag{3.10}$$

$$b(T) = -1.75\left(\frac{T_0}{T}\right)^3. \tag{3.11}$$

We note that the logarithmic term ensures that the magnitude of Φ and $\bar{\Phi}$ is constrained to be in the region between -1 and 1, i.e. the possible attainable values for the normalized trace of an element of the SU(3). Finally, Fukushima proposed a Polyakov loop potential in [43]

$$\frac{U_{\text{Fuku}}}{T^4} = -\frac{b}{T^3}\left(54e^{-a\,T_0/T}\Phi\bar{\Phi} + \ln\left[1 - 6\,\Phi\bar{\Phi} + 4(\Phi^3 + \bar{\Phi}^3) - 3(\Phi\bar{\Phi})^2\right]\right), \tag{3.12}$$

where the constants are $a = 664/270$ and $b = (196.2\,\text{MeV})^3$ and we have added dependence upon the transition temperature, T_0.

A problem with all the Polyakov loop potentials proposed is that they are independent of the number of flavors and of the baryon chemical potential. However, we know that, for example, the transition temperature for the deconfinement transition is a function of N_f. In other words, one ought to incorporate the back-reaction from the fermions to the gluonic sector. In ref. [44], the authors use perturbative arguments to estimate the effects of the number of flavors and the baryon chemical potential on the transition temperature T_0. The functional form of T_0 is [45]

$$T_0 = T_\tau e^{-1/\left(\alpha_0\, b(N_f,\mu)\right)}, \tag{3.13}$$

where

$$b(N_f,\mu) = \frac{1}{6\pi}(11N_c - 2N_f) - \frac{16}{\pi}N_f\frac{\mu^2}{(\hat{\gamma}\,T_\tau)^2}, \tag{3.14}$$

and $T_\tau = 1.77\,\text{GeV}$, $\alpha_0 = 0.304$. $\hat{\gamma}$ controls the curvature of T_0 as a function of μ, and again following [45] we experiment with a range of values to study the effects. This is further discussed in the following section.

Let us finally make a few remarks about the complexity of the effective action. In the mean-field approximation [47–50] of the PNJL and PQM models at finite μ_B, the effective action is complex if one considers it a function of the complex variables Φ and $\bar{\Phi}$. If one ignores the imaginary part of the effective potential, the effective potential becomes a real function of real variables. One can then find a minimum of the effective potential in the usual way. However, in this approach, one obtains $\Phi = \bar{\Phi}$, which is in disagreement with lattice results. In our calculations, we restrict Φ and $\bar{\Phi}$ to be real and we find $\Phi \neq \bar{\Phi}$, thus avoiding the problem.

JHEP04(2014)187

4 Numerical implementation and the glue potential

To find the equilibrium state values of the order parameters ϕ, Φ and $\bar{\Phi}$ we numerically solve the flow equation (2.6) with the boundary condition specified by the tree level potential, eq. (2.4), on a grid in ϕ-Φ-$\bar{\Phi}$-space with $\phi \in [0, 126]\,\mathrm{MeV}$ and $\Phi, \bar{\Phi} \in [0, 1]$ (Φ and $\bar{\Phi}$ are real, as discussed section 3). Doing this at various values of T, B and μ gives us $U_{k=0}(\phi, \Phi, \bar{\Phi}; T, B, \mu)$, which we construct as a dimensionless quantity. In the derivation of the flow equation we have used $O(4)$ symmetry, thus for the boundary condition of the flow we set $h = 0$, then when minimising with respect to ϕ we minimise $U_{k=0} - h\phi$. The resulting surface, $U_{k=0}(\Phi, \bar{\Phi})$ is very smooth thus we use interpolation to save computation time. Additional runs at intermediate values show that errors due to the interpolation are on the order of 0.1%. Before we minimise with respect to the deconfinement order parameters we must add the gluonic potential. Thus Φ and $\bar{\Phi}$ are obtained from the minimisation of $U_{k=0}(\Phi, \bar{\Phi}) + U_{\mathrm{glue}}(\Phi, \bar{\Phi})/\Lambda^4$, where 'glue' stands for one of 'poly', 'log' or 'Fuku' as given in section 3.

We use the following (dimensionless) bare parameters: $m_\Lambda^2 = 0.075$, $\lambda_\Lambda = 9.2$, $g = 3.2258$ and $h = 0.0146$ and we have $\Lambda = 500\,\mathrm{MeV}$ which give constituent quark masses of $300\,\mathrm{MeV}$, a sigma mass of $\sim 478\,\mathrm{MeV}$ and pion masses of $\sim 140\,\mathrm{MeV}$, that is, our results are calculated at the physical point. Changing the energy of the ultraviolet cutoff from 500 to 800 MeV, gives an increase of approximately 3% to the chiral phase transition at low μ, and approximately 10% at low T. Additional details about the implementation at $\Phi = \bar{\Phi} = 1$ can be found in [17].

As the results presented here are calculated at the physical point all of the phase transitions are crossover 'transitions' and thus all critical temperatures are pseudo-critical temperatures. We must therefore define how we can calculate these transitions. Since we have discretized the variables in the computation of the effective potential, calculating the inflection point directly from the output data is very inaccurate. Thus one way to define the transition temperature is to fit the data points for the order parameter in question with a function and then define the transition temperature, T_{x}, as the inflection point of the fitted curve. For the chiral transition we use this method, with the fit based on $\arctan(x)$. However, using this method for the deconfinement transition we run into problems as the functional form of the underlying curve changes with changing μ (see the left panel of figure 3). An alternative way of defining this transition is when the order parameter, $\Phi(T)$, is equal to $\frac{1}{2}$, this we define as $T_{\Phi/2}$. To find this point we interpolate with third-order polynomial interpolation. Figure 1 illustrates this for $\mu = 0$. The left panel shows the data points (crosses) for ϕ as a function of T. The open circle indicates the inflection point of the fitted curve, i.e. T_ϕ, while the cross indicates the temperature when the normalized chiral order parameter satisfies $\phi/\phi(T = 0) = \frac{1}{2}$, we denote this $T_{\phi/2}$. The right panel shows the same, but now for the deconfinement order parameter Φ and the green curve is now the interpolation used to determine $T_{\Phi/2}$.

Following ref. [44], we introduced an N_f and μ_B-dependent transition temperature T_0 via eq. (3.13). In figure 2, we show the effects of varying the parameter $\hat{\gamma}$ in eq. (3.14) on the deconfinement transition in the $\mu - T$ plane for zero magnetic field and utilizing the

JHEP04(2014)187

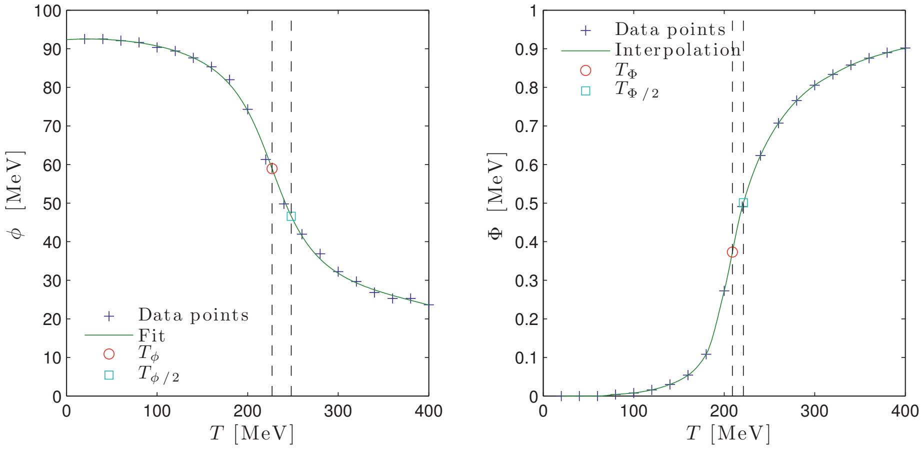

Figure 1. Methods used to determine the transition temperatures for the chiral transition (left) and deconfinement transition (right). Both plots are for $\mu = 0$. See main text for details.

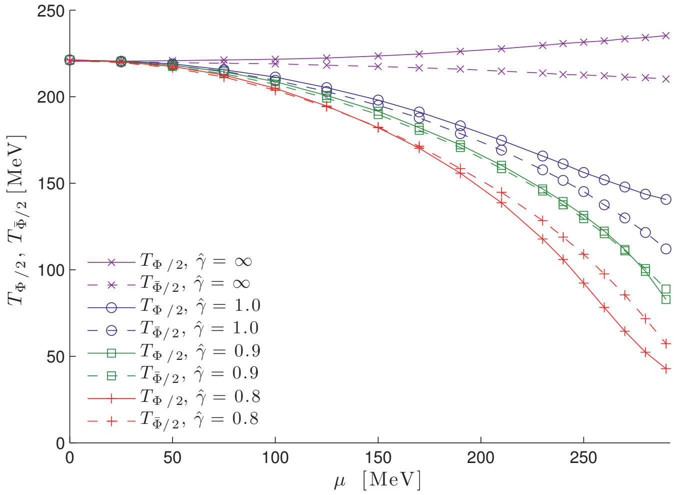

Figure 2. Phase diagram for the deconfinement transition with $B = 0$ and various values of the parameter $\hat{\gamma}$. See main text for details.

polynomial gluonic potential, eq. (3.5). The solid lines show $T_{\Phi/2}$ while the dashed lines show $T_{\bar{\Phi}/2}$ for the same values of $\hat{\gamma}$. We note that both Φ and $\bar{\Phi}$ are real and coincide for $\mu = 0$ but differ at non-zero μ. Furthermore, for a μ_B-independent T_0 (= 208 MeV) the transition temperature is almost independent of the baryon chemical potential μ (magenta lines). The red, green, and blue lines show the results for $\hat{\gamma} = 0.8$, 0.9, and 1.0, respectively. The bending of the curves decreases as a function of $\hat{\gamma}$ which is reasonable since this

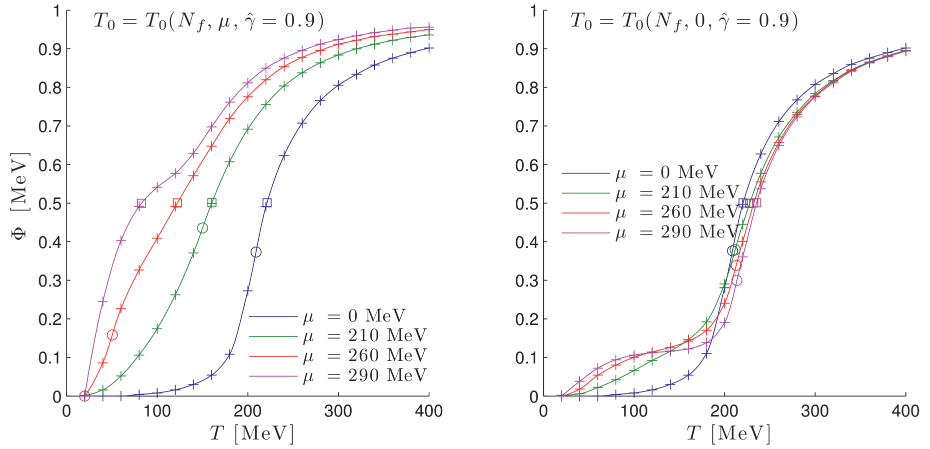

Figure 3. Order parameter Φ as a function of T for various values of the chemical potential μ with (left) and without (right) a μ dependent gluonic transition temperature, T_0. $+$s are the data points, lines are the interpolations thereof, $\square$s give $T_{\Phi/2}$ and $\circ$s approximate T_Φ.

parameter enters in the denominator of the parametrization (3.14) of $b(N_f, \mu)$. At $\hat{\gamma} \approx 0.9$ we find the strongest μ dependence which still preserves $T_{\Phi/2} \geq T_{\bar{\Phi}/2}$ thus in the remaining figures in this paper (figures 3–8) we use $\hat{\gamma} = 0.9$. Finally, we remark that the qualitative behavior is the same for finite magnetic field B. We will present more results for various B-fields in the next section.

In figure 3, we show the order parameter $\Phi(T)$ as a function of T for $\mu = 0$ (blue), $\mu = 210$ (green), $\mu = 260$ (red), and $\mu = 290$ (magenta) with and without a μ dependent gluonic potential. In the left panel, the results are for $T_0 = T_0(N_f, \mu)$, while in the right panel $T_0 = T_0(N_f, 0)$ i.e. independence from μ. Comparing the two panels we see the result shown in figure 2, that only with a μ dependent transition temperature T_0 do we obtain significant change in the deconfinement order parameter when varying μ. Additionally we see in the right panel that at high μ (magenta in particular) there is an initial increase in Φ around $T = 50\,\text{MeV}$, which comes from the mesonic and fermionic potential, $U_{k=0}$, and then around 208 MeV there is the typical increase, driven largely by the gluonic potential, U_{glue}. We then see in the left panel, with a μ dependent T_0, that the effect of U_{glue} mirrors that of $U_{k=0}$ and the deconfinement transition thus decreases with increasing μ.

Figure 3 also illustrates the aforementioned difficulties in defining the deconfinement transition at large μ. It is seen that $T_{\Phi/2} \sim T_\Phi$ at low μ, but for $\mu \gtrsim 230\,\text{MeV}$ this is no longer true. In addition to this, the numerics become more time consuming at low T, thus for values of $T \gtrsim 30\,\text{MeV}$ our results only approximate the behavior of the model. For these reasons we have only calculated the phase diagram up to $\mu = 290\,\text{MeV}$.[4]

---

[4] We have also observed the splitting of the chiral transition reported in [46] without the Polyakov loop, but have not resolved that region in detail with the Polyakov loop.

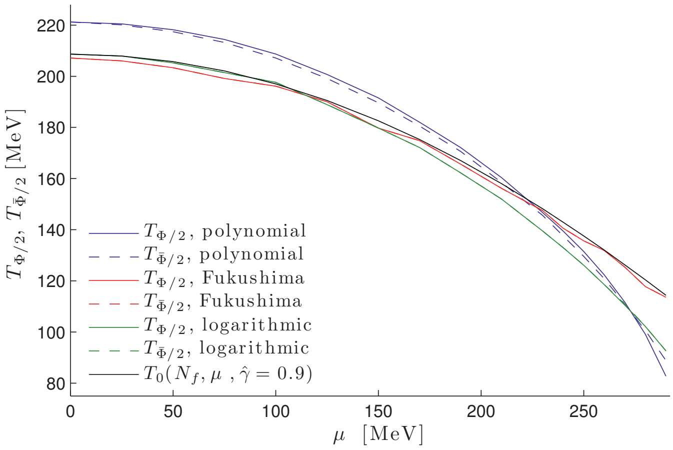

Figure 4. Phase diagram for the deconfinement transition for different glue potentials and $B = 0$. Also shown is the transition temperature $T_0 = T_0(N_f, \mu, \hat{\gamma} = 0.9)$ for pure glue for comparison.

In figure 4, we show the phase diagram for the deconfinement transition with the three different glue potentials introduced in section 3 at $B = 0$. The blue lines are the polynomial potential (3.5), the red lines are the logarithmic potential (3.9), and the green lines are the Fukushima potential (3.12). The black line shows the transition temperature $T_0 = T_0(N_f, \mu, \hat{\gamma} = 0.9)$ for pure glue for comparison. We note that the black curve is almost the same as the curve for the Fukushima potential (red), implying that the coupling to the quarks has almost no influence on the deconfinement transition.

As was observed in [41] we find with the logarithmic potential that $\Phi = \bar{\Phi}$ for all values of μ, we also find this to be true with the Fukushima potential. We also find with the Fukushima potential, and to a lesser degree with the logarithmic potential, that the deconfinement transition temperature is dominated by the gluonic potential. This was also backed up by direct investigation of the Φ and $\bar{\Phi}$ as functions of T.

In figure 5, we show the phase diagram for the chiral transition using the different gluonic potentials. We also show the phase diagram for the quark-meson model without the Polyakov loop, i.e. for $\Phi = 1$. The lines show that the particular form of the gluonic potential is not as influential as we saw in the case of the deconfinement transition. At zero μ and B, T_ϕ decreases by 2% and 3% for the logarithmic and Fukushima potentials respectively. Only with $\mu \gtrsim 260\,\text{MeV}$ do we see a significantly larger deviation than this.

5 Results at finite magnetic field

In this section, we will present our main results and discuss them in some detail. In figure 6, we show the phase diagram for the chiral and the deconfinement transitions for $B = 0$ (blue lines) and for $|qB| = 5.3m_\pi^2$. The results are obtained using the polynomial glue potential (3.5). We will discuss the results in detail in connection with figure 7,

JHEP04(2014)187

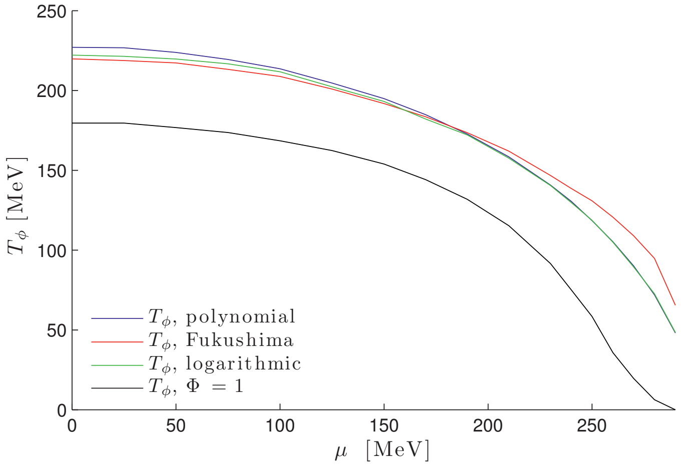

Figure 5. Phase diagram for the chiral transition for $B = 0$ with different glue potentials however the same gluoinic transition temperature $T_0 = T_0(N_f, \mu, \hat{\gamma} = 0.9)$. Also shown is the transition temperature for $\Phi = 1$, i.e. for the quark-meson model without the Polyakov loop.

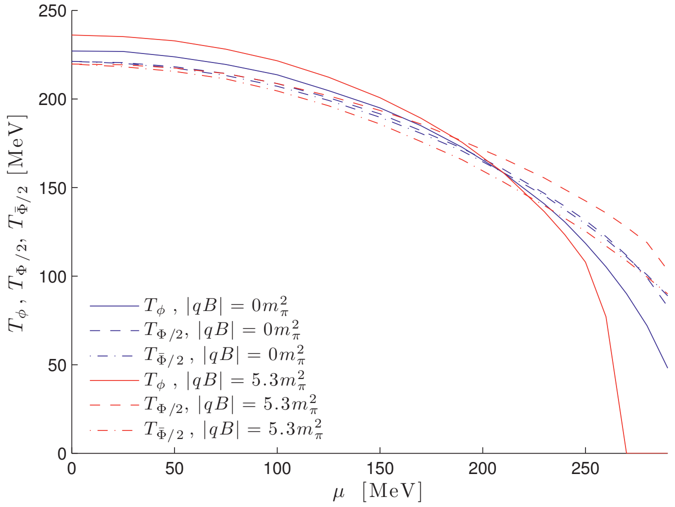

Figure 6. Phase diagram for the deconfinement and chiral transitions for $B = 0$ and the largest magnetic field, $|qB| = 5.3\ m_\pi^2$ with the Polynomial potential.

where we show the chiral and deconfinement transition temperatures as a function of B for different values of μ.

In figure 7, we show the transition temperatures for the chiral and deconfinement transitions as functions of B for different values of μ. The solid blue lines indicate the

JHEP04(2014)187

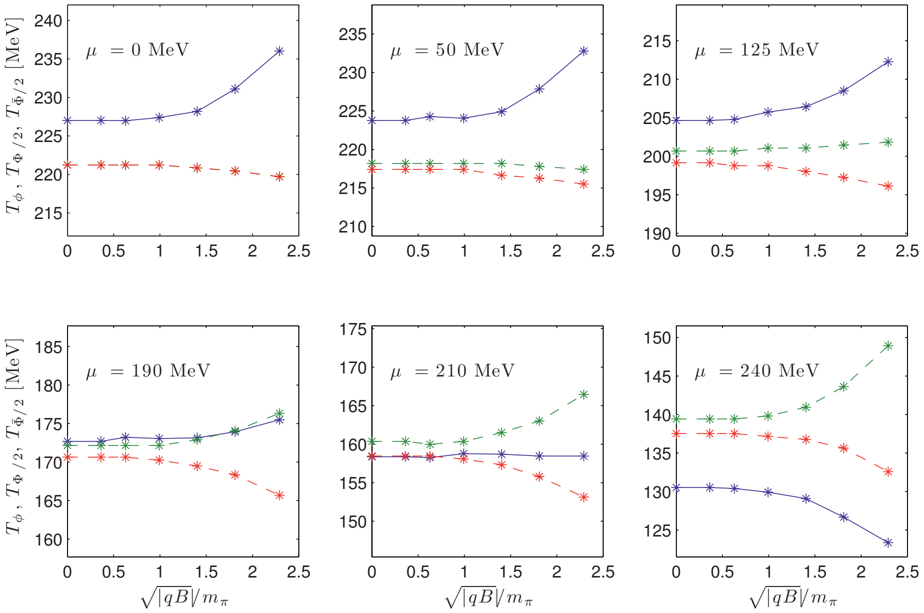

Figure 7. Transition temperatures for the chiral and deconfinement transitions as functions of B for different values of μ. Solid blue lines denote T_ϕ while dashed lines correspond to the deconfinement transition with green giving $T_{\Phi/2}$, red giving $T_{\bar{\Phi}/2}$.

chiral transition, T_ϕ, while the dashed green lines are $T_{\Phi/2}$ and the dashed red lines are $T_{\bar{\Phi}/2}$. In the left upper panel, $\mu = 0$ and $\Phi = \frac{1}{2}$ and $\bar{\Phi} = \frac{1}{2}$ coincide for all B. We note that the transition temperature for the chiral transition is increasing for values of μ up to approximately $\mu = 210\,\text{MeV}$ where it is flat (lower middle panel). For larger chemical potentials, the transition temperature for chiral transition is a decreasing function. This shows the magnetic catalysis for small μ and inverse catalysis for large μ which we discuss below. For nonzero μ we see that the splitting between Φ and $\bar{\Phi}$ increases with μ and also with the strength of the magnetic field B. For small values of μ, $T_{\Phi/2}$ and $T_{\bar{\Phi}/2}$ are almost independent of B, while for large values, $T_{\Phi/2}$ increases with increasing B while $T_{\bar{\Phi}/2}$ decreases with B. This behavior indicates that the relative importance of the fermionic and mesonic fields also increases with larger B and μ although we have not identified a mechanism behind this behavior.

In figure 8, we show the phase diagram for the chiral phase transition for different values of the magnetic field B with coupling to the Polyakov loop variable (solid lines) and without (dashed lines). Inset shows the transition temperature as a function of B for vanishing μ in the two cases. We first notice that the critical temperature increases with the magnetic field for small values of the chemical potential μ. The basic mechanism is that of magnetic catalysis [51–53], namely that the chiral condensate increases as a function of the magnetic field. It is interesting to note that the increase of the transition temperature

JHEP04(2014)187

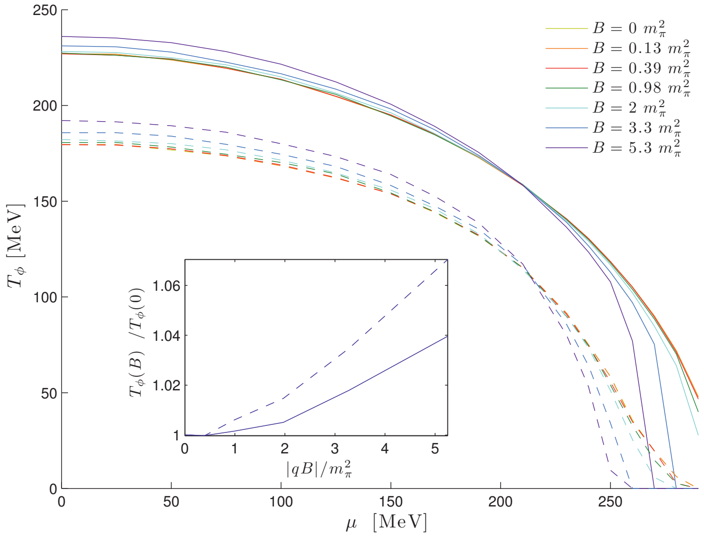

Figure 8. Phase diagram for the chiral transition for different values of the magnetic field B with (solid lines) and without (dashed lines) the Polyakov loop using the polynomial potential. Inset shows the critical temperature as a function of B for $\mu = 0$ with (solid lines) and without (dashed lines) the Polyakov loop.

as a function of B is smaller when we couple the chiral sector to the gluonic sector. For large values of the chemical potential μ, the critical temperature is a decreasing function of the magnetic field. This is inverse catalysis [54, 55]. We also find that the transition temperature is increased signficantly for all values of μ with the addition of the Polyakov loop. Below $\mu \sim 200\,\mathrm{MeV}$ T_ϕ increases by approximately 25% and above this density we find greater increases in T_ϕ. The Polyakov loop acts to suppress the finite temperature, fermionic contribution to the effective potential at all temperatures, although particularly at low temperatures. Thus we expect some increase in T_ϕ but its magnitude is of interest as it shows that the confining dynamics does play an important role in the chiral transition within this model. In this region we find $T_{\phi,\,\mathrm{Fuku}} - T_{\phi,\,\mathrm{log/poly}} \approx 20\,\mathrm{MeV}$. The relative increase in magnetic field is more greatly affected by the choice of potential, with the relative increase in T_ϕ being approximately 20% less with the logarithmic and Fukushima potentials as opposed to the polynomial potential shown in figure 8.

Very recently, the existence of a new critical point associated with the deconfinement transition of strongly interacting matter at finite T and B, but vanishing μ has been suggested [56]. The basic idea is that quarks effectively decouple in the presence of very large magnetic fields due to their increasing mass as a function of B. In this case, one should be able to describe the system with an effective theory of pure gluondynamics. Although this effective theory is anisotropic, it is likely that it has a first-order transition just like isotropic pure-glue QCD. Since QCD with physical quark masses exhibit a crossover and

JHEP04(2014)187

not a first-order transition, there ought to be a critical point in the $T - B$ plane, where the line of first-order transition ends. However we find no evidence within the range of magnetic fields we examine of a transformation from the observed cross-over transition to a first order transition for the deconfinement order parameter.

6 Summary and outlook

In this work we have used the functional renormalization group to calculate the phase diagram with respect to the chiral and deconfinement transitions for the Polyakov loop extended quark-meson model. We first investigated the effects of the gluonic potential, showing that the deconfinement transision is quantitavely dependent upon the exact implementation, and in some cases even qualitatively dependent. Most noticeably $T_{\Phi/2} - T_{\bar{\Phi}/2}$ is only non-zero when using the polynomial potential (3.5). This potential was also the least dominating in that the fermionic and mesonic degrees of freedom had a much larger effect upon the deconfinement order parameters, Φ and $\bar{\Phi}$. However for all three potentials the gluonic potential dominated the dynamics. At high μ we see a double humped structure in these order parameters. This made the evaluation of $T_{\Phi/2}$ and $T_{\bar{\Phi}/2}$ difficult and we can not find a first order transition around $\mu \sim 300\,\mathrm{MeV}$ (given by Herbst et al. [45]) although we saw indications of this.

We find magnetic catalysis at low μ in agreement with other model calculations, however we see a weakening of its effects with the addition of the Polyakov loop. At large μ the inverse magnetic catalysis found in the quark-meson model [17] is also found here. When using the polynomial potential we a find splitting of $T_{\Phi/2}$ and $T_{\bar{\Phi}/2}$ at non-zero μ. This splitting increases with increasing magnetic field strength and quark chemical potential (other than for the very highest μ value). In addition T_ϕ increases significantly for all values of μ shows that the Polyakov loop plays an important role in the chiral transition. In contrast to the confinement transition, we found that the chiral transition is not sensitive to the choice of the gluon potential.

In the recent papers [6, 24], the authors suggest a resolution of the discrepancy between the model calculations and the lattice simulations. The chiral condensate can be written as

$$\langle\bar{\psi}\psi\rangle = \frac{1}{\mathcal{Z}(B)} \int d\mathcal{U} e^{-S_g} \det\left(\not{D}(B) + m\right) \mathrm{Tr}\left(\not{D}(B) + m\right)^{-1}, \tag{6.1}$$

where the partition function is

$$\mathcal{Z}(B) = \int d\mathcal{U} e^{-S_g} \det\left(\not{D}(B) + m\right), \tag{6.2}$$

and S_g is the pure-glue action. Thus there are two contributions to the chiral condensate, namely the operator itself (called valence contribution) and the change of typical gauge configurations sampled, coming from the determinant in eq. (6.1) (called sea contribution). At least for small magnetic fields one can disentangle these contributions by defining

$$\langle\bar{\psi}\psi\rangle^{\mathrm{val}} = \frac{1}{\mathcal{Z}(0)} \int d\mathcal{U} e^{-S_g} \det\left(\not{D}(0) + m\right) \mathrm{Tr}\left(\not{D}(B) + m\right)^{-1}, \tag{6.3}$$

$$\langle\bar{\psi}\psi\rangle^{\mathrm{sea}} = \frac{1}{\mathcal{Z}(B)} \int d\mathcal{U} e^{-S_g} \det\left(\not{D}(B) + m\right) \mathrm{Tr}\left(\not{D}(0) + m\right)^{-1}. \tag{6.4}$$

JHEP04(2014)187

At zero temperature, both contributions are positive leading to magnetic catalysis. At temperatures around the transition temperature, the valence condensate is still positive while the sea condensate is negative. Hence there is a competition between the two leading to a net inverse catalysis. The sea contribution can be viewed as a back reaction of the fermions on the gauge fields and this effect is not present in the model calculations as there are no dynamical gauge fields. If such a back reaction can be incorporated in the model calculations, one may be able to obtain agreement with the lattice simulations. One interesting attempt that was made recently, used a B-dependent parametrization of the transition temperature T_0 [28] in analogy with the flavor and μ_B dependence of T_0. Given the constraint that there is magnetic catalysis at zero temperature and that the chiral transition is a crossover, the authours found that the PQM model leads to thermal magnetic catalysis in the entire allowed parameter space. The calculations presented in [28] were in the mean-field approximation and whether the inclusion of bosonic fluctuations changes this picture is not known. In that case, we are still missing a key ingredient within these models and the disagreement with lattice remains a major challenge to model builders.

Acknowledgments

The authors would like to thank Kazuhiko Kamikado, Takuya Kanazawa, and Jonas R. Glesaaen for valuable discussions.

Open Access. This article is distributed under the terms of the Creative Commons Attribution License (CC-BY 4.0), which permits any use, distribution and reproduction in any medium, provided the original author(s) and source are credited.

References

[1] D.E. Kharzeev, L.D. McLerran and H.J. Warringa, *The effects of topological charge change in heavy ion collisions: 'event by event P and CP-violation'*, *Nucl. Phys.* **A 803** (2008) 227 [`arXiv:0711.0950`] [INSPIRE].

[2] V. Skokov, A.Y. Illarionov and V. Toneev, *Estimate of the magnetic field strength in heavy-ion collisions*, *Int. J. Mod. Phys.* **A 24** (2009) 5925 [`arXiv:0907.1396`] [INSPIRE].

[3] A. Bzdak and V. Skokov, *Event-by-event fluctuations of magnetic and electric fields in heavy ion collisions*, *Phys. Lett.* **B 710** (2012) 171 [`arXiv:1111.1949`] [INSPIRE].

[4] J.M. Lattimer and M. Prakash, *Neutron star observations: prognosis for equation of state constraints*, *Phys. Rept.* **442** (2007) 109 [`astro-ph/0612440`] [INSPIRE].

[5] D. Kharzeev, K. Landsteiner, A. Schmitt and H.-U. Yee eds., *Strongly interacting matter in magnetic fields*, *Lect. Notes Phys.* **871** (2013) 1 [INSPIRE].

[6] G.S. Bali et al., *The QCD phase diagram for external magnetic fields*, *JHEP* **02** (2012) 044 [`arXiv:1111.4956`] [INSPIRE].

[7] G.S. Bali et al., *QCD quark condensate in external magnetic fields*, *Phys. Rev.* **D 86** (2012) 071502 [`arXiv:1206.4205`] [INSPIRE].

[8] M. D'Elia, S. Mukherjee and F. Sanfilippo, *QCD phase transition in a strong magnetic background*, *Phys. Rev.* **D 82** (2010) 051501 [`arXiv:1005.5365`] [INSPIRE].

[9] M. D'Elia and F. Negro, *Chiral properties of strong interactions in a magnetic background*, *Phys. Rev.* **D 83** (2011) 114028 [`arXiv:1103.2080`] [INSPIRE].

[10] A.J. Mizher, M.N. Chernodub and E.S. Fraga, *Phase diagram of hot QCD in an external magnetic field: possible splitting of deconfinement and chiral transitions*, *Phys. Rev.* **D 82** (2010) 105016 [`arXiv:1004.2712`] [INSPIRE].

[11] S. Fayazbakhsh and N. Sadooghi, *Phase diagram of hot magnetized two-flavor color superconducting quark matter*, *Phys. Rev.* **D 83** (2011) 025026 [`arXiv:1009.6125`] [INSPIRE].

[12] R. Gatto and M. Ruggieri, *Dressed Polyakov loop and phase diagram of hot quark matter under magnetic field*, *Phys. Rev.* **D 82** (2010) 054027 [`arXiv:1007.0790`] [INSPIRE].

[13] R. Gatto and M. Ruggieri, *Deconfinement and chiral symmetry restoration in a strong magnetic background*, *Phys. Rev.* **D 83** (2011) 034016 [`arXiv:1012.1291`] [INSPIRE].

[14] K. Kashiwa, *Entanglement between chiral and deconfinement transitions under strong uniform magnetic background field*, *Phys. Rev.* **D 83** (2011) 117901 [`arXiv:1104.5167`] [INSPIRE].

[15] D.C. Duarte, R.L.S. Farias and R.O. Ramos, *Optimized perturbation theory for charged scalar fields at finite temperature and in an external magnetic field*, *Phys. Rev.* **D 84** (2011) 083525 [`arXiv:1108.4428`] [INSPIRE].

[16] V. Skokov, *Phase diagram in an external magnetic field beyond a mean-field approximation*, *Phys. Rev.* **D 85** (2012) 034026 [`arXiv:1112.5137`] [INSPIRE].

[17] J.O. Andersen and A. Tranberg, *The chiral transition in a magnetic background: finite density effects and the functional renormalization group*, *JHEP* **08** (2012) 002 [`arXiv:1204.3360`] [INSPIRE].

[18] M. Ruggieri, M. Tachibana and V. Greco, *Renormalized vs. nonrenormalized chiral transition in a magnetic background*, *JHEP* **07** (2013) 165 [`arXiv:1305.0137`] [INSPIRE].

[19] K. Kamikado and T. Kanazawa, *Chiral dynamics in a magnetic field from the functional renormalization group*, *JHEP* **03** (2014) 009 [`arXiv:1312.3124`] [INSPIRE].

[20] M. Ferreira, P. Costa and C. Providência, *Deconfinement, chiral symmetry restoration and thermodynamics of* $(2+1)$*-flavor hot QCD matter in an external magnetic field*, *Phys. Rev.* **D 89** (2014) 036006 [`arXiv:1312.6733`] [INSPIRE].

[21] E.S. Fraga and L.F. Palhares, *Deconfinement in the presence of a strong magnetic background: an exercise within the MIT bag model*, *Phys. Rev.* **D 86** (2012) 016008 [`arXiv:1201.5881`] [INSPIRE].

[22] K. Fukushima and Y. Hidaka, *Magnetic catalysis versus magnetic inhibition*, *Phys. Rev. Lett.* **110** (2013) 031601 [`arXiv:1209.1319`] [INSPIRE].

[23] T. Kojo and N. Su, *The quark mass gap in a magnetic field*, *Phys. Lett.* **B 720** (2013) 192 [`arXiv:1211.7318`] [INSPIRE].

[24] F. Bruckmann, G. Endrodi and T.G. Kovacs, *Inverse magnetic catalysis and the Polyakov loop*, *JHEP* **04** (2013) 112 [`arXiv:1303.3972`] [INSPIRE].

[25] J. Chao, P. Chu and M. Huang, *Inverse magnetic catalysis induced by sphalerons*, *Phys. Rev.* **D 88** (2013) 054009 [`arXiv:1305.1100`] [INSPIRE].

[26] M. Ferreira, P. Costa, D.P. Menezes, C. Providência and N. Scoccola, *Deconfinement and chiral restoration within the* SU(3) *Polyakov-Nambu-Jona-Lasinio and entangled Polyakov-Nambu-Jona-Lasinio models in an external magnetic field*, *Phys. Rev.* **D 89** (2014) 016002 [`arXiv:1305.4751`] [INSPIRE].

[27] V.D. Orlovsky and Y.A. Simonov, *The quark-hadron thermodynamics in magnetic field*, *Phys. Rev.* **D 89** (2014) 054012 [`arXiv:1311.1087`] [INSPIRE].

[28] E.S. Fraga, B.W. Mintz and J. Schaffner-Bielich, *A search for inverse magnetic catalysis in thermal quark-meson models*, *Phys. Lett.* **B 731** (2014) 154 [`arXiv:1311.3964`] [INSPIRE].

[29] C. Wetterich, *Average action and the renormalization group equations*, *Nucl. Phys.* **B 352** (1991) 529 [INSPIRE].

[30] D. Ebert, K.G. Klimenko, M.A. Vdovichenko and A.S. Vshivtsev, *Magnetic oscillations in dense cold quark matter with four fermion interactions*, *Phys. Rev.* **D 61** (2000) 025005 [`hep-ph/9905253`] [INSPIRE].

[31] S.S. Avancini, D.P. Menezes, M.B. Pinto and C. Providência, *The QCD critical end point under strong magnetic fields*, *Phys. Rev.* **D 85** (2012) 091901 [`arXiv:1202.5641`] [INSPIRE].

[32] K. Fukushima, *Chiral effective model with the Polyakov loop*, *Phys. Lett.* **B 591** (2004) 277 [`hep-ph/0310121`] [INSPIRE].

[33] E. Megias, E. Ruiz Arriola and L.L. Salcedo, *Polyakov loop in chiral quark models at finite temperature*, *Phys. Rev.* **D 74** (2006) 065005 [`hep-ph/0412308`] [INSPIRE].

[34] D.F. Litim, *Optimized renormalization group flows*, *Phys. Rev.* **D 64** (2001) 105007 [`hep-th/0103195`] [INSPIRE].

[35] N. Strodthoff, B.-J. Schaefer and L. von Smekal, *Quark-meson-diquark model for two-color QCD*, *Phys. Rev.* **D 85** (2012) 074007 [`arXiv:1112.5401`] [INSPIRE].

[36] K. Kamikado, N. Strodthoff, L. von Smekal and J. Wambach, *Fluctuations in the quark-meson model for QCD with isospin chemical potential*, *Phys. Lett.* **B 718** (2013) 1044 [`arXiv:1207.0400`] [INSPIRE].

[37] O. Lourenço, M. Dutra, A. Delfino and M. Malheiro, *Hadron-quark phase transition in a hadronic and Polyakov-Nambu-Jona-Lasinio models perspective*, *Phys. Rev.* **D 84** (2011) 125034 [`arXiv:1201.1239`] [INSPIRE].

[38] B.-J. Schaefer, M. Wagner and J. Wambach, *Thermodynamics of* $(2+1)$*-flavor QCD: confronting models with lattice studies*, *Phys. Rev.* **D 81** (2010) 074013 [`arXiv:0910.5628`] [INSPIRE].

[39] C. Ratti, M.A. Thaler and W. Weise, *Phases of QCD: lattice thermodynamics and a field theoretical model*, *Phys. Rev.* **D 73** (2006) 014019 [`hep-ph/0506234`] [INSPIRE].

[40] F. Karsch, E. Laermann and A. Peikert, *Quark mass and flavor dependence of the QCD phase transition*, *Nucl. Phys.* **B 605** (2001) 579 [`hep-lat/0012023`] [INSPIRE].

[41] S. Roessner, C. Ratti and W. Weise, *Polyakov loop, diquarks and the two-flavour phase diagram*, *Phys. Rev.* **D 75** (2007) 034007 [`hep-ph/0609281`] [INSPIRE].

[42] C. Ratti, S. Roessner, M.A. Thaler and W. Weise, *Thermodynamics of the PNJL model*, *Eur. Phys. J.* **C 49** (2007) 213 [`hep-ph/0609218`] [INSPIRE].

[43] K. Fukushima, *Phase diagrams in the three-flavor Nambu-Jona-Lasinio model with the Polyakov loop*, *Phys. Rev.* **D 77** (2008) 114028 [*Erratum ibid.* **D 78** (2008) 039902] [`arXiv:0803.3318`] [INSPIRE].

[44] B.-J. Schaefer, J.M. Pawlowski and J. Wambach, *The phase structure of the Polyakov-quark-meson model*, *Phys. Rev.* **D 76** (2007) 074023 [`arXiv:0704.3234`] [INSPIRE].

[45] T.K. Herbst, J.M. Pawlowski and B.-J. Schaefer, *The phase structure of the Polyakov-quark-meson model beyond mean field*, *Phys. Lett.* **B 696** (2011) 58 [`arXiv:1008.0081`] [INSPIRE].

[46] T.K. Herbst, J.M. Pawlowski and B.-J. Schaefer, *Phase structure and thermodynamics of QCD*, *Phys. Rev.* **D 88** (2013) 014007 [`arXiv:1302.1426`] [INSPIRE].

[47] A. Dumitru, R.D. Pisarski and D. Zschiesche, *Dense quarks, and the fermion sign problem, in a* $\mathrm{SU}(N)$ *matrix model*, *Phys. Rev.* **D 72** (2005) 065008 [`hep-ph/0505256`] [INSPIRE].

[48] K. Fukushima and Y. Hidaka, *A model study of the sign problem in the mean-field approximation*, *Phys. Rev.* **D 75** (2007) 036002 [`hep-ph/0610323`] [INSPIRE].

[49] S. Roessner, T. Hell, C. Ratti and W. Weise, *The chiral and deconfinement crossover transitions: PNJL model beyond mean field*, *Nucl. Phys.* **A 814** (2008) 118 [`arXiv:0712.3152`] [INSPIRE].

[50] B.W. Mintz, R. Stiele, R.O. Ramos and J. Schaffner-Bielich, *Phase diagram and surface tension in the three-flavor Polyakov-quark-meson model*, *Phys. Rev.* **D 87** (2013) 036004 [`arXiv:1212.1184`] [INSPIRE].

[51] K.G. Klimenko, *Three-dimensional Gross-Neveu model at nonzero temperature and in an external magnetic field*, *Z. Phys.* **C 54** (1992) 323 [INSPIRE].

[52] V.P. Gusynin, V.A. Miransky and I.A. Shovkovy, *Catalysis of dynamical flavor symmetry breaking by a magnetic field in* $(2+1)$*-dimensions*, *Phys. Rev. Lett.* **73** (1994) 3499 [*Erratum ibid.* **76** (1996) 1005] [`hep-ph/9405262`] [INSPIRE].

[53] I.A. Shovkovy, *Magnetic catalysis: a review*, *Lect. Notes Phys.* **871** (2013) 13 [`arXiv:1207.5081`] [INSPIRE].

[54] T. Inagaki, D. Kimura and T. Murata, *Four fermion interaction model in a constant magnetic field at finite temperature and chemical potential*, *Prog. Theor. Phys.* **111** (2004) 371 [`hep-ph/0312005`] [INSPIRE].

[55] F. Preis, A. Rebhan and A. Schmitt, *Inverse magnetic catalysis in dense holographic matter*, *JHEP* **03** (2011) 033 [`arXiv:1012.4785`] [INSPIRE].

[56] T.D. Cohen and N. Yamamoto, *New critical point for QCD in a magnetic field*, *Phys. Rev.* **D 89** (2014) 054029 [`arXiv:1310.2234`] [INSPIRE].

Paper II

Inverse magnetic catalysis and regularization in the quark-meson model.
JHEP, 1502:205, 2015.

Published for SISSA by Springer

Received: October 24, 2014
Revised: December 16, 2014
Accepted: January 6, 2015
Published: February 6, 2015

Inverse magnetic catalysis and regularization in the quark-meson model

JHEP02(2015)042

Jens O. Andersen,[a] **William R. Naylor**[a] **and Anders Tranberg**[b]

[a] *Department of Physics, Norwegian University of Science and Technology,*
Høgskoleringen 5, N-7491 Trondheim, Norway
[b] *Faculty of Science and Technology, University of Stavanger,*
N-4036 Stavanger, Norway

E-mail: `andersen@tf.phys.ntnu.no`, `william.naylor@ntnu.no`, `anders.tranberg@uis.no`

Abstract: Motivated by recent work on inverse magnetic catalysis at finite temperature, we study the quark-meson model using both dimensional regularization and a sharp cutoff. We calculate the critical temperature for the chiral transition as a function of the Yukawa coupling in the mean-field approximation varying the renormalization scale and the value of the ultraviolet cutoff. We show that the results depend sensitively on how one treats the fermionic vacuum fluctuations in the model and in particular on the regulator used. Finally, we explore a B-dependent transition temperature for the Polyakov loop potential $T_0(B)$ using the functional renormalization group. These results show that even arbitrary freedom in the function $T_0(B)$ does not allow for a decreasing chiral transition temperature as a function of B. This is in agreement with previous mean-field calculations.

Keywords: Quark-Gluon Plasma, Chiral Lagrangians, Phase Diagram of QCD, Sigma Models

ArXiv ePrint: 1410.5247

Open Access, © The Authors.
Article funded by SCOAP^3.

doi:10.1007/JHEP02(2015)042

Contents

1 **Introduction** 1

2 **The quark-meson model** 2

3 **Mean-field approximation** 3

4 **Numerical results** 5

5 **Discussion and conclusion** 9

---

1 Introduction

In recent years QCD in a strong magnetic field has received considerable attention. This interest has partly been spurred by non-central heavy-ion collisions at the Relativistic Heavy-Ion Collider and the Large Hadron Collider. In these experiments, time-dependent magnetic fields on the order of $|eB| \sim 5m_\pi^2$ are created [1–3] and so detailed knowledge of strongly interacting matter in external fields is necessary.

At $T = 0$, the response of the QCD vacuum to an external magnetic field is well-known. Lattice calculations as well as calculations using the Nambu-Jona-Lasinio (NJL) model [4–10], the quark-meson (QM) model [11], Schwinger-Dyson equations for QED [12] and QCD [13], and the Walecka model [14] show that the chiral condensate increases as a function of the external magnetic field B. Moreover, even the weakest magnetic fields induce a chiral condensate and thus dynamical chiral symmetry breaking if chiral symmetry is intact at $B = 0$.

The fact that the chiral condensate at zero temperature grows as a function of the magnetic field might lead to the expectation that the critical temperature for the chiral transition (T_c) increases as well. Indeed, mean-field calculations employing the NJL model or the Polyakov loop extended NJL (PNJL) [15–17] model as well as the (P)QM model [18–23] show that the critical temperature is an increasing function of the magnetic field. This qualitative behavior is independent of the masses of the σ and π mesons. Additionally, the inclusion of mesonic fluctuations by applying the functional renormalization group (FRG) does not qualitatively change this picture [24–27].

Results from lattice calculations tell a different story. It is seen that the behaviour of T_c with B is only increasing at unrealistically large values of the pion masses [28, 29], however with physical pion masses T_c is seen to decrease with B [30–34]. A number of groups have begun altering the standard treatment of chiral models to include a mechanism for this inverse magnetic catalysis around T_c [35–41]. Two such alterations to the PQM model are to allow either the Yukawa coupling, or the transition temperature of the gluonic sector, to vary with magnetic field. The former is further motivated by two recent papers utilizing the NJL model that were able to demonstrate inverse magnetic catalysis around T_c by varying the four-point coupling [37, 38]. However, in a recent paper by Fraga et al. [35] it was shown that neither of these freedoms were sufficient to obtain inverse magnetic catalysis around T_c, other than for a limited range of low values of the magnetic field.

Motivated both by the seemingly conflicting results coming from the NJL model, and the extension of the work of Fraga et al. [35] to a functional renormalization group (FRG) treatment we investigate the effects of varying the Yukawa coupling, g, within the QM model. We use two different regularization schemes, namely dimensional regularization (DR) and a sharp cutoff. It is seen that simply varying g whilst employing a sharp cutoff gives results that are quantitatively and qualitatively dependent upon the scale of the cutoff, whilst using DR one obtains results that are independent of the renormalization scale. We also investigate varying the transition temperature of the gluonic potential within the PQM model using the FRG and find, in agreement with the prediction of [35], that the FRG does not allow for inverse magnetic catalysis over an extended range of magnetic field values.

It is worth noting that varying the coupling g in an arbitrary fashion amounts to modelling the B-dependence of physics beyond the NJL/QM models through an effective coupling $g(B)$. Ideally, such a dependence would be derived directly from QCD, or encoded through some well-motivated higher-dimensional effective operators dependent upon both g and B. But as we will see below (see also [35]), even a completely general $g(B)$ seems to be insufficient to provide inverse catalysis, irrespective of its origin. In a sense this is a much stronger conclusion than considering just a single realization of such a dependence. Following [35], we therefore explicitly refrain from specifying the origin of the B-dependence og g. We will reach a similar conclusion to [35], but also demonstrate that it has certain loop-holes.

The paper is organized as follows. In section 2, we briefly discuss the quark-meson model. In section 3, we calculate the effective potential in the mean-field approximation using different regularizations. In section 4, we present our results for the phase diagram as a function of g, $\Lambda_{\mathrm{UV/DR}}$ (the cutoff/DR scale) and finally T_0. In section 5 we discuss the results and briefly summarize our work.

2 The quark-meson model

The quark-meson model is a low-energy effective theory for chiral symmetry in QCD. In two-flavor QCD it couples the $O(4)$-symmetric linear sigma model to a massless quark doublet via the Yukawa coupling g. The Euclidean Lagrangian in a magnetic field is then given by

$$\begin{aligned}\mathcal{L} = {}& \frac{1}{2}\left[(\partial_\mu\sigma)^2 + (\partial_\mu\pi_0)^2\right] + (D_\mu\pi^+)^\dagger D_\mu\pi^+ + \frac{1}{2}m^2\left(\varphi^\dagger\varphi\right) + \frac{\lambda}{24}\left(\varphi^\dagger\varphi\right)^2 - h\sigma \\ & + \bar{\psi}\left[\gamma_\mu D_\mu + g(B)(\sigma - \gamma_5\boldsymbol{\tau}\cdot\boldsymbol{\pi})\right]\psi\ ,\end{aligned} \tag{2.1}$$

where the covariant derivative is $D_\mu = \partial_\mu - iq_f A_\mu^{\mathrm{EM}}$, with q_f a diagonal matrix of the electric charges of the up and down quarks. $\boldsymbol{\tau}$ are the Pauli matrices, $\varphi^\dagger = (\sigma, \pi_0, \pi_1, \pi_2)$

and $\pi^{\pm}=\frac{1}{\sqrt{2}}(\pi_1 \pm i\pi_2)$. The fermion field is an isospin doublet,

$$\psi = \begin{pmatrix} u \\ d \end{pmatrix} \ , \tag{2.2}$$

which, as stated, couples to the mesonic sector via the Yukawa coupling $g(B)$, where we have indicated explicitly that this will be allowed to vary with B. We make no assumptions as to the manner of this dependence, and simply investigate the available parameter space when any such dependence is allowed (as was done in [35]).

In the absence of external gauge fields the Lagrangian (2.1) is $O(4)$ symmetric if $h=0$ and $O(3)$ symmetric if $h\neq 0$. In the presence of a background Abelian gauge field, the $O(4)$ symmetry is reduced to an $O(2)\times O(2)$ symmetry, because of the different electric charges of the u and d quarks.

Chiral symmetry (or approximate chiral symmetry when $h\neq 0$) is broken in the vacuum by a nonzero expectation value ϕ for the sigma field. Expanding σ around this mean field ϕ we define

$$\sigma = \phi + \tilde{\sigma} \ , \tag{2.3}$$

where $\tilde{\sigma}$ is a quantum fluctuating field with vanishing expectation value. The tree-level potential is then

$$\mathcal{V}_0 = \frac{1}{2}m^2\phi^2 + \frac{\lambda}{24}\phi^4 - h\phi \ . \tag{2.4}$$

3 Mean-field approximation

In the one-loop approximation, one takes into account the Gaussian fluctuations around the mean-field ϕ. The one-loop effective potential can then be written as a sum of the tree-level term (2.4) and the one-loop contributions from the sigma, the pions, and the quarks. Furthermore, it is a common approximation in the QM model to omit the quantum and thermal fluctuations of the bosons, i.e. treat them at tree level [18, 42].

The one-loop contribution to the effective potential is then given by

$$\begin{aligned} \mathcal{V}_1 &= -\sum_f \mathrm{Tr}\log\left[i\gamma_\mu D_\mu + m_f\right] \\ &= \sum_{P_0,f,n,s} -\frac{|q_fB|}{2\pi}\int_{p_z}\log\left[P_0^2+p_z^2+m_f^2+|q_fB|(2n+1-s)\right] \ , \end{aligned} \tag{3.1}$$

where the trace is over Dirac and color indices and in space-time and $m_u=m_d=g(B)\phi$. Summing over the Matsubara frequencies in eq. (3.1), we find

$$\mathcal{V}_1 = -\sum_{f,n,s}\frac{|q_fB|}{2\pi}\int_{p_z}\left\{\sqrt{p_z^2+m_f^2+|q_fB|(2n+1-s)} - 2T\log\left[1+e^{-\beta\sqrt{p_z^2+m_f^2+|q_fB|(2n+1-s)}}\right]\right\} \ . \tag{3.2}$$

The integral over p_z for the zero temperature term is divergent and is typically regularized using dimensional regularization in $d = 1 - 2\epsilon$ dimensions. The sum over Landau levels is then subsequently regulated using ζ-function regularization. The resulting expression is then expanded around $\epsilon = 0$ and the poles in ϵ are removed by renormalization of the parameters in the Lagrangian in the usual way. The details of this calculation can be found in [23]. The result for the renormalized one-loop effective potential reads

$$\begin{aligned}\mathcal{V}_{\mathrm{DR}} = {} & \frac{1}{2}m^2\phi^2 + \frac{\lambda}{24}\phi^4 - h\phi + \frac{N_c m_q^4}{(4\pi)^2}\sum_f\left[\log\frac{\Lambda_{\mathrm{DR}}^2}{|2q_fB|} + 1\right] - \frac{N_c}{2\pi^2}\sum_f (q_fB)^2\Big[\zeta^{(1,0)}(-1,x_f) \\ & +\frac{1}{2}x_f\log x_f\Big] - N_c\sum_{s,f,k}\frac{|q_fB|T}{\pi^2}\int_0^\infty dp\log\left[1 + e^{-\beta\sqrt{p^2+M_q^2}}\right]\ ,\end{aligned} \tag{3.3}$$

where $x_f = \frac{m_f^2}{|2q_fB|}$ and $M_f^2 = \sqrt{m_f^2 + |q_fB|(2k+1-s)}$, Λ_{DR} is the renormalization scale associated with the modified minimal subtraction scheme and $\zeta(a,x)$ is the Hurwitz zeta-function.

Although not often employed in renormalizable theories, there is nothing that prevents from using a sharp ultraviolet cutoff Λ_{UV} to regulate the divergent integrals. The effective potential is then

$$\begin{aligned}\mathcal{V}_{\mathrm{cut}} = {} & \frac{1}{2}m^2\phi^2 + \frac{\lambda}{24}\phi^4 - h\phi + \frac{2N_c}{(4\pi)^2}\sum_f\Big\{ - \Lambda_{\mathrm{UV}}\sqrt{\Lambda_{\mathrm{UV}}^2 + m_f^2}(2\Lambda_{\mathrm{UV}}^2 + m_f^2) \\ & +m_f^4\log\frac{\Lambda_{\mathrm{UV}} + \sqrt{\Lambda_{\mathrm{UV}}^2 + m_f^2}}{m_f} - \frac{1}{4}m_f^4 - 4(q_fB)^2\left[\zeta^{(1,0)}(-1,x_f) - \frac{1}{2}(x_f^2 - x_f)\log x_f\right]\Big\} \\ & -N_c\sum_{s,f,k}\frac{|q_fB|T}{\pi^2}\int_0^\infty dp\log\left[1 + e^{-\beta\sqrt{p^2+M_q^2}}\right]\ .\end{aligned} \tag{3.4}$$

Comparing the two expressions, eqs. (3.3) and (3.4), we see that they have similar structure, other than the presence of an additional term coupling various powers of $m_f = g\phi$ and Λ_{UV}. Additionally the finite temperature term is independent of the regularization scheme.

The effective potential $\mathcal{V}_{\mathrm{DR}}(\phi)$ ($\mathcal{V}_{\mathrm{cut}}(\phi)$) depends upon the parameters λ, m^2, g, h and Λ_{DR} (Λ_{UV}). As we will explore the dependence of the transition temperatures on Λ_{DR} and Λ_{UV}, these are left as completely 'free'. Without explicit symmetry breaking the pions are true Goldstone bosons, i.e. we need not fix m_π as it is automatically zero. At nonzero pion mass we adjust h to set m_π. The pion decay constant, f_π, and sigma mass m_σ in the vacuum, $T = B = 0$, are fixed by tuning λ and m^2. All these must be tuned for every different value of Λ_{DR} or Λ_{UV} and of course they will be different for the different regularization schemes. We use the values $f_\pi = 93\,\mathrm{MeV}$ and $m_\sigma = 530\,\mathrm{MeV}$ throughout this paper, and at the physical point $m_\pi = 139\,\mathrm{MeV}$. Finally the Yukawa coupling, $g = g(B)$, at $B = 0$ is set to 3.2258 such that the constituent quark mass is $g\phi = 300\,\mathrm{MeV}$. However at finite B and T we will allow this to vary whilst holding m^2 and λ fixed.

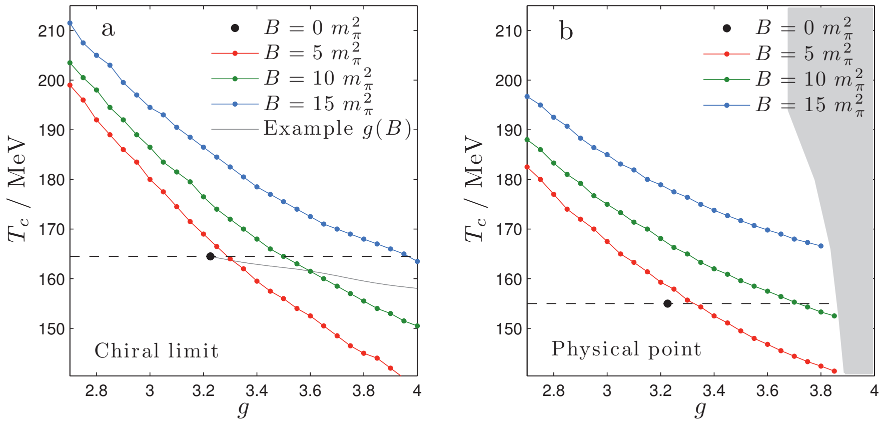

Figure 1. Chiral transition temperature as a function of possible value of the Yukawa coupling for the chiral limit (1a) and the physical point (1b). The plots show that a function $g(B)$ starting at $g = 3.2258$, •, can give inverse magnetic catalysis up to around 10 m_π^2 at the physical point. Beyond this the theory breaks down (grey region). See text for details.

4 Numerical results

Our initial motivation was to use the FRG to see if the conclusions in ref. [35] would be altered when including mesonic fluctuations. It turns out that FRG seems to open for the possibility of inverse magnetic catalysis. However, the flow equation involves integration of momenta k from a sharp ultraviolet cutoff Λ_{FRG} down to $k = 0$ and the naive use of this cutoff proves problematic.

Following ref. [35], in figure 1, we plot the critical temperature for the chiral transition as a function of the Yukawa coupling $g(B)$ for various values of B. Figure 1a gives the results in the chiral limit, while figure 1b is at the physical point. The curves are obtained using the dimensionally regulated mean-field result, eq. (3.3), with $\Lambda_{\text{DR}} = 182\,\text{MeV}$, as was used in [23]. The results shown in figure 1 are in approximate agreement with those of Fraga et al. [35]. At the physical point (1b) we see that the critical temperature becomes undefined at high B and $g(B)$, as given by the grey region. We return to this point shortly.

Figure 1 is understood as follows: at $B = 0$ the constituent quark mass fixes the Yukawa coupling, and thus the chiral transition temperature is fixed to be 165 MeV (155 MeV at the physical point), as is given by •. The dashed black line is simply a visual guide to distinguish catalysis from inverse catalysis. Moving to finite magnetic field the value of the Yukawa coupling as a function of B and T is not known, thus we allow for any possible dependence. Any particular function $g(B)$ is a curve beginning at • and successively intersecting the various contours of increasing B. One such function $g(B)$ is given by the grey line in figure 1a. If the functional dependence is given by

$$g(B) = g(0)\left[1 + a(B/m_\pi^2)^b\right] \tag{4.1}$$

JHEP02(2015)042

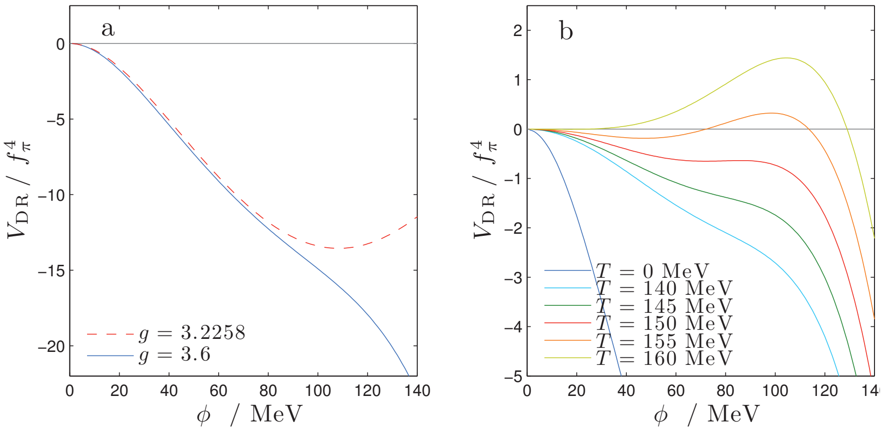

Figure 2. 2a gives the mean-field potential in the chiral limit for $g = 3.2258$ and 3.6 at $T = 0$. We see at $g = 3.6$ that the theory has an unstable vacuum. 2b is the potential with $g = 3.6$ for increasing T. It is seen that the potential develops a local minimum at positive, finite ϕ before the transition temperature, which lies at 161.5 MeV. In both plots $B = 10\ m_\pi^2$.

then this grey line corresponds approximately to $a = 0.0008$ and $b = 2.2$. Here g increases with B in such a way as to give inverse magnetic catalysis up to at least 12 m_π^2. An even simpler function is a line moving vertically upwards from •. This corresponds to the standard case, where one assumes the Yukawa coupling is independent of B and T i.e. $a = b = 0$. In this case, of course, we find T_c, increasing with B, i.e. magnetic catalysis.

After inspection of figure 1a it seems quite possible to create a function $g(B)$ such that we have inverse magnetic catalysis over a large range of magnetic field strength. However the complete picture is more complex as is shown at the physical point, given in figure 1b. Firstly, the change in the definition of the critical temperature (from a second order transition, to a cross over with a pseudocritical temperature) flattens the curves of constant B such that a greater change in g is required for the same change in B and the total range of B values over which one could have inverse catalysis is reduced (for example the blue $B = 15\ m_\pi^2$ curve may never cross the dashed line even if it could be continued to infinitely high g). More problematic than this, at large g (given by the grey region), the theory breaks down. We now explain this with the help of figure 2.

As is well known, at very large values of the field ϕ the mean-field potential becomes unbounded from below, due to the log term in the zero temperature expression (eq. (3.3) for the DR scheme). This term is proportional to the fourth power of the quark mass, so it is greatly influenced by varying the Yukawa coupling. This is evident from figure 2a, where we see at $T = 0$ MeV, $B = 10\ m_\pi^2$ that changing g from 3.2258 to 3.6, the local minimum disappears altogether giving us unbounded (unphysical) results, indeed for $g > 3.35$ this is the case. Thus if g is *only* a function of B then we may not vary it higher than 3.35. However, in figure 2b we now show the change in the potential with T with $B = 10\ m_\pi^2$,

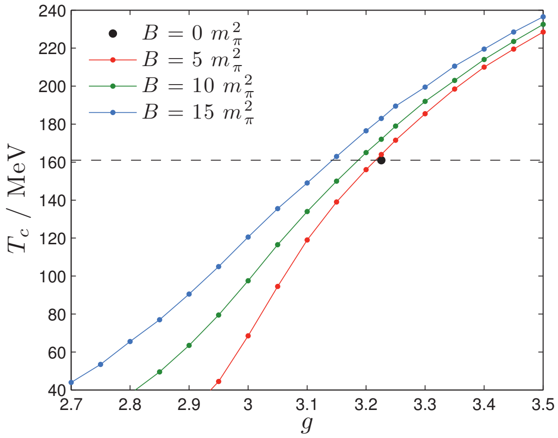

Figure 3. T_c plotted against g using a sharp cutoff of 800 MeV. It is seen that a decreasing function $g(B)$ could give inverse magnatic catalysis, however, as noted in the text, this result depends heavily upon the value of the cutoff.

$g = 3.6$ and in the chiral limit. As T increases, we first develop a local minimum, like we have in the zero T, $g = 3.2258$ case, and then the potential undergoes the usual chiral phase transition. Because the transition temperature in the chiral limit essentially involves investigating the potential around $\phi = 0$ we are able to define the transition temperature even for very large values of g and B. But as g is pushed higher and higher, the region where we have a local minimum becomes smaller, both in T and ϕ. For this reason at finite B we will allow g to be a function of both B and T such that we have the maximum flexibility in g with which to obtain inverse magnetic catalysis. At the physical point the definition of the pseudocritical temperature involves investigation of a finite value of the field ϕ, in our case where it is equal to half the zero temperature value (but note this is not changed when investigating the inflection point). In this case even moderate values of g and B give unphysical results, as is given by the grey region in figure 1b. This is the primary reason that disallows inverse magnetic catalysis even allowing g to be a function of both B and T.

We now turn out attention to the QM model with a sharp cutoff, choosing a value of 800 MeV, as was used in our previous calculations using FRG [25, 26]. The plot corresponding to the previous figure 1 is given in figure 3. These results are qualitatively the same as those we found using the FRG. The observed behaviour is reversed as compared with the dimensionally regulated result, most obviously T_c is an increasing function of g for any fixed B is, while it was a decreasing function in the dimensionally regulated theory. In addition we see that it is possible to choose a function $g(B, T)$ that gives inverse magnetic catalysis. Both as the curves become steeper as we move from 3.2258 to approximately 3 (the region of interest here), but also because g must decrease to obtain inverse magnetic catalysis, thus avoiding the problems of an unbounded potential seen above. However we

JHEP02(2015)042

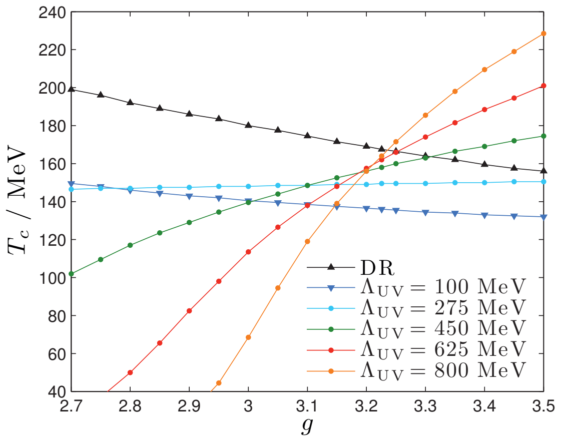

Figure 4. T_c with $g(B)$ for various values of U_{DR} and U_{UV} for both regularization schemes. For the dimensionally regularized theory only a single curve (black 'up' triangles) is given as all values of the renormalization scale between 100 and 800 MeV have T_c within ± 2 MeV of the curve given, which is calculated using $\Lambda = 182\,\mathrm{MeV}$. In the sharp cutoff theory with $\Lambda = 100\,\mathrm{MeV}$ (blue 'down' triangles) the phase transition is of first order, all other transition are second order. The plot shows the heavy dependence of the cutoff theory on the value of the cutoff.

stress that this result is heavily dependent upon the cutoff used and thus this conclusion should not be used out of context. We now turn our attention to this cutoff dependence.

In figure 4 we plot T_c for only a single value of the magnetic field, instead varying the cutoff. The parameter fixing we discussed in section 3 is done for each different value of Λ_{DR} and Λ_{UV}, thus at $g = 3.2258$, f_π, m_σ, m_π and m_q are equal for each curve. We plot only a single value of Λ_{DR} for the theory using DR as the results are within ±2 MeV for all cutoff values between 100 and 800 MeV. For both regularization schemes the finite T terms are exactly the same, and the zero T components are also very similar with exception that the sharp cutoff theory adds a term of the form $-\Lambda_{\mathrm{UV}}\sqrt{\Lambda_{\mathrm{UV}}^2 + m_f^2}(2\Lambda_{\mathrm{UV}}^2 + m_f^2)$. Figure 4 shows that using a large cutoff this term begins to dominate the behaviour as we increase g, lowering the potential and thus increasing T_c.

It has been suggested that the backreaction of the quarks to the gluons plays a primary role in inverse magnetic catalysis [33], thus a natural first step towards inverse magnetic catalysis in Polyakov loop coupled models would be via tuning the gluonic potential. In [35] this was done at mean-field level, where they concluded that it was not possible to obtain inverse magnetic catalysis by simply varying the gluonic transition temperature, T_0. We show that this result remains unchanged with the inclusion of mesonic fluctuations in figure 5, which is calculated using the FRG. We do not introduce the full machinery of the FRG, instead referring the reader to [26]. The methods are the same as in that paper, other than that we rerun the calculation for varying values of T_0, which is a free parameter in the model. For the physical observables f_π, m_f, m_π and m_σ, the values are the same as

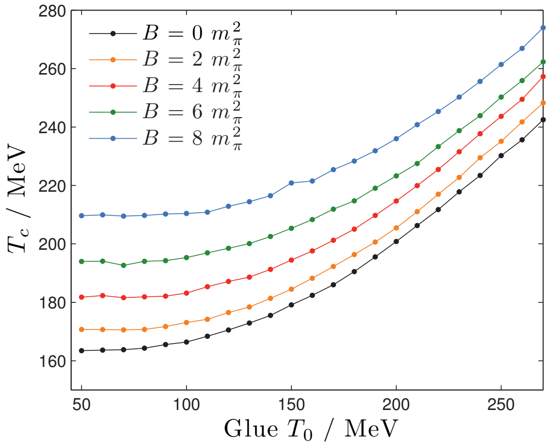

Figure 5. T_c with varying T_0 for various values of B. Note that the scaling in B is more gradual than in previous plots. We see that it is not possible to have inverse magnetic catalysis given any possible function $T_0(B)$ if we also require that $T_c(B = 0) \sim T_d(B = 0)$.

we used in the physical point, mean-field calculations and we have $\Lambda_{\text{FRG}} = 800\,\text{MeV}$. The figure can be read in the same way as figure 1, but with T_0 in the place of g. At $B = 0$, T_0 is usually taken as $\sim 210\,\text{MeV}$ with two flavours of quarks. This value also ensures that T_c is approximately equal to the deconfinement transition temperature, T_d. Using this as the zero-B starting point we see that the curves are simply too flat (and become increasingly so as we decrease T_0) to allow for inverse magnetic catalysis up to magnetic fields over $B \sim 4\ m_\pi^2$. Thus we find in agreement with the prediction of [35] that using the FRG, there is no possible function $T_0(B)$ which could give inverse magnetic catalysis.

5 Discussion and conclusion

In the quark-meson model, one chooses a regularization prescription and fixes the associated scale ($\Lambda = \Lambda_{\text{DR}}$, Λ_{UV}, Λ_{FRG}) and then sets m^2, λ, h and g to obtain the correct values of the particle masses and pion decay constant in the vacuum. In doing so the model's dependence upon Λ is essentially cancelled out. The model is useful because we may then vary external parameters without introducing strong Λ dependence and thus investigate physics outside of the vacuum. But in varying g there is no guarantee that the model will be Λ independent, and as figure 4 shows, when using a cutoff this is not the case. The real problem here, in terms of modelling inverse magnetic catalysis, is not only that it is not possible to generate meaningful results in the mean-field approximation using a sharp cutoff, but that it is not possible to do so using the FRG, as it suffers from exactly the same problems.

Usually it is the case that the inclusion of mesonic fluctuations has some quantitative effect upon the chiral transition temperature but that the results remain qualitatively the

JHEP02(2015)042

same. However we have seen from lattice results that inverse magnetic catalysis is dependent upon the pion mass. But usually in model calculations only the mesonic fluctuations are dependent upon the pion mass, thus indicating their importance. Moreover varying the pion mass amounts to varying m^2 and λ in eq. (3.3) or (3.4). But as there is no coupling between g and either of these variables, varying m_π simply shifts all of the curves in figure 1 either up or down, something we have checked explicitly. Thus to fully reproduce the lattice results at mean-field by varying g (if it was even possible) one would need $g(B, T, m_\pi)$.

We agree with the basic result of Fraga et al. [35], that within the QM model it is not possible to reproduce lattice results by simply utilizing $g(B)$, even if we allow complete freedom in this functional dependence. However, as we use different regularization the reason for this is very different. Moreover we find within our own results that the transition temperature as a function of g depends in detail of how one treats the vacuum fluctuations. It is not only a question of whether to include them or not, as in the case of the order of the transition, but it also depends upon the exact implementation of the regularization scheme. Allowing g to run with B acknowledges that there exists physics not captured by the quark-meson model yet vital in mapping out the chiral phase diagram. But this physics must be incorperated in such a way that reliable computations can still be made. This is not the case when simply varying g using a sharp cutoff and only approximately true in dimensional regularization.

We have refrained from explicitly stating where the effective B-dependence comes from. In full renormalizable QCD the B-dependence can not depend on the regularization, and the expectation is therefore that any effective theory should share this feature. The way forward seems to be to augment the PNJL or PQM model with a selection of additional operators and perform a consistent renormalization of the quantum theory. In particular any such operators would provide additional counterterms to cancel out residual cutoff dependence through some additional renormalization condition.

Acknowledgments

AT is supported by a Villum Foundation Young Investigator Grant.

Open Access. This article is distributed under the terms of the Creative Commons Attribution License (CC-BY 4.0), which permits any use, distribution and reproduction in any medium, provided the original author(s) and source are credited.

References

[1] D.E. Kharzeev, L.D. McLerran and H.J. Warringa, *The Effects of topological charge change in heavy ion collisions: 'Event by event P and CP-violation'*, Nucl. Phys. **A 803** (2008) 227 [`arXiv:0711.0950`] [INSPIRE].

[2] V. Skokov, A.Y. Illarionov and V. Toneev, *Estimate of the magnetic field strength in heavy-ion collisions*, Int. J. Mod. Phys. **A 24** (2009) 5925 [`arXiv:0907.1396`] [INSPIRE].

[3] A. Bzdak and V. Skokov, *Event-by-event fluctuations of magnetic and electric fields in heavy ion collisions*, Phys. Lett. **B 710** (2012) 171 [`arXiv:1111.1949`] [INSPIRE].

[4] S.P. Klevansky and R.H. Lemmer, *Chiral symmetry restoration in the Nambu-Jona-Lasinio model with a constant electromagnetic field*, Phys. Rev. **D 39** (1989) 3478 [INSPIRE].

[5] D. Ebert, K.G. Klimenko, M.A. Vdovichenko and A.S. Vshivtsev, *Magnetic oscillations in dense cold quark matter with four fermion interactions*, Phys. Rev. **D 61** (2000) 025005 [`hep-ph/9905253`] [INSPIRE].

[6] K.G. Klimenko, *Three-dimensional Gross-Neveu model at nonzero temperature and in an external magnetic field*, Z. Phys. **C 54** (1992) 323 [INSPIRE].

[7] V.P. Gusynin, V.A. Miransky and I.A. Shovkovy, *Catalysis of dynamical flavor symmetry breaking by a magnetic field in (2+1)-dimensions*, Phys. Rev. Lett. **73** (1994) 3499 [*Erratum ibid.* **76** (1996) 1005] [`hep-ph/9405262`] [INSPIRE].

[8] V.P. Gusynin, V.A. Miransky and I.A. Shovkovy, *Dimensional reduction and catalysis of dynamical symmetry breaking by a magnetic field*, Nucl. Phys. **B 462** (1996) 249 [`hep-ph/9509320`] [INSPIRE].

[9] C.N. Leung, Y.J. Ng and A.W. Ackley, *Schwinger-Dyson equation approach to chiral symmetry breaking in an external magnetic field*, Phys. Rev. **D 54** (1996) 4181 [`hep-th/9512114`] [INSPIRE].

[10] D.S. Lee, C.N. Leung and Y.J. Ng, *Chiral symmetry breaking in a uniform external magnetic field*, Phys. Rev. **D 55** (1997) 6504 [`hep-th/9701172`] [INSPIRE].

[11] E.J. Ferrer and V. de la Incera, *Magnetic catalysis in the presence of scalar fields*, Phys. Lett. **B 481** (2000) 287 [`hep-ph/0004113`] [INSPIRE].

[12] C.N. Leung and S.-Y. Wang, *Gauge independent approach to chiral symmetry breaking in a strong magnetic field*, Nucl. Phys. **B 747** (2006) 266 [`hep-ph/0510066`] [INSPIRE].

[13] N. Mueller, J.A. Bonnet and C.S. Fischer, *Dynamical quark mass generation in a strong external magnetic field*, Phys. Rev. **D 89** (2014) 094023 [`arXiv:1401.1647`] [INSPIRE].

[14] A. Haber, F. Preis and A. Schmitt, *Magnetic catalysis in nuclear matter*, Phys. Rev. **D 90** (2014) 125036 [`arXiv:1409.0425`] [INSPIRE].

[15] R. Gatto and M. Ruggieri, *Dressed Polyakov loop and phase diagram of hot quark matter under magnetic field*, Phys. Rev. **D 82** (2010) 054027 [`arXiv:1007.0790`] [INSPIRE].

[16] R. Gatto and M. Ruggieri, *Deconfinement and Chiral Symmetry Restoration in a Strong Magnetic Background*, Phys. Rev. **D 83** (2011) 034016 [`arXiv:1012.1291`] [INSPIRE].

[17] K. Kashiwa, *Entanglement between chiral and deconfinement transitions under strong uniform magnetic background field*, Phys. Rev. **D 83** (2011) 117901 [`arXiv:1104.5167`] [INSPIRE].

[18] E.S. Fraga and A.J. Mizher, *Chiral transition in a strong magnetic background*, Phys. Rev. **D 78** (2008) 025016 [`arXiv:0804.1452`] [INSPIRE].

[19] A.J. Mizher, M.N. Chernodub and E.S. Fraga, *Phase diagram of hot QCD in an external magnetic field: possible splitting of deconfinement and chiral transitions*, Phys. Rev. **D 82** (2010) 105016 [`arXiv:1004.2712`] [INSPIRE].

[20] D.C. Duarte, R.L.S. Farias and R.O. Ramos, *Optimized perturbation theory for charged scalar fields at finite temperature and in an external magnetic field*, Phys. Rev. **D 84** (2011) 083525 [`arXiv:1108.4428`] [INSPIRE].

[21] M. Ruggieri, M. Tachibana and V. Greco, *Renormalized vs. Nonrenormalized Chiral Transition in a Magnetic Background*, *JHEP* **07** (2013) 165 [arXiv:1305.0137] [INSPIRE].

[22] M. Ruggieri, L. Oliva, P. Castorina, R. Gatto and V. Greco, *Critical Endpoint and Inverse Magnetic Catalysis for Finite Temperature and Density Quark Matter in a Magnetic Background*, *Phys. Lett.* **B 734** (2014) 255 [arXiv:1402.0737] [INSPIRE].

[23] J.O. Andersen and R. Khan, *Chiral transition in a magnetic field and at finite baryon density*, *Phys. Rev.* **D 85** (2012) 065026 [arXiv:1105.1290] [INSPIRE].

[24] V. Skokov, *Phase diagram in an external magnetic field beyond a mean-field approximation*, *Phys. Rev.* **D 85** (2012) 034026 [arXiv:1112.5137] [INSPIRE].

[25] J.O. Andersen and A. Tranberg, *The Chiral transition in a magnetic background: Finite density effects and the functional renormalization group*, *JHEP* **08** (2012) 002 [arXiv:1204.3360] [INSPIRE].

[26] J.O. Andersen, W.R. Naylor and A. Tranberg, *Chiral and deconfinement transitions in a magnetic background using the functional renormalization group with the Polyakov loop*, *JHEP* **04** (2014) 187 [arXiv:1311.2093] [INSPIRE].

[27] K. Kamikado and T. Kanazawa, *Chiral dynamics in a magnetic field from the functional renormalization group*, *JHEP* **03** (2014) 009 [arXiv:1312.3124] [INSPIRE].

[28] M. D'Elia, S. Mukherjee and F. Sanfilippo, *QCD Phase Transition in a Strong Magnetic Background*, *Phys. Rev.* **D 82** (2010) 051501 [arXiv:1005.5365] [INSPIRE].

[29] M. D'Elia and F. Negro, *Chiral Properties of Strong Interactions in a Magnetic Background*, *Phys. Rev.* **D 83** (2011) 114028 [arXiv:1103.2080] [INSPIRE].

[30] G. Endrodi, Z. Fodor, S.D. Katz and K.K. Szabo, *The QCD phase diagram at nonzero quark density*, *JHEP* **04** (2011) 001 [arXiv:1102.1356] [INSPIRE].

[31] G.S. Bali, F. Bruckmann, G. Endrodi, Z. Fodor, S.D. Katz et al., *QCD quark condensate in external magnetic fields*, *Phys. Rev.* **D 86** (2012) 071502 [arXiv:1206.4205] [INSPIRE].

[32] G.S. Bali, F. Bruckmann, G. Endrodi, Z. Fodor, S.D. Katz et al., *The QCD phase diagram for external magnetic fields*, *JHEP* **02** (2012) 044 [arXiv:1111.4956] [INSPIRE].

[33] F. Bruckmann, G. Endrodi and T.G. Kovacs, *Inverse magnetic catalysis and the Polyakov loop*, *JHEP* **04** (2013) 112 [arXiv:1303.3972] [INSPIRE].

[34] G.S. Bali, F. Bruckmann, G. Endrodi, F. Gruber and A. Schaefer, *Magnetic field-induced gluonic (inverse) catalysis and pressure (an)isotropy in QCD*, *JHEP* **04** (2013) 130 [arXiv:1303.1328] [INSPIRE].

[35] E.S. Fraga, B.W. Mintz and J. Schaffner-Bielich, *A search for inverse magnetic catalysis in thermal quark-meson models*, *Phys. Lett.* **B 731** (2014) 154 [arXiv:1311.3964] [INSPIRE].

[36] M. Ferreira, P. Costa, D.P. Menezes, C. Providência and N. Scoccola, *Deconfinement and chiral restoration within the* SU(3) *Polyakov-Nambu-Jona-Lasinio and entangled Polyakov-Nambu-Jona-Lasinio models in an external magnetic field*, *Phys. Rev.* **D 89** (2014) 016002 [arXiv:1305.4751] [INSPIRE].

[37] R.L.S. Farias, K.P. Gomes, G.I. Krein and M.B. Pinto, *Importance of asymptotic freedom for the pseudocritical temperature in magnetized quark matter*, *Phys. Rev.* **C 90** (2014) 025203 [arXiv:1404.3931] [INSPIRE].

[38] M. Ferreira, P. Costa, O. Lourenço, T. Frederico and C. Providência, *Inverse magnetic catalysis in the (2+1)-flavor Nambu-Jona-Lasinio and Polyakov-Nambu-Jona-Lasinio models*, *Phys. Rev.* **D 89** (2014) 116011 [`arXiv:1404.5577`] [inSPIRE].

[39] E.J. Ferrer, V. de la Incera and X.J. Wen, *Quark Antiscreening at Strong Magnetic Field and Inverse Magnetic Catalysis*, `arXiv:1407.3503` [inSPIRE].

[40] A. Ayala, M. Loewe, A.J. Mizher and R. Zamora, *Inverse magnetic catalysis for the chiral transition induced by thermo-magnetic effects on the coupling constant*, *Phys. Rev.* **D 90** (2014) 036001 [`arXiv:1406.3885`] [inSPIRE].

[41] A. Ayala, M. Loewe and R. Zamora, *Inverse magnetic catalysis in the linear σ-model with quarks*, *Phys. Rev.* **D 91** (2015) 016002 [`arXiv:1406.7408`] [inSPIRE].

[42] O. Scavenius, A. Mócsy , I.N. Mishustin and D.H. Rischke, *Chiral phase transition within effective models with constituent quarks*, *Phys. Rev.* **C 64** (2001) 045202 [`nucl-th/0007030`] [inSPIRE].

Paper III

Confronting effective models for deconfinement in dense quark matter
with lattice data.
Submitted to Physical Review D *arXiv:1505.05925*, 2015.

Prepared for submission to JHEP

Confronting effective models for deconfinement in dense quark matter with lattice data

arXiv:1505.05925v2 [hep-ph] 25 May 2015

Jens O. Andersen,[a] **Tomáš Brauner**[b] **and William Naylor**[a]

[b] *Department of Physics, Norwegian University of Science and Technology, Høgskoleringen 5, 7491 Trondheim, Norway*

[a] *Institute for Theoretical Physics, Vienna University of Technology, Wiedner Hauptstraße 8–10, 1040 Vienna, Austria*

E-mail: `jens.andersen@ntnu.no`, `brauner@hep.itp.tuwien.ac.at`, `william.naylor@ntnu.no`

Abstract: Ab initio numerical simulations of the thermodynamics of dense quark matter remain a challenge. Apart from the infamous sign problem, lattice methods have to deal with finite volume and discretization effects as well as with the necessity to introduce sources for symmetry-breaking order parameters. We study these artifacts in the Polyakov-loop-extended Nambu-Jona-Lasinio model, and compare its predictions to existing lattice data for cold and dense two-color matter with two flavors of Wilson quarks. To achieve even qualitative agreement with lattice data *requires* the introduction of two novel elements in the model: (i) explicit chiral symmetry breaking in the effective contact four-fermion interaction, referred to as the chiral twist, and (ii) renormalization of the Polyakov loop. The feedback of the dense medium to the gauge sector is modeled by a chemical-potential-dependent scale in the Polyakov-loop potential. In contrast to previously used analytical ansätze, we determine its dependence on the chemical potential from lattice data for the expectation value of the Polyakov loop. Finally, we propose to add a two-derivative operator to our effective model. This term acts as an additional source of explicit chiral symmetry breaking, mimicking an analogous term in the lattice Wilson action.

Keywords: Deconfinement, Nambu–Jona-Lasinio model, Polyakov loop

Contents

1 Introduction **1**

2 Two-color QCD **3**
- 2.1 Chiral perturbation theory 4
- 2.2 The puzzle and its resolution 6

3 The model **6**
- 3.1 Classification of operators 7
- 3.2 Effects of chiral symmetry breaking 8

4 Vacuum physics **9**
- 4.1 Parameter fixing 11
- 4.2 Role of the chiral twist 11

5 Zero temperature: chiral restoration **12**
- 5.1 Role of the diquark source 12
- 5.2 Role of the quark mass 14
- 5.3 Role of the chiral twist 15

6 Nonzero temperature: deconfinement **18**
- 6.1 Renormalization of the Polyakov loop 18
- 6.2 Zero chemical potential 19
- 6.3 Chemical potential dependence 20

7 Conclusions and outlook **23**

A Chiral model with a Wilson term **25**
- A.1 Three-momentum cutoff 25
- A.2 Pauli-Villars regularization 26
- A.3 Vacuum physics 27

1 Introduction

Hadronic matter in extreme conditions such as high temperature or high density has received considerable attention over the past decades. However, direct numerical simulations of the theory of strong interactions — quantum chromodynamics (QCD) — at nonzero baryon density are a formidable challenge due to the infamous sign problem. Large efforts have been made to overcome this problem (see for instance refs. [1–3] for some recent proposals), yet with limited success so far. At present, the only tools for quantitative analysis of dense nuclear matter are phenomenological effective models and, to some extent, continuum functional methods [4, 5].

Lattice simulations and phenomenological models can be of mutual benefit: while numerical simulations can provide a firm model-independent basis for effective continuum approaches, results obtained by the latter can be easily extrapolated to conditions where lattice techniques are difficult to apply. However, there is a gap that needs to be bridged to make this interaction possible. Lattice simulations have to deal with several artifacts, namely the effects of finite volume and spacetime discretization, as well as the need for external sources to pick a unique ground state whenever continuous symmetries are expected to be spontaneously broken. Usually, it is much easier to introduce these effects in models, rather than eliminate them from lattice simulations.

The main goal of the present paper is to do exactly that. We effectively re-introduce the effects of external sources and spacetime discretization using a phenomenological continuum model and focus on discriminating between physics and lattice artifacts. Our work is based upon results of recent simulations of two-color QCD (2cQCD) at high baryon density, using two flavors of Wilson-type quarks [6, 7]. These are compared to an effective model of the Nambu-Jona-Lasinio (NJL) type [8–10], augmented with the Polyakov loop, which is an (approximate) order parameter for deconfinement [11–13]. We discuss in detail the model under the constraints of spacetime and internal symmetries. Starting from a classification of all operators allowed in the Lagrangian by symmetries, we propose two modifications:

- Incorporation of explicit chiral symmetry breaking in the four-fermion interaction.
- Addition of a two-derivative kinetic term, mimicking the lattice Wilson term.

We then show that the modification of the four-fermion interaction is *required* for the model predictions to be consistent with lattice results, at least away from the continuum limit (at fixed lattice spacing).

We would like to stress that it is not our purpose here to carry out a precise numerical fit of the effective model to available lattice data. We rather wish to gain qualitative insight with a reasonable number of free parameters, and thus to prepare the ground for a future more detailed quantitative study. The simple setting used here allows us to study separately, and make robust conclusions about, the various physical ingredients entering the problem, namely the chiral restoration at high density and low temperature as well as deconfinement at high temperature and moderate-to-high density.

The outline of the paper is as follows. In section 2 we review the most important properties of 2cQCD (see ref. [14] for a recent review). Section 3 is devoted to a detailed discussion of the model. We classify all novel operators up to dimension six, allowed by the symmetries, and give a brief overview of the qualitative changes brought about by the non-standard operators. Since we modify one of the interaction terms, it is mandatory to first analyze how it affects the physics in the vacuum. This is done in section 4, where we also fix the parameters in the quark (NJL) sector of the model. The next two sections constitute the core of the paper, where we investigate various lattice artifacts in accordance with our main program. In section 5, we work at zero temperature, allowing us to separate the physics of flavor symmetry from deconfinement issues and the Polyakov loop. We analyze in turn the effects of a diquark source, the dependence on the quark mass, and the modified interaction term. In section 6, we add the gauge sector to the model and study the thermodynamics at nonzero temperature; the renormalization of the Polyakov loop is a new element here. Subsequently, we extract the chemical potential dependence of the temperature scale in the Polyakov-loop potential, which essentially determines the position of the deconfinement crossover. In section 7 we summarize and conclude. Some calculation details can be found in appendix A, where we analyze in detail the consequences of the two-derivative (Wilson) kinetic term for quarks.

2 Two-color QCD

In this paper, 2cQCD means a non-Abelian gauge theory with the SU(2) gauge group and N_f degenerate flavors of fundamental quarks. Two-color QCD differs in many respects from real-world, three-color QCD, most of them stemming from the fact that the fundamental representation of SU(2) is pseudoreal. For instance, a color singlet can only be made out of an even number of quarks, hence baryons in 2cQCD are bosons. Consequently, *dilute* nuclear matter is expected to be formed by a Bose-Einstein condensate (BEC) of bosonic baryons rather than by a Fermi sea of nucleons.

Next comes the question of the low-energy hadronic spectrum, which is of importance for the thermodynamics at low temperatures. The lowest-lying states in the spectrum are determined by the spontaneously broken flavor symmetry in the (2c)QCD vacuum. Here the pseudoreality of quarks implies that the usual $\mathrm{SU}(N_f)_\mathrm{L} \times \mathrm{SU}(N_f)_\mathrm{R} \times \mathrm{U}(1)_\mathrm{B}$ chiral symmetry of QCD in the limit of vanishing quark masses is embedded in an extended $\mathrm{SU}(2N_f)$ flavor symmetry group [15, 16]. The chiral condensate in the vacuum breaks this to $\mathrm{Sp}(2N_f)$, leading to $2N_f^2 - N_f - 1$ Goldstone bosons. These include $N_f^2 - 1$ pseudoscalar mesons, and $N_f(N_f - 1)/2$ diquark-antidiquark pairs. Nonzero (degenerate) quark masses make these modes massive. Forming an irreducible multiplet of the $\mathrm{Sp}(2N_f)$ symmetry, these states are all degenerate with a common mass that we denote by m_π.

The determinant of the Dirac operator of 2cQCD is necessarily real and for an even number of degenerate quark flavors it is also positive [17]. Consequently, the theory does not suffer from the sign problem and Monte Carlo simulations of dense matter are possible. In the following, we will focus exclusively on the simplest case of two quark flavors. In this case, the usual pion triplet is augmented by a single diquark-antidiquark pair carrying baryon number but no isospin. This determines the basic topology of the phase diagram of 2cQCD. Nonzero baryon chemical potential μ_B breaks the flavor symmetry down to the usual $\mathrm{SU}(2)_\mathrm{L} \times \mathrm{SU}(2)_\mathrm{R} \times \mathrm{U}(1)_\mathrm{B}$ chiral group; this is natural as the additional symmetry generators following from the pseudoreality of the quark representation do not commute with the baryon number operator. For nonzero (degenerate) quark masses, only the $\mathrm{SU}(2)_\mathrm{V} \times \mathrm{U}(1)_\mathrm{B}$ subgroup is exact.

When $\mu_\mathrm{B} \geq m_\pi$, the diquarks are expected to undergo BEC, which breaks $\mathrm{U}(1)_\mathrm{B}$ spontaneously. Since $\mathrm{U}(1)_\mathrm{B}$ is an exact symmetry, the baryon superfluid phase is necessarily separated from the vacuum by a phase transition. As the chemical potential is further increased, one eventually enters a Bardeen-Cooper-Schrieffer-like (BCS-like) regime where the thermodynamics is dominated by a Fermi sea of quarks that form weakly bound Cooper pairs. The order parameter for $\mathrm{U}(1)_\mathrm{B}$ symmetry breaking now is a composite diquark operator, which has the same quantum numbers as the order parameter in the BEC phase. The two regimes should therefore be smoothly connected [18]; in this context one speaks of a BEC-BCS crossover [19].[1]

If we instead crank up the temperature at zero baryon chemical potential, we expect the physics to be more-or-less similar to that of three-color QCD. Around some pseudocritical temperature T_c, we expect a rapid crossover from hadronic to quark degrees of freedom, accompanied by a rise in the expectation value of the Polyakov loop. This is loosely referred to as deconfinement. In the same range of temperatures, the chiral condensate melts, and we enter the quark-gluon plasma phase.

In lattice simulations of 2cQCD with Wilson fermions, the symmetry of the theory is affected in a twofold manner. Firstly, Lorentz invariance is broken to a discrete symmetry group of the spacetime lattice, which may result in a certain degree of anisotropy. At the same time, the Wilson term in the action acts as an additional source of explicit breaking of flavor symmetry which only disappears in the continuum limit. Since it breaks the flavor symmetry in exactly the same way as the quark masses do it may not be possible to distinguish the two sources of symmetry breaking in low-energy observables.

In our model calculations, we will focus on two classes of observables: symmetry-breaking order parameters (condensates) and thermodynamic quantities such as pressure or baryon density. We now summarize the expectations for these observables and then describe the relevant lattice results in order to set the stage for our analysis.

2.1 Chiral perturbation theory

The flavor symmetry of 2cQCD and its spontaneous breaking are most conveniently encoded in the low-energy effective theory for the pseudo-Goldstone modes, namely chiral perturbation theory (χPT) [21, 22]. Following the notation of refs. [16, 23], the pions and diquarks are expressed in terms of a $2N_f \times 2N_f$ antisymmetric unimodular unitary matrix Σ, in terms of which the leading-order χPT Lagrangian in Minkowski space reads

$$\mathscr{L}_{\chi\mathrm{PT}} = \frac{1}{2} f_\pi^2 \operatorname{tr}(D_\mu \Sigma D^\mu \Sigma^\dagger) + H \operatorname{Re}\operatorname{tr}(J\Sigma). \tag{2.1}$$

Here f_π is the pion decay constant and the covariant derivative D_μ includes the baryon number chemical potential μ_B, $D_\mu\Sigma \equiv \partial_\mu\Sigma - \mathrm{i}\delta_{\mu 0}\mu_\mathrm{B}(B\Sigma + \Sigma B^T)$, where B is the baryon number operator. The matrix J in general contains sources that couple to scalar or pseudoscalar quark bilinears. Here we will need the scalar source m_0 (quark mass), and the diquark source j, in terms of which we have $J = m_0\Sigma_1^\dagger + j\Sigma_2^\dagger$. In the case of two flavors, the matrix basis can be chosen such that

---

[1] Here we identify the position of the BEC-BCS crossover with the region where the quark chemical potential measured with respect to its constituent mass changes sign. Another useful measure of the crossover is provided by the diquark wave function, recently studied in 2cQCD in ref. [20].

$$B = \frac{1}{2}\begin{pmatrix} \mathbb{1} & 0 \\ 0 & -\mathbb{1} \end{pmatrix}, \qquad \Sigma_1 = \begin{pmatrix} 0 & -\mathbb{1} \\ \mathbb{1} & 0 \end{pmatrix}, \qquad \Sigma_2 = \begin{pmatrix} \tau_2 & 0 \\ 0 & \tau_2 \end{pmatrix} \tag{2.2}$$

in the 2×2 block form, where τ_2 is a Pauli matrix. Finally, the coupling H can be fixed by expanding the Lagrangian (2.1) to second order in the fluctuations about the vacuum, or by using the Gell-Mann-Oakes-Renner relation, leading to $H = f_\pi^2 m_\pi^2 / m_0$.

As the low-energy spectrum contains excitations carrying baryon number, the leading-order chiral Lagrangian (2.1) can be used to study the phase diagram of 2cQCD at zero temperature and nonzero baryon density.[2] The ground state at finite density is most easily visualized by using a Lie algebra isomorphism to cast the coset space SU(4)/Sp(4) equivalently as SO(6)/SO(5) [23]. The unitary matrix Σ can thus be mapped onto a unit 6-vector $\vec{n}$ via the relation $\Sigma = \vec{n} \cdot \vec{\Sigma}$, where Σ_i is a set of suitably chosen basis matrices. Depending on the values of the chemical potential(s) and the external sources, the ground state therefore moves on a unit sphere. In the absence of an isospin chemical potential μ_I and other sources except m_0, j, the symmetry of the problem can be exploited to rotate the ground state into the (n_1, n_2) plane, corresponding to a chiral condensate and a diquark condensate with a fixed phase. The ground state can thus be parametrized by a single angle θ such that $n_1 = \cos\theta$ and $n_2 = \sin\theta$.

For the time being, we will assume that $j = 0$. The effects of the diquark source will be discussed in detail in section 5.1. The static part of the Lagrangian (2.1), whose *maximum* is to be found, then becomes

$$\mathscr{L}^{\mathrm{stat}}_{\chi\mathrm{PT}} = 2 f_\pi^2 \mu_\mathrm{B}^2 \sin^2\theta + 4 f_\pi^2 m_\pi^2 \cos\theta. \tag{2.3}$$

As expected, the chiral-symmetry-breaking state $\theta = 0$ is stable for $\mu_\mathrm{B} < m_\pi$. As μ_B further increases, the equilibrium starts rotating into the diquark direction, and the angle of rotation θ is given by [16]

$$\cos\theta = \frac{m_\pi^2}{\mu_\mathrm{B}^2}. \tag{2.4}$$

This result is a priori expected to hold only within the range of validity of χPT, in particular only in the BEC regime where bosonic degrees of freedom dominate the physics of dense two-color matter. It should therefore be emphasized that, in fact, it remains at least qualitatively accurate even for much higher values of μ_B. A numerical solution of the NJL model shows that eq. (2.4) holds also for chemical potentials rather deep in the BCS phase where a Fermi sea of quarks has been formed. The agreement between the two approaches, based on completely different degrees of freedom, persists at zero temperature up to $\mu_\mathrm{B} \approx 3 m_\pi$ [26]. This can be attributed to the fact that in this range of μ_B, the physics at zero temperature is almost entirely driven by the condensates; the contribution of quark quasiparticles is negligible.

---

[2] Including the effects of nonzero temperature requires calculating loops, and hence going to the next-to-leading order in the derivative expansion [24, 25].

2.2 The puzzle and its resolution

The above discussion hints that the quantitative aspects of the phase diagram of 2cQCD are determined by its symmetries even far beyond the region where one would expect it. The results of lattice simulations are in a stark contrast to this naive expectation. Most importantly, the lattice data indicate a fast transition to a BCS regime just above $\mu_{\mathrm{B}} = m_\pi$; the expected bosonic BEC phase, if present at all, is not resolved. Moreover, in the BCS regime, 2cQCD behaves as a system of weakly interacting, almost massless quarks. This conclusion is supported by two independent pieces of evidence [6]:

- The values of pressure and baryon number density, when normalized to their values for an ideal gas of massless quarks — the Stefan-Boltzmann (SB) limit — exhibit a plateau at $\mu_{\mathrm{B}} \gtrsim m_\pi$ close to one. The precise height of this plateau is currently hard to determine, but its existence seems to be confirmed.

- The expectation value of the color-singlet diquark operator scales with μ_{B}^2 in the same range of chemical potentials, reminiscent of the density of states at a sharp Fermi surface of massless relativistic fermions.

An additional, related piece of evidence is provided by the fact that the critical temperature T_d for diquark condensation saturates at high μ_{B} at a value roughly given by $T_d \approx T_c/2$ [7], whereas the picture of the order parameter rotating on a unit sphere, sketched above, would naively suggest a vastly different value, $T_d \approx T_c$.

How can we reconcile these observations with the universal model-independent predictions of χPT? The simple and short answer is: we *cannot*. The SB scaling of thermodynamic observables requires that the quarks are almost massless and their quasiparticle gap, proportional to the diquark condensate, is very small as well. It is obvious that this cannot be true simultaneously in χPT, according to which the sum of squares of the chiral and diquark condensates is constant.

It is apparent that the key physical ingredient required is the rapid transition to a BCS-like gas of almost massless and gapless quarks at $\mu_{\mathrm{B}} \gtrsim m_\pi$. Once this is achieved, the other features — μ_{B}^2-scaling of the expectation value of the diquark operator and the suppression of T_d — should follow naturally. χPT as well as effective models based on the same symmetries lead to predictions that are at odds with this requirement. We therefore expect explicit chiral symmetry breaking to play a crucial role. However, as we demonstrate in section 5.2, tuning the current quark mass even to unreasonably high values is not sufficient. In the remainder of this paper, we therefore take a rather radical approach to the problem in which we abandon the chiral symmetry altogether. We introduce explicit symmetry breaking into the effective four-quark interaction and show that this leads to the desired effect. The possible origin of this symmetry breaking is discussed in section 7.

3 The model

Our model is of PNJL type, which is based on quark degrees of freedom. Thus the only field variable is the quark spinor ψ. For the time being, we focus on the quark sector. The gauge sector will be discussed in detail later, when the effects of nonzero temperature are introduced. The form of the Lagrangian is constrained by spacetime and internal symmetries, which we assume to be as follows: Poincaré invariance plus the discrete symmetries of charge conjugation, parity, and time reversal, *global* SU(2) color symmetry, and Sp(4) flavor symmetry. We therefore abandon the full SU(4) flavor group. This group is explicitly broken down to the Sp(4) subgroup by (degenerate) quark masses and the Wilson term in the lattice action. The Sp(4) subgroup therefore constitutes the true flavor symmetry of both lattice and continuum 2cQCD with massive quarks.

Finally, we make one more step which goes beyond the usual PNJL model building. We do not restrict ourselves to the simplest possible Lagrangian consisting of a quark kinetic term and a four-quark interaction. Instead, we classify all terms in the Lagrangian consistent with the above symmetries up to dimension six.[3] This is in agreement with the effective field theory philosophy where all operators up to a given dimension allowed by symmetry should be included [27].

3.1 Classification of operators

We start by classifying the operators according to their canonical dimension. The operators are written schematically with their indices suppressed.

- **Order 3.** The only parity-even Lorentz scalar that respects baryon number, SU(2) color and isospin invariance is the quark mass term $\bar\psi\psi$. The Sp(4) symmetry is automatically implied, but the full SU(4) group is explicitly broken.
- **Order 4.** Schematically, the operator must be of the $\bar\psi D\psi$ type to respect baryon number. Lorentz invariance and parity together with the SU(2) color and isospin invariance single out the usual quark kinetic term $\bar\psi \not{D}\psi$. The full SU(4) symmetry is automatically implied.
- **Order 5.** Here we have two possibilities respecting baryon number conservation and Lorentz invariance, namely $D_\mu\bar\psi D^\mu\psi$ and $D_\mu\bar\psi[\gamma^\mu,\gamma^\nu]D_\nu\psi$. The latter is, however, irrelevant for our purposes since we only consider a purely temporal background gauge field, representing the baryon chemical potential and the Polyakov loop. Parity, SU(2) color and isospin invariance then single out the operator $D_\mu\bar\psi D^\mu\psi$. The Sp(4) symmetry is automatically implied, but the full SU(4) group is explicitly broken. We will refer to this operator as the *Wilson term* since it closely resembles the corresponding operator in the lattice Wilson action.
- **Order 6.** Here we have two schematic possibilities respecting baryon number, namely $\bar\psi DDD\psi$ and $(\bar\psi\psi)^2$. Lorentz invariance requires the former to contain an odd number of Dirac matrices, hence it represents a higher-order correction to the kinetic term which automatically preserves chiral symmetry. We will therefore drop it from further consideration since we do not expect that it leads to any qualitatively new effects. The non-derivative operator, on the other hand, is a standard NJL-type four-quark

---

[3] Dimension-six operators are needed to describe quark interactions.

interaction. There are many operators of this type that respect a given symmetry, as can be seen by performing a Fierz transformation of the basic one-gluon-exchange type of operator [10]. In the mean-field approximation, we want to build an invariant interaction out of fermion bilinears that carry the quantum numbers of the low-energy degrees of freedom. The degrees of freedom that must be present in the model are the pseudo-Goldstone bosons: the pion triplet (represented by $\bar{\psi}\mathrm{i}\gamma_5\vec{\tau}\psi$) and the isospin-singlet diquark, which is represented by $\bar{\psi}^{\mathcal{C}}\gamma_5\sigma_2\tau_2\psi$ (where $\mathcal{C}$ stands for charge conjugation and σ_2 is the Pauli matrix in color space). Furthermore, the operator with the quantum numbers of a true scalar, $\bar{\psi}\psi$, must be added in order to account for the chiral condensate. The two Sp(4)-invariant interactions that can be built out of the squares of these operators are

$$(\bar{\psi}\psi)^2 \qquad \text{and} \qquad (\bar{\psi}\mathrm{i}\gamma_5\vec{\tau}\psi)^2 + |\bar{\psi}^{\mathcal{C}}\gamma_5\sigma_2\tau_2\psi|^2. \tag{3.1}$$

The above considerations suggest the following generic NJL-type Lagrangian,

$$\mathscr{L}_{\mathrm{NJL}} = \bar{\psi}(\mathrm{i}\not{D} - m_0)\psi + \kappa D_\mu\bar{\psi}D^\mu\psi + G(\bar{\psi}\psi)^2 + \lambda G\left[(\bar{\psi}\mathrm{i}\gamma_5\vec{\tau}\psi)^2 + |\bar{\psi}^{\mathcal{C}}\gamma_5\sigma_2\tau_2\psi|^2\right], \tag{3.2}$$

where the covariant derivative $D_\mu\psi$ includes the baryon chemical potential, and later in section 6 also the constant background gauge field representing the Polyakov loop. The dimensionless parameter λ is in the remainder of this paper referred to as the *chiral twist*. The minimal NJL model for three-color QCD amounts to skipping the last operator inside the brackets, and setting $\kappa = 0$ and $\lambda = 1$ [9]. The two-color version including the diquark channel, with $\kappa = 0$ and $\lambda = 1$, was first introduced in ref. [28] and subsequently used by several other groups [29–32]. In the following subsection, we will discuss the consequences of the modifications introduced here.

3.2 Effects of chiral symmetry breaking

The classification of invariant operators has automatically guided us to introduce two new couplings in the Lagrangian. Let us start with the Wilson term proportional to κ. As already mentioned, it mimics the discretization artifacts introduced by the lattice Wilson action. The presence of a two-derivative bilinear operator in the Lagrangian leads to doubling of the fermion degrees of freedom. For small κ, we expect the new fermion species to be heavy with mass scaling as $1/\kappa$. Since the Wilson term breaks chiral symmetry explicitly, it will enhance the chiral condensate in the vacuum. Regarding thermodynamics, we expect the effects of the Wilson term to be most pronounced at high temperatures since the new fermion is heavy and thus difficult to excite thermally. In addition, the presence of a heavy fermion may lead to undesirable artifacts at high baryon density, namely the appearance of a second Fermi surface at high μ_{B} and low temperature. Some of the quantitative consequences of the Wilson term will be worked out in appendix A.

It is the chiral twist that will play a pivotal role in our analysis. As we abandon chiral symmetry here, the scalar and pseudoscalar channels are no longer forced to appear with the same strength. However, the diquark and pion operators do enter through a fixed combination, as required by the exact Sp(4) symmetry of two-flavor 2cQCD. This guarantees exact mass degeneracy of pions and diquarks, and therefore that the critical chemical potential for diquark condensation at zero temperature equals the *pion* mass.

A detailed analysis of the consequences of our model (3.2) with the modified interaction constitutes the bulk of the remainder of the paper. Yet some qualitative observations can be made already now. It is clear that the existence of a bound state in the pion channel requires $\lambda > 0$. Since the strength of attraction in the scalar channel remains fixed to G, the constituent quark mass in the vacuum will be unaffected by λ. As a consequence, the pion will become less strongly bound and its mass will increase with decreasing λ. The location of the BEC-BCS crossover at zero temperature will therefore shift towards lower values of μ_B/m_π and it is conceivable that the BEC region can be eliminated altogether. In the following, we will therefore consider only the range $0 < \lambda \leq 1$.

Since the coupling in the diquark channel also decreases with λ, we expect the diquark condensate to be suppressed. This will sharpen the quark Fermi surface and move the system closer to the SB limit. An additional effect which follows from our analysis below, is that the chiral condensate will also be suppressed as compared to the naive expectation based on eq. (2.4). Suppressing both the diquark and the chiral condensate, the chiral twist is therefore exactly what we need in order to explain the rapid crossover to the gas of weakly coupled almost massless quarks.

4 Vacuum physics

In the remainder of the paper, except for appendix A, we set $\kappa = 0$. The composite bosonic degrees of freedom σ, $\vec{\pi}$, Δ, and Δ^* are introduced by the Hubbard-Stratonovich transformation, adding to the Lagrangian (3.2) the term

$$\Delta\mathscr{L}_\mathrm{NJL} = -\frac{1}{4G}(\sigma+2G\bar{\psi}\psi)^2 - \frac{1}{4\lambda G}(\vec{\pi}+2\lambda G\bar{\psi}\mathrm{i}\gamma_5\vec{\tau}\psi)^2 - \frac{1}{4\lambda G}|\Delta^* - 2\lambda G\bar{\psi}\mathrm{i}\gamma_5\sigma_2\tau_2\psi^\mathcal{C}|^2. \tag{4.1}$$

The Lagrangian is now bilinear in the quark fields and we can integrate them out exactly. This leads to the effective bosonic action

$$S^\mathrm{eff}_\mathrm{NJL} = -\int \mathrm{d}t\,\mathrm{d}^3\boldsymbol{x}\left(\frac{\sigma^2}{4G} + \frac{\vec{\pi}^2 + |\Delta|^2}{4\lambda G}\right) - \mathrm{i}\,\mathrm{Tr}\log\mathscr{D}, \tag{4.2}$$

where

$$\mathscr{D} \equiv \begin{pmatrix} \mathrm{i}\not{D} - M - \mathrm{i}\gamma_5\vec{\pi}\cdot\vec{\tau} & \Delta\gamma_5 \\ -\Delta^*\gamma_5 & \mathrm{i}\not{D} - M + \mathrm{i}\gamma_5\vec{\pi}\cdot\vec{\tau} \end{pmatrix} \tag{4.3}$$

is the Dirac operator acting on the Nambu space spanned by red quarks and green antiquarks. We have introduced the shorthand notation $M \equiv m_0 + \sigma$ for the constituent quark mass, and denoted by "Tr" the functional trace.

In the following, we work in the mean-field approximation. This means that after taking functional derivatives of the action (4.2) as appropriate, all bosonic fields are set equal to a constant. The integrals that appear are ultraviolet divergent and we need to regulate them. With the exception of appendix A, we will use a simple sharp three-momentum cutoff Λ. Depending on the cutoff, writing the expressions in a manifestly

Lorentz-covariant form may involve some manipulations that are not justified from a strictly mathematical point of view. This is, however, a well-known issue [9].

The vacuum of 2cQCD is characterized by broken chiral symmetry. Differentiating eq. (4.2) with respect to m_0, we find that the chiral condensate of a single quark flavor is related to the σ condensate by

$$\langle \bar{u}u \rangle = -\frac{\sigma}{4G}. \tag{4.4}$$

The latter is found from the stationary point condition $\delta S^{\text{eff}}_{\text{NJL}}/\delta\sigma = 0$. This yields[4]

$$\sigma = 16\mathrm{i}GN_cM\int\frac{\mathrm{d}^4k}{(2\pi)^4}\frac{1}{k^2-M^2} = 8GN_cM\int\frac{\mathrm{d}^3\boldsymbol{k}}{(2\pi)^3}\frac{1}{\epsilon_{\boldsymbol{k}}}, \tag{4.5}$$

where the quark dispersion relation in the vacuum is

$$\epsilon_{\boldsymbol{k}} \equiv \sqrt{\boldsymbol{k}^2+M^2}. \tag{4.6}$$

The spectrum of pseudo-Goldstone bosons can be determined from the polarization function (inverse propagator), which is obtained by taking a second functional derivative of the action. We already know that in the vacuum pions and diquarks are degenerate, so we just state the result for the pion polarization function, simplified by using eq. (4.5),

$$\chi(p^2) = -\frac{1}{2G}\left(\frac{1}{\lambda}-\frac{\sigma}{M}\right)+4N_cp^2I(p^2), \tag{4.7}$$

where

$$I(p^2) \equiv -\mathrm{i}\int\frac{\mathrm{d}^4k}{(2\pi)^4}\frac{1}{[(k+p)^2-M^2](k^2-M^2)}. \tag{4.8}$$

In the chiral limit, $M=\sigma$ and we can immediately see the effect of explicit chiral symmetry breaking by the chiral twist: the pion is exactly massless only for $\lambda=1$. In general the pion mass squared is given by the zero of the inverse propagator, $\chi(m_\pi^2)=0$. Using the the gap equation (4.5) once more, we can rewrite this as

$$1 = 8\lambda GN_c\int\frac{\mathrm{d}^3\boldsymbol{k}}{(2\pi)^3}\left(\frac{1}{2\epsilon_{\boldsymbol{k}}+m_\pi}+\frac{1}{2\epsilon_{\boldsymbol{k}}-m_\pi}\right). \tag{4.9}$$

Using the Lehmann spectral representation of the pion propagator, we can determine the coupling $g_{\pi qq}$ of the one-pion state to the pseudoscalar quark bilinear $\bar{\psi}\mathrm{i}\gamma_5\vec{\tau}\psi$,

$$\frac{1}{g^2_{\pi qq}} = \chi'(p^2)\Big|_{p^2=m_\pi^2} = 16N_c\int\frac{\mathrm{d}^3\boldsymbol{k}}{(2\pi)^3}\frac{\epsilon_{\boldsymbol{k}}}{(4\epsilon^2_{\boldsymbol{k}}-m^2_\pi)^2}. \tag{4.10}$$

From this result, one can obtain the coupling of the one-pion state to the axial vector current, that is, the pion decay constant f_π. The resulting expression is

$$f_\pi = \frac{g_{\pi qq}}{2Gm^2_\pi}\left(\frac{M}{\lambda}-\sigma\right). \tag{4.11}$$

---

[4] We keep the dependence of the analytic formulas on the number of colors N_c explicit in order to facilitate a comparison with the three-color case.

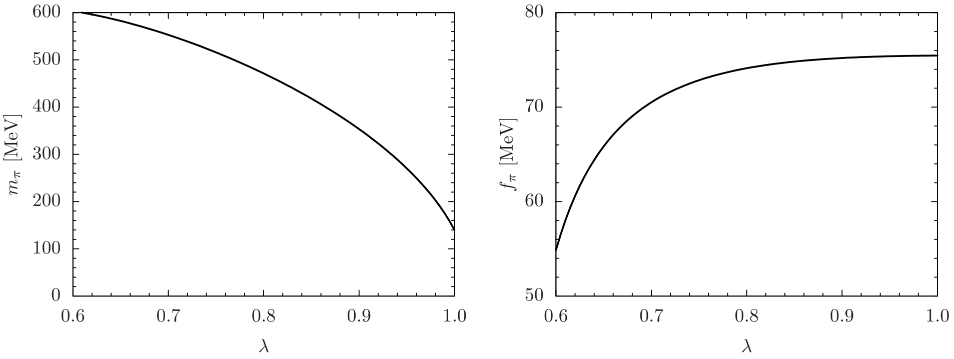

Figure 1. Pion mass (left panel) and decay constant (right panel) as a function of λ. All other parameters are fixed according to eq. (4.13).

4.1 Parameter fixing

The NJL model (3.2) with $\kappa = 0$ and $\lambda = 1$ is defined by the three parameters m_0, G, and Λ, which should be determined by a fit to three independent observables. It is customary to use the chiral condensate, pion decay constant and pion mass for that purpose. We follow ref. [30] and determine the values of these input quantities in 2cQCD from their physical, three-color counterparts using a naive scaling with the number of colors N_c,

$$\langle \bar{u}u \rangle = -(218\text{ MeV})^3, \quad f_\pi = 75.4\text{ MeV}, \quad m_\pi = 140\text{ MeV} \qquad \text{(physical input)}. \tag{4.12}$$

Equations (4.4), (4.9), and (4.11) then give us the following values

$$G = 7.23\text{ GeV}^{-2}, \quad \Lambda = 657\text{ MeV}, \quad m_0 = 5.4\text{ MeV} \qquad \text{(fitted parameters)}, \tag{4.13}$$

which we will use throughout the rest of the paper unless explicitly stated otherwise. The coupling λ will be treated as a tunable parameter.

4.2 Role of the chiral twist

As explained in section 3.2, we expect that the pion mass increases with decreasing λ. It is clear from the left panel of figure 1 that the effect is actually rather large. At $\lambda \approx 0.95$, the pion mass is increased by a factor of two, and at around $\lambda \approx 0.6$, it reaches the (unphysical) threshold for decay into a quark-antiquark pair. (The σ condensate in the vacuum is to great precision equal to 300 MeV for our choice of parameters.) At the same time, the pion decay constant starts to drop rapidly (right panel of figure 1), which indicates that the pion ceases to behave as a Goldstone boson. The interval $[0.6, 1]$ therefore defines the range of reasonable values for λ to which we will restrict ourselves in the following.

To gain a more analytic insight into the λ-dependence of physical observables, we take the derivative of eq. (4.9) with respect to λ. Using eq. (4.10) allows us to rewrite the result in the form of an exact differential equation,

$$\frac{\mathrm{d}m_\pi^2}{\mathrm{d}\lambda} = -\frac{g_{\pi qq}^2}{2\lambda^2 G}. \tag{4.14}$$

In the chiral limit, the pion mass will scale asymptotically as $m_\pi \propto \sqrt{1-\lambda}$ for $\lambda \to 1$. Using in addition eq. (4.11), we readily obtain another differential equation, this time for the pion decay constant,

$$f_\pi^2 = \frac{1}{2G}(M-\lambda\sigma)^2 \frac{\mathrm{d}}{\mathrm{d}\lambda}\frac{1}{m_\pi^2}. \tag{4.15}$$

This expression together with the asymptotic scaling $m_\pi \propto \sqrt{1-\lambda}$ explains the very weak λ-dependence of f_π for λ close to one, see the right panel of figure 1. The fact that f_π is almost constant in the range $\lambda \in [0.8, 1]$ also justifies a posteriori our treatment of λ as a tunable parameter: since the quark mass, and hence the pion mass, is a free parameter on the lattice anyway, we have some freedom in tuning both m_0 and λ without affecting the physical observables $\langle \bar{u}u \rangle$ and f_π, and do not have to refit our parameters anew for each value of λ.

5 Zero temperature: chiral restoration

In this section, we will investigate the effects of tuning various parameters on different physical quantities at zero temperature. We focus on the chiral and diquark condensates, the pressure, and the baryon number density. We can therefore drop the pion field $\vec{\pi}$ in eq. (4.2). Evaluating the action for constant σ and Δ and going to Euclidean space gives the thermodynamic potential

$$\Omega_{\mathrm{NJL}}^{T=0} = \frac{\sigma^2}{4G} + \frac{|\Delta|^2}{4\lambda G} - 2N_c \sum_{\pm} \int \frac{\mathrm{d}^3\boldsymbol{k}}{(2\pi)^3} E_{\boldsymbol{k}}^{\pm}, \tag{5.1}$$

where the quark quasiparticle dispersion relations are defined by[5]

$$E_{\boldsymbol{k}}^{\pm} \equiv \sqrt{(\xi_{\boldsymbol{k}}^{\pm})^2 + |\Delta|^2}, \qquad \xi_{\boldsymbol{k}}^{\pm} \equiv \epsilon_{\boldsymbol{k}} \pm \mu. \tag{5.2}$$

The values of the condensates for a given μ are found by direct numerical minimization of the thermodynamic potential. The pressure is equal to $-\Omega_{\mathrm{NJL}}^{T=0}$ conventionally shifted by a constant so that the pressure is zero in the vacuum. The baryon number density is obtained by taking the derivative of the pressure with respect to μ_{B}, giving

$$n_{\mathrm{B}}^{T=0} = N_c \int \frac{\mathrm{d}^3\boldsymbol{k}}{(2\pi)^3} \left(\frac{\xi_{\boldsymbol{k}}^+}{E_{\boldsymbol{k}}^+} - \frac{\xi_{\boldsymbol{k}}^-}{E_{\boldsymbol{k}}^-} \right), \tag{5.3}$$

where we have separated the particle and antiparticle contributions.

5.1 Role of the diquark source

The first lattice simulations of dense 2cQCD with Wilson quarks were performed with a fixed external source j for the diquark operator [33, 34]; only recently has the extrapolation to vanishing source been studied. However, these attempts were based on fitting three data points by a simple analytical ansatz for the j-dependence. Ref. [6] resorted to a linear extrapolation, but as pointed out in ref. [7], none of the three ansätze used therein (linear, power-law, and power-law with an offset) led to satisfactory results.

---

[5] For the quark degrees of freedom, we choose to work with the *quark* number chemical potential μ, given by $\mu = \mu_{\mathrm{B}}/2$.

In principle, adding a diquark source to the NJL model is straightforward and is analogous to introducing the quark mass m_0 as a source for the $\bar{\psi}\psi$ operator. All we need to do is to make the shift $\Delta \to \Delta + j$ in the fermion part of the thermodynamic potential (5.1). However, since we want to gain *analytic* insight into the scaling of the Δ condensate in the limit $j \to 0$, numerical solution of the NJL model is not satisfactory. Instead we once again employ χPT. We have confidence in this since the NJL model and χPT give numerically very similar results in a large range of chemical potentials [26].

We showed below eq. (2.1) how the diquark source enters the χPT Lagrangian. Following ref. [16], we relate the diquark source to the quark mass by introducing a new angle ϕ, and express the chemical potential in terms of a dimensionless parameter x, via

$$j = m_0 \tan\phi \equiv m_0 \tilde{j}, \qquad x \equiv \frac{\mu_\mathrm{B}}{m_\pi}. \tag{5.4}$$

The static part of the Lagrangian (2.3) with the added diquark source term can then be rewritten as a dimensionless potential,

$$V(\theta) \equiv -\frac{\mathscr{L}_{\chi\mathrm{PT}}^{\mathrm{stat}}}{4 f_\pi^2 m_\pi^2} = -\frac{1}{2}x^2 \sin^2\theta - \cos\theta - \tilde{j}\sin\theta = -\frac{1}{2}x^2\sin^2\theta - \frac{\cos(\theta-\phi)}{\cos\phi}. \tag{5.5}$$

Finally introducing the shorthand notation $\delta \equiv \sin\theta$ for the normalized diquark condensate, the stationarity condition $\delta V(\theta)/\delta\theta = 0$ takes the simple form,

$$\tilde{j} = \frac{\delta}{\sqrt{1-\delta^2}} - x^2\delta. \tag{5.6}$$

Note that for $\tilde{j} = 0$, we recover the nontrivial solution for the chiral condensate (2.4), now expressed as $\cos\theta = \sqrt{1-\delta^2} = 1/x^2$. It is easy to see that for any $\tilde{j} > 0$, eq. (5.6) admits a unique positive solution $\delta(\tilde{j})$.

The presence of the condensate in the ground state is reflected by a specific asymptotic scaling of this solution in the limit $\tilde{j} \to 0$. The asymptotic expansion of $\delta(\tilde{j})$ can be found by an iterative solution of eq. (5.6), leading to

$$\begin{aligned} \delta(\tilde{j}) &= \frac{\tilde{j}}{1-x^2} - \frac{\tilde{j}^3}{2(1-x^2)^4} + \mathcal{O}(\tilde{j}^5), && (x<1), \\ \delta(\tilde{j}) &= (2\tilde{j})^{1/3} - \frac{\tilde{j}}{2} + \frac{(2\tilde{j})^{5/3}}{24} + \mathcal{O}(\tilde{j}^3), && (x=1), \\ \delta(\tilde{j}) &= \sqrt{1-\frac{1}{x^4}} + \frac{\tilde{j}}{x^2(x^4-1)} - \frac{3x^2\tilde{j}^2}{2(x^4-1)^{5/2}} + \mathcal{O}(\tilde{j}^3), && (x>1). \end{aligned} \tag{5.7}$$

The $x = 1$ part is most easily obtained by writing eq. (5.6) as $\tilde{j} = 4\tan^3\frac{\theta}{2}/(1-\tan^4\frac{\theta}{2})$, first solving for $\theta(\tilde{j})$, and then converting this into a series for $\delta(\tilde{j})$. In contrast, the solutions in the regions $x < 1$ and $x > 1$ are simple Taylor expansions. Moreover, for $x < 1$ the expansion only contains odd powers of $\tilde{j}$, reflecting the unbroken discrete symmetry of eq. (5.6), under which both $\tilde{j}$ and δ change sign. We stress that in *both* regions $x < 1$

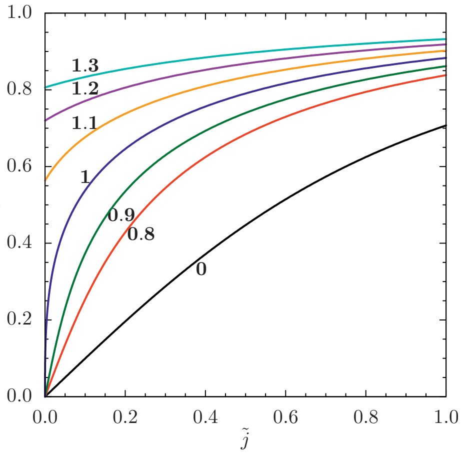

Figure 2. Dependence of the rescaled diquark condensate δ on the dimensionless source $\tilde{j}$ for several different values of the parameter $x = \mu_\mathrm{B}/m_\pi$ (given in bold).

and $x > 1$, the condensate is a linear function of the source in the limit $\tilde{j} \to 0$, but the series convergence becomes slower and slower as the phase transition is approached. A rough upper bound on the range of values of $\tilde{j}$ in which a linear extrapolation makes sense, can be obtained by comparing the first two $\tilde{j}$-dependent terms of the expansion, giving $\tilde{j} \lesssim |x^2 - 1|^{3/2}$ for x close to one in both regions. The convergence of the expansion can also be judged from the exact numerical solution of eq. (5.6), shown in figure 2.

5.2 Role of the quark mass

We argued in section 2.2 that reproducing the fast transition to a gas of weakly interacting almost massless quarks at $\mu_\mathrm{B} \geq m_\pi$, as seen on the lattice, requires strong explicit breaking of chiral symmetry. It might be tempting to the think that this effect is due to a large current quark mass. In this section, we therefore set $\lambda = 1$ and investigate the dependence on m_0 at zero temperature using the mean-field approximation (5.1).

Since the transition to the baryon superfluid phase is expected to occur at $\mu_\mathrm{B} = m_\pi$, it makes sense to trade the chemical potential for the dimensionless parameter $x = \mu_\mathrm{B}/m_\pi$ for the sake of comparison. This is done in figure 3, where the solutions to the gap equations for the chiral and diquark condensates are shown for several values of m_0. It is obvious, after proper rescaling, that the prediction of χPT (2.4), indicated by a dashed line in the figure, works quite well even for unreasonably heavy quarks. (One would probably not expect an approach based on spontaneously broken symmetry to still work even when the mass of the pseudo-Goldstone boson reaches the scale of the ultraviolet cutoff.) It is also clear that just tuning the quark mass not is sufficient for our purposes, even for the largest values of m_0: the size of the quasiquark gap Δ remains largely unaffected.[6] Moreover the

---

[6] The distortion of the curves at high m_0 and μ_B should be attributed to the three-momentum cutoff.

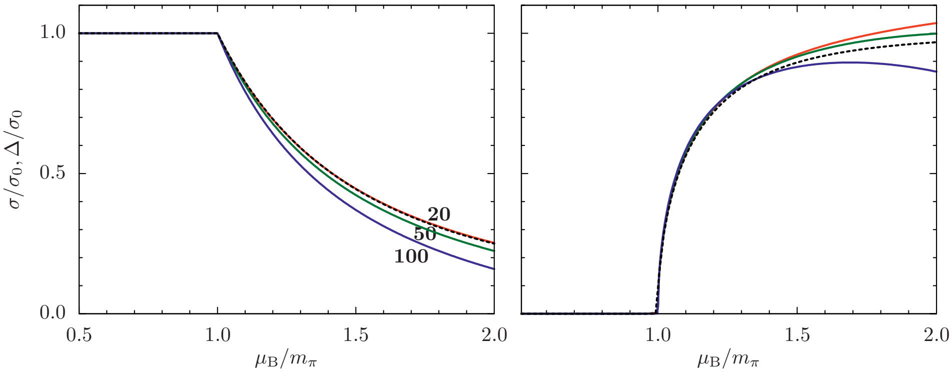

Figure 3. Dependence of the rescaled chiral and diquark condensate on $x = \mu_B/m_\pi$ for several different values of the current quark mass m_0. Here σ_0 is the chiral condensate in the vacuum for given m_0 and the other parameters as in eq. (4.13). The values of m_0 in MeV are indicated in bold (the same color coding is used in both panels). The dashed line shows the prediction of χPT.

slight reduction in the chiral condensate is canceled by the increased current quark mass so that the constituent quark mass is not reduced at all.

The results shown in figure 3 are also in a good agreement with older lattice simulations using *staggered* quarks [17, 35]. There, the prediction (2.4) of χPT was verified numerically for current quark masses varying by an order of magnitude. A tiny reduction of the chiral condensate as compared to eq. (2.4), observed therein, could — exactly as in our case — be ascribed to the relatively large current quark mass. Since the staggered implementation of lattice quarks preserves chiral symmetry, we conclude that heavy quarks alone are not sufficient to explain the thermodynamic behavior in the baryon superfluid phase observed in ref. [6]. An additional source of chiral symmetry breaking is needed. On the lattice, this is provided by the Wilson term in the action. In our NJL model, the chiral twist serves this purpose, as we will now demonstrate.

5.3 Role of the chiral twist

In this section, we fix m_0 to its value given in eq. (4.13), and instead vary the chiral twist. Figure 4 shows the dependence of the chiral and diquark condensates at zero temperature on λ. Since the pion mass is very sensitive to λ, we again plot these quantities against the ratio $x = \mu_B/m_\pi$. The numerical results fully confirm our expectations outlined in section 3.2, namely that the diquark condensate (at fixed x) becomes rather strongly suppressed as λ decreases. At the same time, the chiral condensate is strongly suppressed as well. We note that this is in contrast to χPT where the sum of the two condensates squared is constant. The suppression of both condensates simultaneously is exactly what we want.

How small should λ be to reach a quantitative agreement with the lattice results of refs. [6, 7]? The suppression of the diquark condensate leads to a suppression of the critical temperature T_d. In this paper, we are not going to compute the critical temperature, but

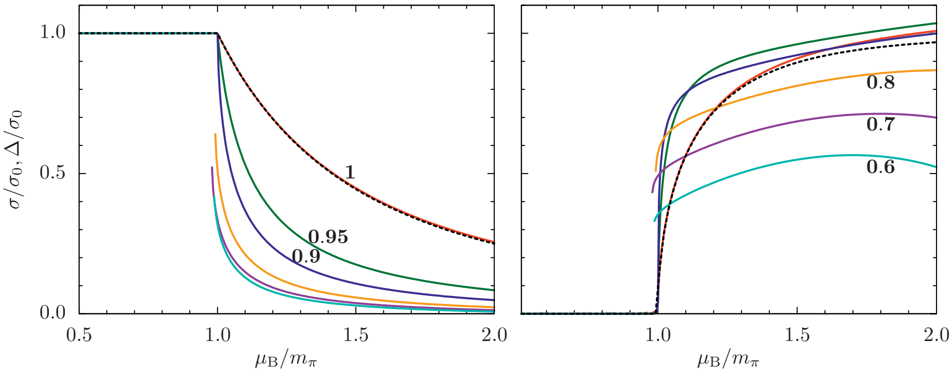

Figure 4. Dependence of the rescaled chiral (left panel) and diquark (right panel) condensate on $x = \mu_B/m_\pi$ for several values of λ (shown in bold). Here $\sigma_0 \approx 300$ MeV is the chiral condensate in the vacuum for our parameter set (4.13). The dashed line indicates the prediction of χPT.

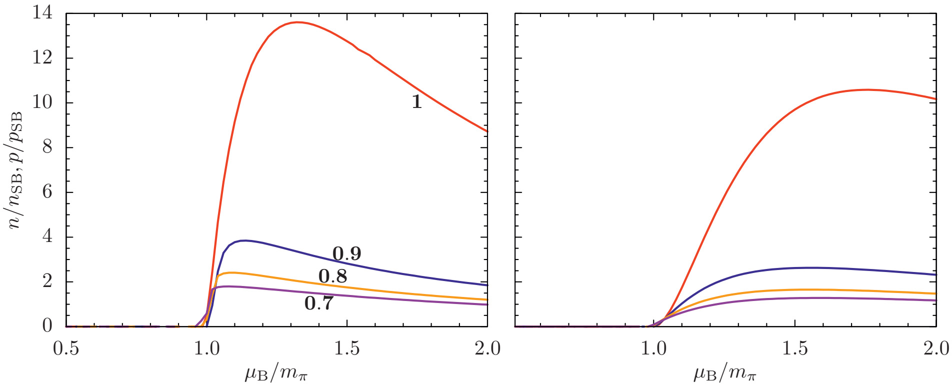

Figure 5. Dependence of baryon number density (left panel) and pressure (right panel) on chemical potential for several values of λ (shown in bold, the same color coding as in figure 4 is used). Both quantities are normalized to the SB values for a gas of free massless quarks.

we can make at least an estimate.[7] Since in the weak-coupling BCS theory as well as in its extension including the most important corrections due to fluctuations, the critical temperature is proportional to the pairing gap at zero temperature, and since we want $T_d \approx T_c/2$, we need to reduce the diquark condensate roughly by a factor of two. This suggests that λ should fall somewhere in the range $[0.6, 0.7]$.

Let us next consider the thermodynamic observables baryon number density and pressure. (Since we are at zero temperature, the energy density is linearly dependent on these two via the Gibbs-Duhem relation.) Both quantities are plotted in figure 5. The peak just

---

[7] It would be easy to do in the mean-field approximation, but that would miss an important physical ingredient, namely the order parameter fluctuations. We briefly discuss this point in the conclusions.

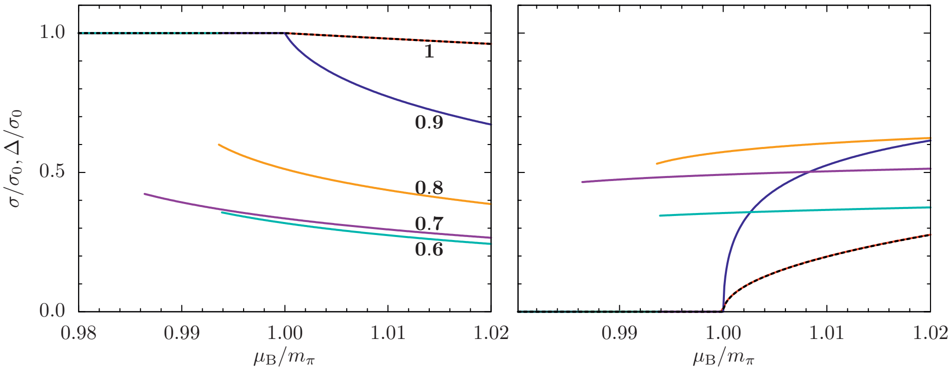

Figure 6. Detail of figure 4 close to the phase transition. The same color coding is used.

after the onset of diquark condensation at $\mu_\mathrm{B} = m_\pi$, well formed at $\lambda = 1$, is a hallmark of BEC. As λ decreases, it is gradually washed away, and again we need $\lambda \in [0.6, 0.7]$ to be able to conclude that the BEC-like behavior has given way to BCS-like scaling. One should, however, be aware of the fact that the absolute height of the peak is only indicative here, as it is very sensitive to the value of the pion decay constant and thus to the precise values of the parameters used [26].

Before closing this section, we would like to point out a subtle detail concerning the dependence of our results on the chiral twist. As may be seen already in figure 4, the diquark condensation phase transition becomes first order for sufficiently small λ. In order to highlight this feature, we zoom in on figure 4 in the immediate vicinity of the transition. This is shown in figure 6. The discontinuity of the condensates becomes rather strong, yet the location of the transition remains very close to $\mu_\mathrm{B}/m_\pi = 1$. For the values of λ considered here, it remains in the range of $\mu_\mathrm{B}/m_\pi \in [0.98, 1]$. We have confirmed numerically that around the transition point, the thermodynamic potential has two competing local minima, and used this to locate the transition precisely. The first-order transition only appears for sufficiently low values of λ, the critical value being approximately $\lambda_c \approx 0.88$.

While the appearance of a first-order transition was somewhat unexpected to us, it is not in contradiction with symmetry or any other physical principle. The change of the order of the transition may well be an artifact of our model, and we therefore do not analyze it any further. It is nevertheless interesting to note that introducing the chiral twist provides a mechanism for a direct transition from the vacuum to the BCS regime of weakly coupled quarks without the necessity for an intermediate BEC phase. In any case, we remark that the first-order transition is unlikely to be visible in current lattice simulations, since it appears very close to its expected position, and since even a small external diquark source j is likely to turn it into a crossover. This is clear from figure 7, showing details of the transition for $\lambda = 0.8$: an external source as small as 1 MeV is sufficient to smooth out the transition into a crossover.

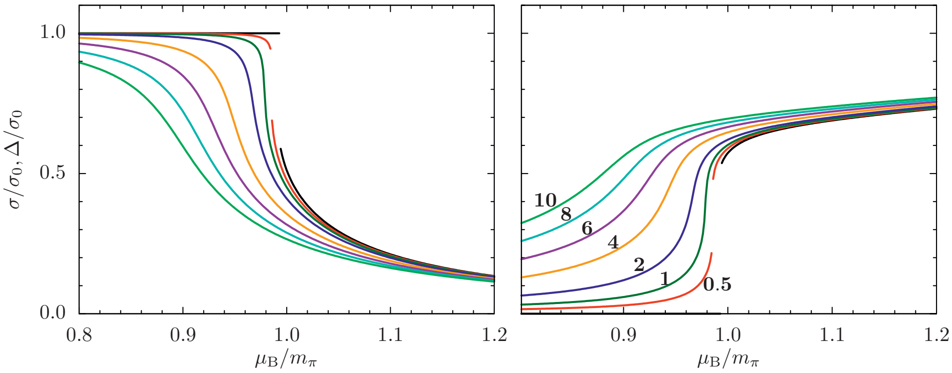

Figure 7. Dependence of the rescaled chiral and diquark condensate on the diquark source j for $\lambda = 0.8$. The values of j in MeV are indicated in bold.

6 Nonzero temperature: deconfinement

At nonzero temperature, the nature of thermal excitations in the system becomes important, and the simple NJL model (3.2) does not capture the equilibrium thermodynamics of (2c)QCD correctly: at low temperatures, the relevant degrees of freedom of 2cQCD are the pions and the diquarks, whereas the NJL model is based on the quark degrees of freedom. We follow the by now standard procedure and take into account the confining property of strong interactions by coupling the model to the Polyakov loop. We have avoided doing so until now for two reasons: (i) there is considerable freedom in the choice of the gauge sector of the model [36], and (ii) the resulting framework is no longer a Lagrangian field theory in the usual sense but merely a statistical model, since there are no dynamical gauge degrees of freedom.

At nonzero temperature, we have to add the effects of thermal quark excitations as well as the gauge sector to eq. (5.1). The full thermodynamic potential of the PNJL model 2cQCD then becomes [30]

$$\Omega_{\text{PNJL}} = \Omega_{\text{gauge}}(\Phi) + \frac{\sigma^2}{4G} + \frac{|\Delta|^2}{4\lambda G} - 2N_c \sum_{\pm} \int \frac{\mathrm{d}^3\boldsymbol{k}}{(2\pi)^3} \Big[E^{\pm}_{\boldsymbol{k}} + T\log\big(1+2\Phi e^{-\beta E^{\pm}_{\boldsymbol{k}}} + e^{-2\beta E^{\pm}_{\boldsymbol{k}}}\big)\Big], \tag{6.1}$$

where Φ is the expectation value of the Polyakov loop and $\Omega_{\text{gauge}}(\Phi)$ is the yet unspecified contribution of the gauge sector.

6.1 Renormalization of the Polyakov loop

Before we proceed with the numerical solution of the model, we have to address a conceptual issue related to the Polyakov loop. On the lattice, the concept of the Polyakov loop is rather subtle as in the naive continuum limit, its expectation value vanishes even in the deconfined phase; the Polyakov loop requires renormalization [37–39]. A simple way to think of it is as follows. The Polyakov loop expectation value can be related to the free energy of a static heavy quark immersed in the colored medium, F_q, via $\Phi \sim e^{-\beta F_q}$. An additive renormalization of the free energy then gives a multiplicative renormalization of the Polyakov loop via

$$\Phi_R = e^{-\beta \Delta F_q} \Phi_0, \tag{6.2}$$

where Φ_0 is its "bare" value. On the lattice, another interpretation of this formula is available. Using the relation $\beta = N_\tau a_s$, where N_τ is the number of lattice points in the temporal direction and a_s is the lattice spacing, we have $e^{-\beta \Delta F_q} = (e^{-a_s \Delta F_q})^{N_\tau} \equiv Z_\Phi^{N_\tau}$. The lattice Polyakov loop is a time-ordered product of N_τ link variables, winding around the temporal direction. Renormalization of each link variable by the constant factor Z_Φ therefore gives rise to a temperature-dependent renormalization of the Polyakov loop.

In practice, the Z_Φ factor is found by imposing a certain renormalization condition. Following refs. [6, 7], we define this condition by prescribing a value $\bar{\Phi}_R$ for the renormalized Polyakov loop at a given reference temperature $\bar{T}$ and $\mu_\mathrm{B} = 0$. This leads to the relation

$$\Phi_R(T, \mu_\mathrm{B}) = \Phi_0(T, \mu_\mathrm{B}) \left[\frac{\bar{\Phi}_R}{\Phi_0(\bar{T}, 0)} \right]^{\bar{T}/T}. \tag{6.3}$$

The Z_Φ factor is kept constant throughout the computation: it is fixed at $\mu_\mathrm{B} = 0$ and the same value is used regardless of the baryon chemical potential.

How should we compare the prediction of our model (6.1) to the renormalized Polyakov loop measured on the lattice? Note that depending on the reference value $\bar{\Phi}_R$, the renormalized Polyakov loop can in principle take on any positive value, whereas the quantity Φ in eq. (6.1) is usually assumed (and for some choices of Ω_gauge enforced) to lie in the range $[0, 1]$. Here we take the point of view that in our model, the finite-valued Φ is already renormalized, but in some a priori unknown scheme. In order to be able to compare our model to lattice results, we therefore first have to minimize the thermodynamic potential (6.1) with respect to Φ, and then perform an additional finite renormalization using eq. (6.3) with the same renormalization condition as used on the lattice.

6.2 Zero chemical potential

We next have to make a choice for the Polyakov loop potential $\Omega_\mathrm{gauge}(\Phi)$. Some of the potentials used in the literature include a large number of free parameters, allowing a precise numerical fit to lattice data [12]. However, since we aim at a qualitative understanding rather than numerical fitting, we prefer to have a model with as few free parameters as possible. We therefore employ the potential already used in the context of 2cQCD in ref. [30], motivated by the lattice strong-coupling expansion [11],

$$\Omega_\mathrm{gauge}(\Phi) = -bT \left[24\Phi^2 e^{-\beta a} + \log(1 - \Phi^2) \right]. \tag{6.4}$$

The parameter a is proportional to the deconfinement temperature T_g in the pure-gauge theory via $a = T_g \log 24$. The parameter b can be related to the string tension. While the parameters of the quark sector of the model are fixed by eq. (4.13) — the chiral twist does not affect the mean-field thermodynamic potential at $\mu_\mathrm{B} = 0$ — the parameters a, b will be determined by a fit to lattice data for the expectation value of the Polyakov loop.

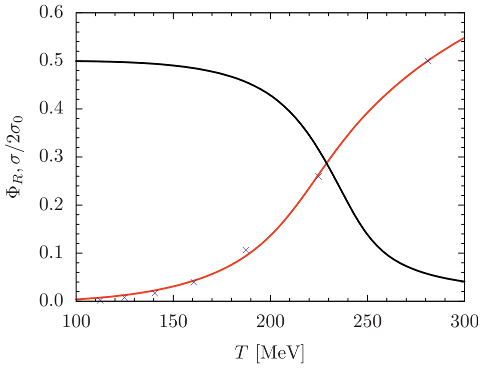

Figure 8. Expectation value of the rescaled chiral condensate (black line) and the Polyakov loop (red line) at $\mu_\mathrm{B} = 0$ as a function of temperature. The data points are taken from ref. [7]; the highest data point is the reference point which defines the renormalization condition. Note that in order to be able to display both curves on the same scale, the chiral condensate is rescaled to equal 1/2 in the vacuum.

To this end, we use the conversion between the lattice and physical units provided by ref. [6], defined by the reference temperature of $\bar{T} = 281$ MeV for $N_\tau = 4$. We then use the renormalization scheme B of ref. [7], in which $\bar{\Phi}_R = 1/2$. Our best fit to the lattice data is shown in figure 8 and corresponds to the values

$$b = (278\text{ MeV})^3, \qquad T_g = 247\text{ MeV}. \tag{6.5}$$

In the same figure, we also display the temperature dependence of the chiral condensate (rescaled for convenience to equal 1/2 in the vacuum). This demonstrates that with the present values of the gauge sector parameters, differing somewhat from those of ref. [30], the chiral and deconfinement crossovers at zero chemical potential appear in the same range of temperatures. Note that the location of the crossover may depend somewhat on the choice of the renormalization condition. We prefer not to give a single value for a pseudocritical temperature due to the ambiguity of this concept.

6.3 Chemical potential dependence

With increasing chemical potential, one generally expects that the deconfinement crossover moves towards lower temperatures due to the back-reaction of the dense medium to the gauge sector. However, it is notoriously difficult to take this back-reaction into account in the PNJL model. A common way around this is to include an explicit μ_B-dependence in the potential Ω_gauge, usually using an analytic ansatz motivated by perturbation theory [40–42]. One should note that introducing such a chemical potential dependence into Ω_gauge leads to an unphysical artifact: it gives an extra contribution to the baryon number density that does not arise from the quark degrees of freedom of the model. However, since $\Omega_\mathrm{gauge} = 0$ at $T = 0$, this artifact does not violate the "Silver Blaze" property stating that at zero temperature, physics is independent of μ_B below the onset of diquark BEC [43].

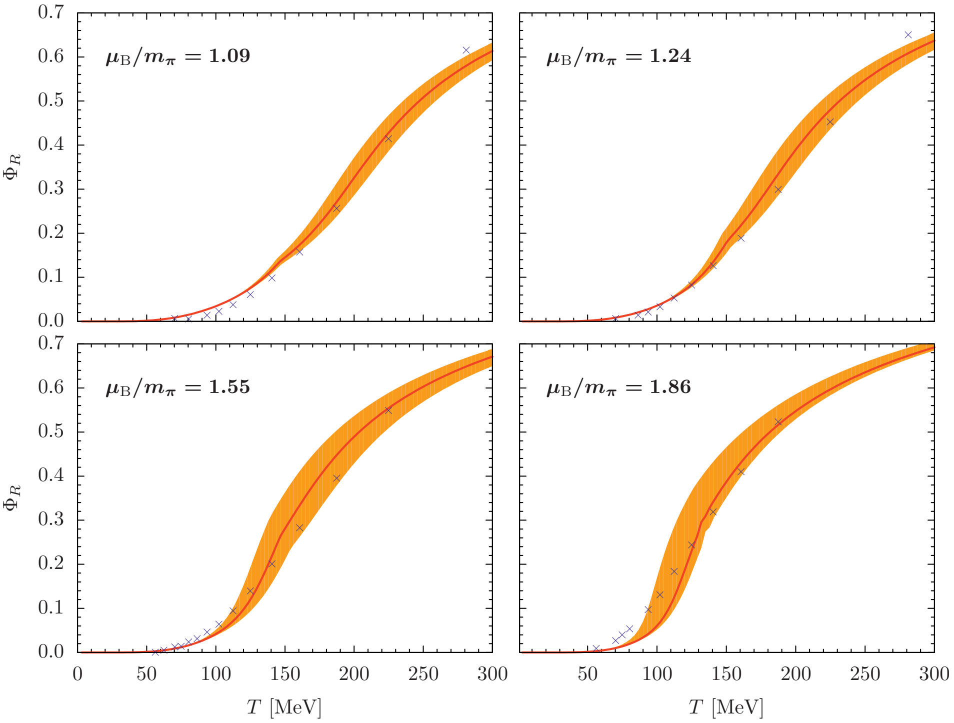

Figure 9. Expectation value of the renormalized Polyakov loop for $\lambda = 0.7$ and several values of μ_B. The red lines represent the best fit of the T_g parameter. The orange bands were obtained by varying T_g in order to estimate the error of the fit. The data points are taken from ref. [7].

Here we would like to make the case that the data for the expectation value of the Polyakov loop at nonzero baryon density of refs. [6, 7], can be exploited to obtain a direct information about the Polyakov loop potential, without resorting to any ansatz. To make it as simple as possible, we assume that b is constant and fixed by eq. (6.5), while the parameter a contains a μ_B-dependent temperature scale,

$$a(\mu_B) = T_g(\mu_B) \log 24. \tag{6.6}$$

This is in accord with the ideas put forward in ref. [40], based on the perturbative running with the physical scale set by the chemical potential. Figure 9 shows a comparison of our model predictions with lattice data for different values of μ_B taken from ref. [7]. In each plot, we have adjusted the value of $T_g(\mu_B)$ to represent the lattice data most faithfully; the quality of the fit can be assessed by varying T_g, indicated by the bands in figure 9. Along with adjusting $T_g(\mu_B)$, the μ_B-independent value $\lambda = 0.7$ was chosen to achieve the best overall fit. Note that this value agrees well with the estimate $\lambda \in [0.6, 0.7]$ obtained in the previous section, based on different observables for a different thermodynamic regime, namely high density and zero temperature.

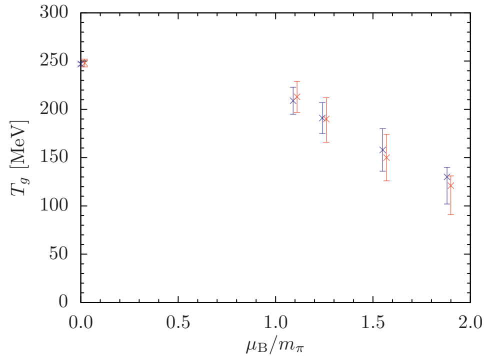

Figure 10. Temperature scale T_g of the Polyakov loop potential (6.4) as a function of μ_{B}/m_π. The blue data points are extracted directly from figure 9; the error bars are defined by the bands therein. The red data points correspond to $m_0 = 48$ MeV, with the other parameters of the NJL model still given by eq. (4.13); this reproduces the pion mass used in ref. [7]. Both data sets correspond to the same values of μ_{B}/m_π, but the red points were slightly displaced for the sake of convenience.

The extracted values of $T_g(\mu_{\mathrm{B}})$ are shown as the blue data points in figure 10, with error bars defined by the bands in figure 9. This plot provides a direct information about the back-reaction of the dense medium to the gauge sector, without the need to employ a particular analytical ansatz for the function $T_g(\mu_{\mathrm{B}})$. If desired, the data points in figure 10 can of course be fitted with a suitably chosen function of μ_{B}.

The effect of tuning the chiral twist on the Polyakov loop crossover can be appreciated with the help of figure 11. For $\lambda = 1$, the crossover tends to be too steep. The reason is that we are in the baryon superfluid phase and the quark gap Δ is too large to allow thermal excitation of quarks. Hence the behavior of the Polyakov loop to a large extent is the same as in the pure gauge theory. Once λ is lowered, the quark gap is reduced and the light quark excitations smear out the crossover. The fact that the curves for different λ converge at high temperatures is easy to understand: at these temperatures, the system has already undergone the phase transition to the normal phase (visible in some of the curves as a small cusp) where the thermodynamic potential is independent of λ altogether. The residual deviation between different curves is a consequence of rescaling μ_{B} by the λ-dependent pion mass for the sake of the plot.

Before closing the section, two remarks are in order. Firstly, we have not made an attempt to fit all the parameters of our model precisely to the lattice data. As a consequence, our pion mass (about 550 MeV for $\lambda = 0.7$) differs by about 25% from its lattice value (720 MeV in physical units). The latter can be reproduced in our model by setting $m_0 = 48$ MeV while keeping the other parameters in eq. (4.13) unchanged. Following the same procedure, that is fitting the parameters a, b at $\mu_{\mathrm{B}} = 0$ to the lattice data and then re-adjusting T_g for each particular value of μ_{B}, we arrive at the red data points shown in figure 10. The proximity of the two data sets demonstrates that our results are rather

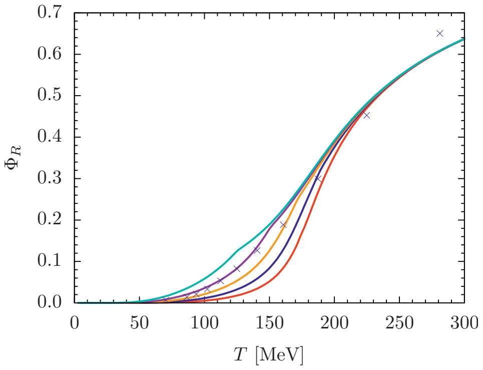

Figure 11. Expectation value of the renormalized Polyakov loop for $\mu_{\mathrm{B}}/m_\pi = 1.24$ and several different values of λ. The same color coding as in figure 4 is used: decreasing λ by steps of 0.1 moves from red ($\lambda = 1$) to cyan ($\lambda = 0.6$).

robust and to a large extent independent of the precise model setup. Note that in this latter calculation, including a nonzero diquark source is essential to achieve a good agreement with the lattice data. The effect of the diquark source on the expectation value of the Polyakov loop is much weaker for the light quark parameter set (4.13), and all results shown in figures 8 and 9 are understood at $j = 0$.

Secondly, as can be seen in figure 9, our model cannot reproduce very well the Polyakov loop data at both low and high temperatures. Reaching agreement here may require going beyond the simple model of eq. (6.4) and introducing a more phenomenological gauge sector potential with a larger number of free parameters, or using input from other methods [44]. Nevertheless, for lower temperatures *and* lower μ_{B}, our simple model can reproduce the lattice data quite well, which makes our conclusions based on symmetry and its explicit breaking rather robust.

7 Conclusions and outlook

In the present paper, we have studied in detail the PNJL model with focus on comparing it to lattice data for 2cQCD. We have discussed extensively the effects of strong explicit chiral symmetry breaking due to finite quark masses and the Wilson term in the lattice action. We argued that taking these effects into account requires a generalization of the standard PNJL model. This is accomplished by introducing the chiral twist that incorporates explicit breaking of chiral symmetry in the four-quark interaction term. Based on diverse pieces of evidence, we have argued for its value in the range $\lambda \in [0.6, 0.7]$, which can *simultaneously* account for the following nontrivial effects:

- Rapid crossover from the vacuum to a BCS-like gas of almost massless and gapless quarks at $\mu_{\mathrm{B}} \gtrsim m_\pi$.

- Strong suppression of the critical temperature T_d for baryon number breaking as compared to the (pseudo)critical temperature T_c for chiral restoration at $\mu_{\mathrm{B}} = 0$.

- Strong broadening of the Polyakov loop crossover within the baryon superfluid phase.

We argued in section 5.2 that these effects cannot be explained by a large current quark mass. However, this statement should be understood *within* the (P)NJL model framework. We cannot discriminate with confidence the effects of explicit chiral symmetry breaking by lattice discretization and by the current quark mass on the level of the 2cQCD Lagrangian. Which of these sources of symmetry breaking is more important can be decided with future lattice simulations by varying the quark mass and lattice spacing.

In addition, we were able to extract the μ_{B}-dependent temperature scale $T_g(\mu_{\mathrm{B}})$ from the lattice data for the expectation value of the Polyakov loop. This is a model-independent result in the sense that it does not rely on a particular analytical ansatz for the μ_{B}-dependence of the Polyakov-loop potential. However, one should not interpret T_g as a deconfinement temperature: while the actual transition from hadronic to quark degrees of freedom is a smooth crossover which does not have a well-defined critical temperature, the quantity T_g is well defined, but depends on the choice of the Polyakov loop potential.

Our simple mean-field model of course has its limitations, most importantly in that it ignores fluctuations of the composite bosonic degrees of freedom. We therefore have to carefully choose observables which are not sensitive to such fluctuations. (Their effect on the phase diagram of 2cQCD was investigated in refs. [45, 46].) Examples of such observables, discussed in this paper, include:

+ Thermodynamical observables at low temperature and high density, where the physics is dominated by a Fermi sea of quarks as well as the chiral and diquark condensates. Indeed, it is well-known that the mean-field BCS pairing theory works quantitatively quite well at weak coupling and zero temperature.

+ Expectation value of the Polyakov loop from low to high temperatures. The Polyakov loop couples only indirectly to, and therefore is very mildly affected by, the colorless diquark degrees of freedom [30]. The dominant matter contribution to the Polyakov loop thermodynamics comes from the colored quarks, which we do take into account.

Observables for which the diquark fluctuations play an essential role, and which we therefore deliberately avoid discussing in this paper, include:

– Critical temperature T_d for baryon superfluidity. This is the main reason why we prefer not to plot the phase diagram of 2cQCD.

– Baryon number density in the confined phase without a diquark condensate (that is, at low T as well as μ_{B}).

There are several open questions that we would like to understand better and we leave them for future work. Firstly, we have not provided any microscopic derivation of the chiral twist. Both interaction terms in eq. (3.2) are expected to arise as we integrate out high-momentum modes in 2cQCD to arrive at a low-energy effective description. In particular, it would be desirable to have an explanation for the fact that $\lambda < 1$. We simply assumed this since it leads to the desired phenomenology.

Secondly, we have not touched upon the fact that in the lattice simulations of ref. [6], a second onset is observed at high $\mu_{\rm B}$, where the thermodynamic quantities rise significantly above their SB limits. At present, we do not have any explanation for this effect.

Finally, we wish to make the case that current and future lattice data for dense two-color QCD should be used to improve our understanding of the real world. To this end, we need a dictionary to translate between models for two-color and three-color QCD. What we have in mind is a framework valid for both two and three colors, augmented by a mapping of the model parameters. For example, one can use the expected scaling based on large-N_c arguments. This was done here and in ref. [30] to fix the parameters of the NJL part of the model. The gauge sector can be treated in similar manner. Once we have a specific analytical model that reproduces or at least fits the data for $T_g(\mu_{\rm B})$, we can extract an improved $\mu_{\rm B}$-dependent Polyakov-loop potential for QCD simply by assuming that its quark-induced part is suppressed by a factor of $1/N_c$ relative to the dominant, gluon contribution. The resulting model will allow one to study, for example, the interplay of chiral symmetry restoration and deconfinement in cold and dense quark matter.

A Chiral model with a Wilson term

In this appendix, we consider the effects of adding a Wilson term to the NJL Lagrangian.

A.1 Three-momentum cutoff

Let us revisit the model of eq. (3.2). In the mean-field approximation, the Lagrangian describes a pair of fermion species with squared masses

$$M_\pm^2 = \frac{1}{2\kappa^2}\left(1 + 2\kappa M \pm \sqrt{1 + 4\kappa M}\right), \tag{A.1}$$

where $M = m_0 + \sigma$. In the limit $\kappa \to 0$, one of the masses approaches M, as expected. The other, however, diverges as $1/\kappa$. In lattice field theory, this mode is interpreted as the Wilson doubler which decouples in the continuum limit.

We shall now argue that a naive three-momentum cutoff Λ is not a suitable regulator in a theory with a heavy doubler. To see this, consider the thermodynamic potential in the vacuum. The thermodynamic potential is given by

$$\Omega_{\rm NJL}^{\rm vac} = \frac{\sigma^2}{4G} - 4N_c \sum_{e=\pm} \int \frac{{\rm d}^3\boldsymbol{k}}{(2\pi)^3}\, \epsilon_{e\boldsymbol{k}}, \tag{A.2}$$

where $\epsilon_{e\boldsymbol{k}} \equiv \sqrt{\boldsymbol{k}^2 + M_e^2}$. The gap equation for the chiral condensate is obtained by taking the derivative with respect to σ. This yields

$$\sigma = \frac{4GN_c}{\kappa} \sum_{e=\pm} \int \frac{{\rm d}^3\boldsymbol{k}}{(2\pi)^3} \frac{1}{\epsilon_{e\boldsymbol{k}}} \left(1 + \frac{e}{\sqrt{1 + 4\kappa M}}\right), \tag{A.3}$$

generalizing eq. (4.5). The core of the problem is visible now. In the limit $\kappa \to 0$, the integrand involving the heavy doubler approaches a nonzero constant. Hence the heavy fermion gives a nonzero contribution to the gap equation even in the limit when its mass goes to infinity. The heavy doubler does not decouple. This can be traced to the fact that the Wilson term modifies the spectrum of the theory, yet the momentum cutoff is sensitive to momenta only, not to masses. We need to use some regularization scheme which affects masses directly.

A.2 Pauli-Villars regularization

Implementing the Pauli-Villars (PV) scheme may be subtle since covariant regulators in general tend to introduce unphysical artifacts at finite temperature and chemical potential. We therefore first derive the naive expression for the thermodynamic potential with the Wilson term, and subsequently introduce the regulator. This will ensure thermodynamic consistency.

Returning to eq. (4.2) and switching to Euclidean space, the mean-field thermodynamic potential reads

$$\Omega_{\mathrm{PNJL}} = \Omega_{\mathrm{gauge}}(\Phi) + \frac{\sigma^2}{4G} + \frac{|\Delta|^2}{4\lambda G} - 2T\sum_n \int \frac{\mathrm{d}^3\boldsymbol{k}}{(2\pi)^3} \log\det\mathcal{G}^{-1}(\omega_n, \boldsymbol{k}), \tag{A.4}$$

where the determinant of the inverse propagator takes the form

$$\begin{aligned}\det\mathcal{G}^{-1} = \Big\{ &\big[(M-\kappa K_\uparrow^2)^2 - K_\uparrow^2\big]\big[(M-\kappa K_\downarrow^2)^2 - K_\downarrow^2\big] \\ &+ 2|\Delta|^2\big[(M-\kappa K_\uparrow^2)(M-\kappa K_\downarrow^2) - K_\uparrow\cdot K_\downarrow\big] + |\Delta|^4 \Big\}^2 .\end{aligned} \tag{A.5}$$

The arrows indicate momenta of red quarks and green antiquarks, $K^\mu_{\uparrow,\downarrow} \equiv (K^0_{\uparrow,\downarrow}, \boldsymbol{k})$, with

$$K^0_\uparrow \equiv \mathrm{i}\omega_n + \mu - \mathrm{i}\alpha, \qquad K^0_\downarrow \equiv \mathrm{i}\omega_n - \mu - \mathrm{i}\alpha. \tag{A.6}$$

Furthermore, $\omega_n \equiv (2n+1)\pi T$ are the fermionic Matsubara frequencies and α is the constant background color gauge field, related to the Polyakov loop variable via $\Phi = \cos(\beta\alpha)$. It is not easy to factorize the determinant (A.5) into simple factors corresponding to free fermionic quasiparticles for general Δ. In the following, we therefore set $\Delta = 0$ and make sure that μ_{B} is low enough so that we do not enter the baryon superfluid phase. Note that as a consequence λ becomes irrelevant for the thermodynamics.

PV regularization is introduced by making the replacement in eq. (A.4)

$$\log\det\mathcal{G}^{-1} \to \sum_j c_j \log\det\mathcal{G}_j^{-1}, \tag{A.7}$$

where the inverse propagator $\mathcal{G}_j^{-1}$ is defined analogously to eq. (A.5) by

$$\det\mathcal{G}_j^{-1} = \Big\{\big[(M-\kappa K_\uparrow^2)^2 + j\Lambda^2 - K_\uparrow^2\big]\big[(M-\kappa K_\downarrow^2)^2 + j\Lambda^2 - K_\downarrow^2\big]\Big\}^2 . \tag{A.8}$$

The coefficients c_j are chosen in order to cancel ultraviolet divergences. Two simple choices, referred to as the PV2 and PV3 schemes, correspond to $j = 0, 1, 2$ with $c_j = \{1, -2, 1\}$ and to $j = 0, 1, 2, 3$ with $c_j = \{1, -3, 3, -1\}$ [9]. The PV2 scheme removes all the divergences, except a residual logarithmic divergence in the thermodynamic potential. This divergence can be eliminated by subtracting the potential at a conveniently chosen reference point. All derivatives of the thermodynamic potential such as the gap equation are rendered finite. The PV3 scheme, on the other hand, renders the thermodynamic potential finite without further subtractions. We choose the PV3 scheme for convenience since the PV2 scheme turns out to be continuous but non-analytic in the limit $\kappa \to 0$.

Since at $\Delta = 0$ the Dirac determinant (A.5) trivially factorizes, it is easy to carry out the Matsubara sum, leading to a generalization of eq. (6.1), valid in the normal phase,

$$\Omega^{\Delta=0}_{\mathrm{PNJL}} = \Omega_{\mathrm{gauge}}(\Phi) + \frac{\sigma^2}{4G} - 2N_c \sum_{e=\pm}\sum_{\pm}\int \frac{\mathrm{d}^3\boldsymbol{k}}{(2\pi)^3}\sum_{j=0}^{3} c_j \Big[E^{j\pm}_{e\boldsymbol{k}} + T\log\big(1 + 2\Phi e^{-\beta E^{j\pm}_{e\boldsymbol{k}}} + e^{-2\beta E^{j\pm}_{e\boldsymbol{k}}}\big)\Big], \tag{A.9}$$

where

$$E^{j\pm}_{e\boldsymbol{k}} \equiv \left|\sqrt{\boldsymbol{k}^2 + M^2_{je}} \pm \mu\right|, \qquad M^2_{je} \equiv \frac{1}{2\kappa^2}\left(1 + 2\kappa M + e\sqrt{1 + 4\kappa M - 4j\kappa^2\Lambda^2}\right). \tag{A.10}$$

The latter generalizes eq. (A.1) for the Wilson masses to the PV regulator modes. Before we work out the physical consequences, it is useful to pause and explain why we introduced the PV regularization via eq. (A.8). Here is our consistency check list:

- The regularization manifestly cancels all divergences. This is easy to see by expanding the logarithm of the regulated determinant (A.8) in powers of Λ. Every factor of $j\Lambda^2$ is suppressed by $1/K^4$ for $\kappa > 0$, or at least $1/K^2$ for $\kappa = 0$. Since the thermodynamic potential has a quartic divergence, three subtractions are sufficient to make it finite.

- For $\kappa = 0$, our prescription reduces to the simple replacement $M^2 \to M^2 + j\Lambda^2$, corresponding to the usual implementation of the PV scheme in Lorentz-invariant theories. However, this naive replacement does not work for nonzero κ.

- Our thermodynamic potential represents a gas of quasiparticles with masses M_{je} at finite chemical potential. Since the regularization does not affect the shift of K^0 by μ, it automatically has the “Silver Blaze” property [43], namely that the physics is completely independent of μ_{B} at $T = 0$ below the onset of diquark condensation. Note that this property is not necessarily preserved is some PV-like regularizations where the whole Gram matrix of the Dirac operator is regulated [47].

A.3 Vacuum physics

As the first step, we have to refit the model parameters owing to the different regularization scheme. The same values for the chiral condensate, pion decay constant, and pion mass given in eq. (4.12), yield the parameter values in the PV3 scheme

$$G = 5.11\ \mathrm{GeV}^{-2}, \quad \Lambda = 1129\ \mathrm{MeV}, \quad m_0 = 5.4\ \mathrm{MeV} \qquad \text{(fitted parameters)}. \tag{A.11}$$

The fact that the same physical observables require a relatively high cutoff and give a comparably small constituent quark mass in covariant regularization schemes is well known [9]. The Wilson coupling κ is treated as a free parameter.

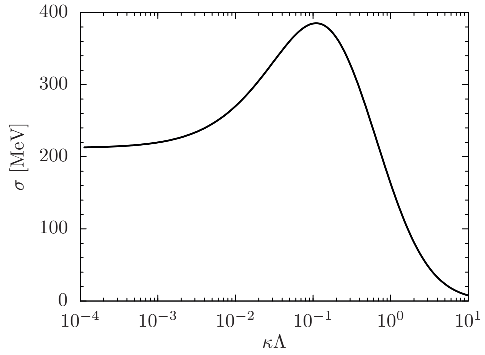

Figure 12. Chiral condensate in the vacuum as a function of the dimensionless combination $\kappa\Lambda$; all the other parameters are fixed by eq. (A.11). Note the logarithmic scale of the horizontal axis.

Figure 12 shows the effect of the κ coupling on the chiral condensate in the vacuum. As expected, the chiral condensate initially grows with κ. However, around $\kappa\Lambda \approx 10^{-1}$, the growth stops and further increasing κ leads to a suppression of the condensate. This is connected to the fact that the PV regulator masses (A.10) become complex, and we therefore do not attach physical significance to this threshold. Large values of κ are not physical anyway since the masses of the two fermion species converge to each other.

In a similar fashion, one can use eq. (A.9) to study the consequences of the Wilson term for thermodynamics quantities. However, we do not perform a detailed analysis here, but just remark that it does not affect the qualitative conclusions made in this paper. At a quantitative level, we expect κ to play a role whenever chiral symmetry is important. In particular, the presence of an extra heavy fermion species should manifest itself in modified thermodynamics at high temperatures.

Acknowledgments

We are grateful to Jon-Ivar Skullerud for making the lattice data from ref. [7] available to us, and for helpful correspondence. We furthermore appreciate discussions and/or correspondence with Paolo Castorina, Kenji Fukushima and Štefan Olejník. One of us (T.B.) would like to thank the Institute for Theoretical Physics, Goethe University Frankfurt for hospitality during the final stage of this project, and to Michael Buballa, Owe Philipsen, Dirk Rischke, David Scheffler, and Armen Sedrakian for useful comments. The work of T.B. was supported by the Austrian Science Fund (FWF), grant No. M 1603-N27.

References

[1] M. Cristoforetti, F. Di Renzo, and L. Scorzato, *New approach to the sign problem in quantum field theories: High density QCD on a Lefschetz thimble*, *Phys. Rev.* **D86** (2012) 074506, [`arXiv:1205.3996`].

[2] G. Aarts, *Complex Langevin dynamics and other approaches at finite chemical potential*, *PoS* **LATTICE2012** (2012) 017, [`arXiv:1302.3028`].

[3] D. Sexty, *Progress in complex Langevin simulations of full QCD at non-zero density*, *Nucl. Phys.* **A931** (2014) 856–860, [`arXiv:1408.6767`].

[4] J. Braun, L. M. Haas, F. Marhauser, and J. M. Pawlowski, *Phase Structure of Two-Flavor QCD at Finite Chemical Potential*, *Phys. Rev. Lett.* **106** (2011) 022002, [`arXiv:0908.0008`].

[5] C. S. Fischer, J. Luecker, and J. A. Mueller, *Chiral and deconfinement phase transitions of two-flavour QCD at finite temperature and chemical potential*, *Phys. Lett.* **B702** (2011) 438–441, [`arXiv:1104.1564`].

[6] S. Cotter, P. Giudice, S. Hands, and J.-I. Skullerud, *Towards the phase diagram of dense two-color matter*, *Phys. Rev.* **D87** (2013) 034507, [`arXiv:1210.4496`].

[7] T. Boz, S. Cotter, L. Fister, D. Mehta, and J.-I. Skullerud, *Phase transitions and gluodynamics in 2-colour matter at high density*, *Eur. Phys. J.* **A49** (2013) 87, [`arXiv:1303.3223`].

[8] U. Vogl and W. Weise, *The Nambu and Jona-Lasinio Model: Its Implications for Hadrons and Nuclei*, *Prog. Part. Nucl. Phys.* **27** (1991) 195–272.

[9] S. P. Klevansky, *The Nambu–Jona-Lasinio model of quantum chromodynamics*, *Rev. Mod. Phys.* **64** (1992) 649–708.

[10] M. Buballa, *NJL-model analysis of dense quark matter*, *Phys. Rept.* **407** (2005) 205–376, [`hep-ph/0402234`].

[11] K. Fukushima, *Chiral effective model with the Polyakov loop*, *Phys. Lett.* **B591** (2004) 277–284, [`hep-ph/0310121`].

[12] C. Ratti, M. A. Thaler, and W. Weise, *Phases of QCD: Lattice thermodynamics and a field theoretical model*, *Phys. Rev.* **D73** (2006) 014019, [`hep-ph/0506234`].

[13] E. Megías, E. Ruiz Arriola, and L. L. Salcedo, *Polyakov loop in chiral quark models at finite temperature*, *Phys. Rev.* **D74** (2006) 065005, [`hep-ph/0412308`].

[14] L. von Smekal, *Universal Aspects of QCD-like Theories*, *Nucl. Phys. Proc. Suppl.* **228** (2012) 179–220, [`arXiv:1205.4205`].

[15] J. B. Kogut, M. A. Stephanov, and D. Toublan, *On two-color QCD with baryon chemical potential*, *Phys. Lett.* **B464** (1999) 183–191, [`hep-ph/9906346`].

[16] J. B. Kogut, M. A. Stephanov, D. Toublan, J. J. M. Verbaarschot, and A. Zhitnitsky, *QCD-like theories at finite baryon density*, *Nucl. Phys.* **B582** (2000) 477–513, [`hep-ph/0001171`].

[17] S. Hands, I. Montvay, S. Morrison, M. Oevers, L. Scorzato, and J. Skullerud, *Numerical study of dense adjoint matter in two color QCD*, *Eur. Phys. J.* **C17** (2000) 285–302, [`hep-lat/0006018`].

[18] D. T. Son and M. A. Stephanov, *QCD at Finite Isospin Density*, *Phys. Rev. Lett.* **86** (2001) 592–595, [`hep-ph/0005225`].

[19] W. Zwerger, *The BCS-BEC Crossover and the Unitary Fermi Gas*, vol. 836 of *Lecture Notes in Physics*. Springer, 2012.

[20] A. Amato, P. Giudice, and S. Hands, *Hadron Wavefunctions as a Probe of a Two Color Baryonic Medium*, `arXiv:1501.0300`.

[21] J. Gasser and H. Leutwyler, *Chiral Perturbation Theory to One Loop*, *Ann. Phys.* **158** (1984) 142–210.

[22] J. Gasser and H. Leutwyler, *Chiral Perturbation Theory: Expansions in the Mass of the Strange Quark*, *Nucl. Phys.* **B250** (1985) 465–516.

[23] T. Brauner, *On the chiral perturbation theory for two-flavor two-color QCD at finite chemical potential*, *Mod. Phys. Lett.* **A21** (2006) 559–570, [`hep-ph/0601010`].

[24] K. Splittorff, D. Toublan, and J. J. M. Verbaarschot, *QCD with two colors at finite baryon density at next-to-leading order*, *Nucl. Phys.* **B620** (2002) 290–314, [`hep-ph/0108040`].

[25] K. Splittorff, D. Toublan, and J. J. M. Verbaarschot, *Thermodynamics of chiral symmetry at low densities*, *Nucl. Phys.* **B639** (2002) 524–548, [`hep-ph/0204076`].

[26] J. O. Andersen and T. Brauner, *Phase diagram of two-color quark matter at nonzero baryon and isospin density*, *Phys. Rev.* **D81** (2010) 096004, [`arXiv:1001.5168`].

[27] S. Weinberg, *The Quantum Theory of Fields*, vol. I. Cambridge University Press, Cambridge, UK, 1995.

[28] C. Ratti and W. Weise, *Thermodynamics of two-color QCD and the Nambu Jona-Lasinio model*, *Phys. Rev.* **D70** (2004) 054013, [`hep-ph/0406159`].

[29] G.-f. Sun, L. He, and P. Zhuang, *BEC-BCS crossover in the Nambu-Jona-Lasinio model of QCD*, *Phys. Rev.* **D75** (2007) 096004, [`hep-ph/0703159`].

[30] T. Brauner, K. Fukushima, and Y. Hidaka, *Two-color quark matter: $U(1)_A$ restoration, superfluidity, and quarkyonic phase*, *Phys. Rev.* **D80** (2009) 074035, [`arXiv:0907.4905`].

[31] S. Imai, H. Toki, and W. Weise, *Quark-hadron matter at finite temperature and density in a two-color PNJL model*, *Nucl. Phys.* **A913** (2013) 71–102, [`arXiv:1210.1307`].

[32] T. Makiyama, Y. Sakai, T. Saito, M. Ishii, J. Takahashi, K. Kashiwa, H. Kouno, A. Nakamura, and M. Yahiro, *Phase structure of two-color QCD at real and imaginary chemical potentials; lattice simulations and model analyses*, `arXiv:1502.0619`.

[33] S. Hands, S. Kim, and J.-I. Skullerud, *Deconfinement in dense two-color QCD*, *Eur. Phys. J.* **C48** (2006) 193–206, [`hep-lat/0604004`].

[34] S. Hands, S. Kim, and J.-I. Skullerud, *Quarkyonic phase in dense two color matter*, *Phys. Rev.* **D81** (2010) 091502, [`arXiv:1001.1682`].

[35] S. Hands, I. Montvay, L. Scorzato, and J. Skullerud, *Diquark condensation in dense adjoint matter*, *Eur. Phys. J.* **C22** (2001) 451–461, [`hep-lat/0109029`].

[36] K. Fukushima, *Phase diagrams in the three-flavor Nambu–Jona-Lasinio model with the Polyakov loop*, *Phys. Rev.* **D77** (2008) 114028, [`arXiv:0803.3318`].

[37] O. Kaczmarek, F. Karsch, P. Petreczky, and F. Zantow, *Heavy quark-antiquark free energy and the renormalized Polyakov loop*, *Phys. Lett.* **B543** (2002) 41–47, [`hep-lat/0207002`].

[38] A. Dumitru, Y. Hatta, J. Lenaghan, K. Orginos, and R. D. Pisarski, *Deconfining phase transition as a matrix model of renormalized Polyakov loops*, *Phys. Rev.* **D70** (2004) 034511, [`hep-th/0311223`].

[39] O. Kaczmarek and F. Zantow, *Static quark-antiquark interactions in zero and finite temperature QCD: I. Heavy quark free energies, running coupling, and quarkonium binding*, *Phys. Rev.* **D71** (2005) 114510, [`hep-lat/0503017`].

[40] B.-J. Schaefer, J. M. Pawlowski, and J. Wambach, *Phase structure of the Polyakov-quark-meson model*, *Phys. Rev.* **D76** (2007) 074023, [`arXiv:0704.3234`].

[41] T. K. Herbst, J. M. Pawlowski, and B.-J. Schaefer, *The phase structure of the Polyakov-quark-meson model beyond mean field*, *Phys. Lett.* **B696** (2011) 58–67, [`arXiv:1008.0081`].

[42] T. K. Herbst, J. M. Pawlowski, and B.-J. Schaefer, *Phase structure and thermodynamics of QCD*, *Phys. Rev.* **D88** (2013) 014007, [`arXiv:1302.1426`].

[43] T. D. Cohen, *Functional Integrals for QCD at Nonzero Chemical Potential and Zero Density*, *Phys. Rev. Lett.* **91** (2003) 222001, [`hep-ph/0307089`].

[44] L. M. Haas, R. Stiele, J. Braun, J. M. Pawlowski, and J. Schaffner-Bielich, *Improved Polyakov-loop potential for effective models from functional calculations*, *Phys. Rev.* **D87** (2013) 076004, [`arXiv:1302.1993`].

[45] N. Strodthoff, B.-J. Schaefer, and L. von Smekal, *Quark-meson-diquark model for two-color QCD*, *Phys. Rev.* **D85** (2012) 074007, [`arXiv:1112.5401`].

[46] N. Strodthoff and L. von Smekal, *Polyakov-quark-meson-diquark model for two-color QCD*, *Phys. Lett.* **B731** (2014) 350–357, [`arXiv:1306.2897`].

[47] D. Nickel and M. Buballa, *Solitonic ground states in (color) superconductivity*, *Phys. Rev.* **D79** (2009) 054009, [`arXiv:0811.2400`].